

STUDIES ON POLYLACTIDE NANOCOMPOSITES WITH  
POLYHEDRAL OLIGOMERIC SILSESQUIOXANE

A THESIS SUBMITTED TO  
THE GRADUATE SCHOOL OF NATURAL AND APPLIED SCIENCES  
OF  
MIDDLE EAST TECHNICAL UNIVERSITY

BY

YELDA MEYVA ZEYBEK

IN PARTIAL FULFILLMENT OF THE REQUIREMENTS  
FOR  
THE DEGREE OF DOCTOR OF PHILOSOPHY  
IN  
POLYMER SCIENCE AND TECHNOLOGY

MAY 2020



Approval of the thesis:

**STUDIES ON POLYLACTIDE NANOCOMPOSITES WITH POLYHEDRAL  
OLIGOMERIC SILSESQUIOXANE**

submitted by **YELDA MEYVA ZEYBEK** in partial fulfillment of the requirements  
for the degree of **Doctor of Philosophy in of Polymer Science and Technology**  
**Department, Middle East Technical University by,**

Prof. Dr. Halil Kalıpçılar  
Dean, Graduate School of **Natural and Applied Sciences**

\_\_\_\_\_

Prof. Dr. Necati Özkan  
Head of Department, **Polymer Science and Technology**

\_\_\_\_\_

Prof. Dr. Cevdet Kaynak  
Supervisor, **Metallurgical and Materials Eng. Dept., METU**

\_\_\_\_\_

**Examining Committee Members:**

Prof. Dr. Necati Özkan  
Polymer Science and Technology Dept., METU

\_\_\_\_\_

Prof. Dr. Cevdet Kaynak  
Metallurgical and Materials Engineering Dept., METU

\_\_\_\_\_

Assist. Prof. Dr. Batur Ercan  
Metallurgical and Materials Engineering Dept., METU

\_\_\_\_\_

Assist. Prof. Dr. Ayşe Çağıl Kandemir  
Mechanical Engineering Dept., TED UNIVERSITY

\_\_\_\_\_

Assist. Prof. Dr. Salih Ertan  
Chemical Engineering Dept., ATILIM UNIVERSITY

\_\_\_\_\_

**DATE:** 28.05.2020

**I hereby declare that all information in this document has been obtained and presented in accordance with academic rules and ethical conduct. I also declare that, as required by these rules and conduct, I have fully cited and referenced all material and results that are not original to this work.**

Name, Last Name : Yelda Meyva Zeybek

Signature :

## **ABSTRACT**

### **STUDIES ON POLYLACTIDE NANOCOMPOSITES WITH POLYHEDRAL OLIGOMERIC SILSESQUIOXANE**

Meyva Zeybek, Yelda

Ph.D., Department of Polymer Science and Technology

Supervisor: Prof. Dr. Cevdet Kaynak

May 2020, 144 pages

The main purpose of the first part of this thesis was to investigate influences of three parameters on the mechanical and thermal properties of the polylactide (PLA) matrix nanocomposites filled with polyhedral oligomeric silsesquioxane (POSS) particles. For the first parameter of “Filler Content”, nanocomposites with 1, 3, 5, 7 wt% basic POSS structure were compared. For the second parameter of “Functional Group”, basic POSS structure having only nonpolar isobutyl groups were compared with three other functionalized POSS structures; i.e. aminopropylisobutyl-POSS (ap-POSS), propanediolisobutyl-POSS (pd-POSS) and octasilane-POSS (os-POSS). For the third parameter of “Copolymer Compatibilization”, all specimens were compared before and after their maleic anhydride (MA) grafted copolymer compatibilization. Specimens were produced with twin-screw extruder melt mixing and shaped under compression molding. Various tests and analyses indicated that the optimum filler content for the improved mechanical properties was 1 wt%; while the optimum structure for strength and modulus was pd-POSS structure, in terms of fracture toughness it was basic POSS structure. Additional use of MA compatibilization was especially effective for the basic POSS and os-POSS particles.

Because of the biocompatible and nontoxic character of both PLA and POSS nanoparticles, recently being a significant alternative for biomedical parts; the main purpose of the second part of this thesis was to investigate performance of the 3D-

printed PLA/POSS nanocomposites with respect to the compression molded PLA/POSS specimens. Due to the higher uniformity and higher homogeneity in the distribution of POSS nanoparticles in each PLA matrix layer, mechanical tests (tensile, flexural, toughness) revealed that the improvements in the strength, elastic modulus and fracture toughness values of the 3D-printed specimens were much higher compared to their compression molded counterparts, the benefits starting from 13% increasing up to 78%. It was also observed that there was almost no deterioration in the physical structure and mechanical properties of the 3D-printed specimens, even after keeping them 120 days at 37°C in a physiological solution prepared by using the standard PBS (Phosphate Buffered Saline) tablet.

It is known that electrospinning is the most practical technique to obtain unique properties of polymer based nanofibrous structures, such as neat PLA and PLA filled with POSS particles. On the other hand, due to the so many different process parameters to consider, production of these fibers are extremely difficult and time consuming. That is, use of a certain statistical optimization technique in the design of experiments would be necessary. Therefore, the main purpose of the third part of this thesis was to determine the optimum electrospinning parameters by applying the Taguchi technique first to neat PLA and then to reveal the applicability of these parameters for the electrospinning of PLA/POSS nanofibers. It was observed that instead of conducting 81 experiments to determine the most significant 4 optimum process parameters for PLA, use of Taguchi L<sub>9</sub> orthogonal array experiment matrix, i.e. conducting only 9 experiments, reduced time, labor and material consumption considerably. Moreover, it was generally concluded that these same parameters could be also used for the electrospinning of PLA/POSS nanofibers after addition of only 3 wt% KCl salt into the polymer solution.

**Keywords:** Polylactide, Polyhedral Oligomeric Silsesquioxane, Melt Mixing, 3D-Printing, Electrospinning

## ÖZ

### **POLİHEDRAL OLİGOMERİK SİLSESKİOKSAN İÇEREN POLİLAKTİT NANOKOMPOZİTLERİ ÜZERİNE ÇALIŞMALAR**

Meyva Zeybek, Yelda

Doktora, Polimer Bilim ve Teknolojisi Bölümü

Tez Yöneticisi: Prof. Dr. Cevdet Kaynak

Mayıs 2020, 144 sayfa

Bu tezin ilk bölümünün ana amacı, üç parametrenin polihedral oligomerik silseskuioksan (POSS) parçacık katkılı polilaktit (PLA) matris nanokompozitlerinin mekanik ve termal özellikleri üzerindeki etkilerini araştırmaktır. İlk parametre olan “Dolgu İçeriği” için ağırlıkça %1, 3, 5, 7 temel POSS yapısı içeren nanokompozitler karşılaştırılmıştır. İkinci parametre olan “Fonksiyonel Grup” için sadece polar olmayan izobütil gruplarına sahip temel POSS yapısı, diğer üç fonksiyonel POSS yapısı ile karşılaştırılmıştır; bunlar aminopropilizobutil-POSS (ap-POSS), propandiolizobutil-POSS (pd-POSS) ve oktasilan-POSS (os-POSS)’dur. Üçüncü parametre olan “Kopolimer İle Uyumlaştırma” için, tüm numuneler maleik anhidrat (MA) graft edilmiş kopolimer ile uyumlaştırılma öncesi ve sonrası karşılaştırılmıştır. Numuneler çift vidalı ekstrüder eriyik karıştırma ile üretilmiş ve basınçlı kalıplama yöntemi ile şekillendirilmiştir. Çeşitli testler ve analizler göstermiştir ki, iyileştirilmiş mekanik özellikler için optimum dolgu miktarı ağırlıkça %1’dir; dayanım ve modül için optimum yapı pd-POSS yapısı iken, kırılma tokluğu açısından ise temel POSS yapısıdır. MA uyumlaştırmasının ek olarak kullanımı özellikle temel POSS ve os-POSS parçacıkları için etkili olmuştur.

Hem PLA hem de POSS nanoparçacıkları biyouyumlu ve toksik olmayan karakterleri ile son zamanlarda biyomedikal parçalar için önemli bir seçenek oluşturmaları nedeniyle; bu tezin ikinci bölümünün ana amacı, 3B-yazıcı ile üretilmiş

PLA/POSS nanokompozitlerinin basınçlı kalıplama ile üretilmiş PLA/POSS numunelerine göre performanslarını incelemektir. Her bir PLA matris katmanında POSS nanoparçacıklarının dağılımındaki daha yüksek üniformluk ve homojenlik nedeniyle, mekanik testler (çekme, eğme, tokluk) ortaya koymuştur ki 3B-yazıcı ile üretilmiş numunelerin dayanım, elastik modül ve kırılma tokluğu değerlerindeki iyileşmeler basınçlı kalıplama ile üretilmiş muadillerine göre çok daha yüksektir, faydaları % 13'ten % 78'e kadar artmıştır. Ayrıca, standart PBS (Fosfat Tamponlu Tuz Çözeltisi) tableti kullanılarak hazırlanan fizyolojik bir solüsyonda 37°C'de 120 gün tutulduktan sonra bile, 3B-yazıcı ile üretilmiş numunelerin fiziksel yapısında ve mekanik özelliklerinde neredeyse hiç bozulma olmadığı gözlenmiştir.

Saf PLA ve POSS parçacık katkılı PLA gibi polimer bazlı nanofiber yapıların üstün özelliklerini elde etmek için en pratik tekniğin elektroğirme olduğu bilinmektedir. Öte yandan, dikkate alınması gereken birçok farklı proses parametresi olması nedeniyle, bu fiberlerin üretimi son derece zor ve zaman alıcıdır. Bu yüzden, deneylerin tasarımında belirli bir istatistiksel optimizasyon tekniğinin kullanılması gerekli olacaktır. Dolayısıyla, bu tezin üçüncü bölümünün ana amacı optimum elektroğirme parametrelerini belirlemek amacıyla Taguchi tekniğini önce saf PLA için uygulamak, ardından da bu optimum parametrelerin PLA/POSS nanofiberleri için uygulanabilirliğini ortaya koymaktır. PLA için en önemli 4 optimum işlem parametresini belirlemek için 81 deney yapmak yerine, Taguchi L9 ortogonal dizi deney matrisinin kullanılması, yani sadece 9 deney yapılması ile zaman, işçilik ve malzeme tüketiminin önemli ölçüde azaldığı gözlenmiştir. Ayrıca, polimer çözeltisine ağırlıkça sadece % 3 KCl tuzu ilave edildikten sonra, saf PLA için belirlenen optimum elektroğirme parametrelerinin aynen PLA/POSS nanofiberleri için de kullanılabileceği sonucuna varılmıştır.

**Anahtar Kelimeler:** Polilaktit, Polihedral Oligomerik Silseskioksan, Eriyik Karıştırma, 3B-Baskı, Elektroğirme



*to my unborn son*

## ACKNOWLEDGEMENTS

I would like to express my gratitude to my supervisor Prof. Dr. Cevdet Kaynak for his guidance, advice and support in this long period. This thesis would not be successful without his significant criticism and suggestions. I would also like to thank my thesis monitoring committee members Prof. Dr. Necati Özkan and Assist. Prof. Dr. Batur Ercan for their valuable contributions throughout the studies.

I would like to thank all the administrative board and technical staff of the METU Metallurgical and Materials Engineering Department for supplying all the research facilities required in this dissertation. I would like to acknowledge METU Central Laboratory for procuring the GPC analyses.

I am also grateful to Assist. Prof. Dr. Salih Ertan from Atılım University for providing some of the POSS particles, and to Assist. Prof. Dr. Gamze Karanfil from Karamanoğlu Mehmetbey University for the discussion during electrospinning studies.

I also thank to my laboratory mates Burcu Sarı, Ulaş Can, and Deniz Varsavaş for their brilliant ideas, friendship and unlimited support; and to Süer Kürklü Kocaoğlu, Serap Yağmur, Çiğdem Güngör, Seda Kül for their endless friendship and backing.

I would also like to express my gratitude to my parents Yasemin Meyva and Doğan Meyva, my lovely sister Nesil Meyva. They were with me in all my hard times in this long process and believed that I could succeed despite all difficulties. Special thanks go to, my soulmate Dr. Özer Zeybek and my little miracle for giving a completely different meaning to my life.

## TABLE OF CONTENTS

<b>ABSTRACT</b> .....	vii
<b>ÖZ</b> .....	ix
<b>ACKNOWLEDGEMENTS</b> .....	xii
<b>TABLE OF CONTENTS</b> .....	xiii
<b>LIST OF TABLES</b> .....	xvi
<b>LIST OF FIGURES</b> .....	xviii
<b>NOMENCLATURE</b> .....	xxii
<b>CHAPTERS</b>	
<b>1. INTRODUCTION</b> .....	1
1.1 Polylactides .....	1
1.2 Polylactide Matrix Composites .....	4
1.3 Polyhedral Oligomeric Silsesquioxane (POSS) .....	6
1.4 Polymer/POSS Nanocomposites .....	8
1.5 3D-Printing Techniques .....	11
1.6 Electrospinning Techniques .....	15
1.7 Taguchi Optimization Method .....	19
<b>2. LITERATURE SURVEY AND AIMS OF THE THESIS</b> .....	23
2.1 Literature Survey on the Effects of Filler Content, Functional Group and Copolymer Compatibilization on the Behavior of PLA/POSS Nanocomposites....	23
2.2 Literature Survey on the Behavior of 3D-Printed PLA Matrix Composites..	26
2.3 Literature Survey on the Electrospinning of Neat PLA and PLA/POSS Nanofibers.....	27
2.4 Purposes of the Dissertation .....	30

<b>3. EXPERIMENTAL WORK</b> .....	33
3.1 Experimental Procedures Used in the First Part of the Thesis.....	33
3.2 Experimental Procedures Used in the Second Part of the Thesis.....	36
3.3 Experimental Procedures Used in the Third Part of the Thesis .....	39
<b>4. RESULTS AND DISCUSSION</b> .....	43
4.1 Effects of Filler Content, Functional Group and Copolymer Compatibilization on the Behavior of PLA/POSS Nanocomposites.....	43
4.1.1 Effects of POSS Content .....	43
4.1.2 Effects of the Functional Groups on the POSS Structure .....	53
4.1.3 Effects of MA Compatibilization .....	67
4.2 Effects of 3D-Printing on the Behavior of PLA/POSS Nanocomposites Compared with Their Compression Molded Counterparts .....	80
4.2.1 Appearances of the 3D-Printed and Compression Molded Specimens .....	81
4.2.2 Mechanical Properties of the 3D-Printed and Compression Molded Specimens .....	84
4.2.3 Thermal Behavior of the 3D-Printed and Compression Molded Specimens .....	94
4.2.4 Behavior of the 3D-Printed Specimens in a Physiological Solution .....	97
4.3 Use of Taguchi Optimization for the Electrospinning Process Parameters of PLA and PLA/POSS Nanofibers .....	98
4.3.1 Preliminary Studies for the Approximate Process Parameters .....	98
4.3.2 Parameter Levels Selected for Taguchi Method.....	100
4.3.3 Results of the Nine Taguchi Experiments Applied for the Neat PLA.....	102
4.3.4 Confirmation Experiment for the PLA Nanofibers .....	108
4.3.5 Applicability of Taguchi Optimum Parameters for the PLA/POSS Nanofibers.....	111

<b>5. CONCLUSIONS</b> .....	115
<b>REFERENCES</b> .....	121
<b>CURRICULUM VITAE</b> .....	139

## LIST OF TABLES

### TABLES

<b>Table 4.1</b> Tensile strength ( $\sigma_{TS}$ ), flexural strength ( $\sigma_{Flex}$ ), tensile modulus ( $E$ ), flexural modulus ( $E_{Flex}$ ); % strain at break (% $\epsilon_f$ ) and fracture toughness ( $K_{IC}$ and $G_{IC}$ ) values of the specimens with different POSS contents.....	46
<b>Table 4.2</b> Transition temperatures ( $T_g$ , $T_c$ , $T_m$ ), enthalpies ( $\Delta H_m$ , $\Delta H_c$ ) and crystallinity percent ( $X_C$ ) of the specimens with different POSS contents during DSC first heating profile.....	51
<b>Table 4.3</b> Thermal degradation temperatures ( $T_{5\%}$ , $T_{10\%}$ , $T_{25\%}$ ) of the specimens with different POSS contents at 5, 10 and 25 wt% mass losses, the maximum mass loss temperature ( $T_{max}$ ) and %Residue at 550°C.....	51
<b>Table 4.4</b> Tensile strength ( $\sigma_{TS}$ ), flexural strength ( $\sigma_{Flex}$ ), tensile modulus ( $E$ ), flexural modulus ( $E_{Flex}$ ); % strain at break (% $\epsilon_f$ ) and fracture toughness ( $K_{IC}$ and $G_{IC}$ ) values of the specimens with 1 wt% POSS having different functional groups.....	61
<b>Table 4.5</b> Transition temperatures ( $T_g$ , $T_c$ , $T_m$ ), enthalpies ( $\Delta H_m$ , $\Delta H_c$ ) and crystallinity percent ( $X_C$ ) of the specimens with 1 wt% POSS having different functional groups, during DSC first heating profile.....	65
<b>Table 4.6</b> Thermal degradation temperatures ( $T_{5\%}$ , $T_{10\%}$ , $T_{25\%}$ ) of the specimens with 1 wt% POSS having different functional groups, at 5, 10 and 25 wt% mass losses, the maximum mass loss temperature ( $T_{max}$ ) and %Residue at 550°C.....	66
<b>Table 4.7</b> Tensile strength ( $\sigma_{TS}$ ), flexural strength ( $\sigma_{Flex}$ ), tensile modulus ( $E$ ), flexural modulus ( $E_{Flex}$ ); % strain at break (% $\epsilon_f$ ) and fracture toughness ( $K_{IC}$ and $G_{IC}$ ) values of the specimens before and after MA compatibilization.....	73
<b>Table 4.8</b> Transition temperatures ( $T_g$ , $T_c$ , $T_m$ ), enthalpies ( $\Delta H_m$ , $\Delta H_c$ ) and crystallinity percent (% $X_C$ ) of the specimens, before and after MA compatibilization, during DSC first heating profile.....	78

<b>Table 4.9</b> Thermal degradation temperatures ( $T_{5\%}$ , $T_{10\%}$ , $T_{25\%}$ ) of the specimens, before and after MA compatibilization, at 5, 10 and 25 wt% mass losses, the maximum mass loss temperature ( $T_{max}$ ) and %Residue at 550°C.....	78
<b>Table 4.10</b> Tensile strength ( $\sigma_{TS}$ ), flexural strength ( $\sigma_{Flex}$ ), tensile modulus ( $E$ ), flexural modulus ( $E_{Flex}$ ), and fracture toughness ( $K_{IC}$ and $G_{IC}$ ) of the 3D-printed and compression molded specimens.....	85
<b>Table 4.11</b> Transition temperatures ( $T_g$ , $T_c$ , $T_m$ ), enthalpies ( $\Delta H_m$ , $\Delta H_c$ ) and crystallinity percent ( $X_C$ ) of the 3D-printed and compression molded specimens during DSC first heating.....	95
<b>Table 4.12</b> Thermal degradation temperatures ( $T_{5\%}$ , $T_{10\%}$ , $T_{25\%}$ ) of the 3D-printed and compression molded specimens at 5, 10 and 25 wt% mass losses, the maximum mass loss temperature ( $T_{max}$ ).....	96
<b>Table 4.13</b> Parameters and levels used in the Taguchi method.....	102
<b>Table 4.14</b> Orthogonal array L <sub>9</sub> ( $3^4$ ) used in the Taguchi method.....	102
<b>Table 4.15</b> Results of nine Taguchi experiments in terms of average fiber diameter and S/N Ratios.....	105
<b>Table 4.16</b> S/N ratio response table including delta and rank data.....	106
<b>Table 4.17</b> Results of the analysis of variance (ANOVA) approach used after the Taguchi experiments.....	108

## LIST OF FIGURES

### FIGURES

<b>Figure 1.1</b> Enantiomers of the lactic acid structure.....	2
<b>Figure 1.2</b> Synthesis routes of PLA from L- and D-lactic acid.....	3
<b>Figure 1.3</b> Chemical structures of non-caged (a,b,c) and caged silsesquioxanes (d,e,f).....	7
<b>Figure 1.4</b> Examples of Polymer/POSS nanocomposites including typical applications.....	9
<b>Figure 1.5</b> Different Polymer/POSS nanocomposite architectures.....	9
<b>Figure 1.6</b> Eight steps of the stereolithography type 3D-printing technique.....	12
<b>Figure 1.7</b> Four principal methods of the 3D-printing techniques: (a) fused deposition modeling (b) inkjet printing (c) stereolithography (d) powder bed fusion.....	12
<b>Figure 1.8</b> Design schematics of the (a) downward, (b) upward and (c) horizontal electrospinning set-ups.....	16
<b>Figure 3.1</b> Chemical structure of PLA.....	33
<b>Figure 3.2</b> Chemical structure of the basic POSS nanoparticles used.....	34
<b>Figure 3.3</b> Front view of the 3D-printer used.....	38
<b>Figure 3.4</b> (a) Three basic components of a typical electrospinning set-up, and (b) General view of the electrospinning equipment used.....	40
<b>Figure 4.1</b> SEM fractographs showing effects of POSS content on the distribution and agglomeration level of particles in the PLA matrix.....	44
<b>Figure 4.2</b> Stress-Strain curves of the specimens with different POSS contents obtained during tensile and 3-point-bending flexural tests.....	47
<b>Figure 4.3</b> Effects of POSS content on the strength ( $\sigma_{TS}$ and $\sigma_{Flex}$ ) and modulus ( $E$ and $E_{Flex}$ ) values of the specimens.....	48
<b>Figure 4.4</b> Effects of POSS content on the ductility ( $\% \varepsilon_f$ ) and fracture toughness ( $K_{IC}$ and $G_{IC}$ ) values of the specimens.....	49



<b>Figure 4.5</b> First heating DSC thermograms of the specimens with different POSS contents.....	52
<b>Figure 4.6.</b> Thermogravimetric curves of the specimens with different POSS contents.....	52
<b>Figure 4.7</b> Functional groups of the four different POSS structures compared in the thesis.....	54
<b>Figure 4.8</b> ATR-FTIR spectra of the (a) four different POSS structures and (b) their PLA matrix nanocomposites including neat PLA .....	56
<b>Figure 4.9</b> SEM fractographs showing effects of POSS functional groups on the distribution and agglomeration level of the particles in PLA matrix, under magnifications of (a) 20000X and (b) 40000X.....	59
<b>Figure 4.10</b> Stress-Strain curves of the specimens, with 1 wt% POSS having different functional groups, obtained during tensile and 3-point bending flexural tests.....	62
<b>Figure 4.11</b> Effects of POSS functional groups on the strength ( $\sigma_{TS}$ and $\sigma_{Flex}$ ) and modulus ( $E$ and $E_{Flex}$ ) values of the specimens.....	63
<b>Figure 4.12</b> Effects of POSS functional groups on the ductility (% $\epsilon_f$ ) and fracture toughness ( $K_{IC}$ and $G_{IC}$ ) values of the specimens.....	64
<b>Figure 4.13</b> First heating DSC thermograms of the specimens with 1 wt% POSS having different functional groups.....	66
<b>Figure 4.14</b> Thermogravimetric curves of the specimens with 1 wt% POSS having different functional groups.....	67
<b>Figure 4.15</b> ATR-FTIR spectra of the PLA-g-MA (i.e. gMA) copolymer and all PLA matrix nanocomposites with MA compatibilization.....	70
<b>Figure 4.16</b> SEM fractographs showing effects of MA compatibilization on the interfacial morphology between PLA matrix and all POSS structures, under the magnifications of (a) 20000X and (b) 40000X.....	71
<b>Figure 4.17</b> Stress-Strain curves of the specimens, before and after MA compatibilization, obtained during tensile and 3-point bending flexural tests.....	74
<b>Figure 4.18</b> Effects of MA compatibilization on the strength ( $\sigma_{TS}$ and $\sigma_{Flex}$ ) and modulus ( $E$ and $E_{Flex}$ ) values of the specimens.....	75

<b>Figure 4.19</b> Effects of MA compatibilization on the ductility ( $\% \epsilon_f$ ) and fracture toughness ( $K_{IC}$ and $G_{IC}$ ) values of the specimens.....	76
<b>Figure 4.20</b> First heating DSC thermograms of the specimens before and after MA compatibilization.....	79
<b>Figure 4.21</b> Thermogravimetric curves of the specimens before and after MA compatibilization.....	80
<b>Figure 4.22</b> Images of the 3D-printed and compression molded specimens shaped for flexural and fracture toughness tests.....	82
<b>Figure 4.23</b> SEM fractographs of the 3D-printed and compression molded specimens.....	83
<b>Figure 4.24</b> Tensile stress-strain curves of the 3D-printed and compression molded specimens.....	84
<b>Figure 4.25</b> Flexural stress-strain curves of the 3D-printed and compression molded specimens.....	86
<b>Figure 4.26</b> Tensile strength and flexural strength of the 3D-printed and compression molded specimens. Note that %increases given on top of the PLA/POSS nanocomposite columns were determined compared to their neat PLA.....	89
<b>Figure 4.27</b> Tensile modulus and flexural modulus of the 3D-printed and compression molded specimens. Note that %increases given on top of the PLA/POSS nanocomposite columns were determined compared to their neat PLA.....	90
<b>Figure 4.28</b> Fracture toughness of the 3D-printed and compression molded specimens. Note that %increases given on top of the PLA/POSS nanocomposite columns were determined compared to their neat PLA.....	91
<b>Figure 4.29</b> %Benefits in the mechanical properties of the 3D-printed specimens compared to their compression molded counterparts.....	93
<b>Figure 4.30</b> First heating DSC thermograms of the 3D-printed and compression molded specimens.....	95
<b>Figure 4.31</b> Thermogravimetric curves of the 3D-printed and compression molded specimens.....	96

<b>Figure 4.32</b> SEM images showing effects of PLA solution concentration on the formation of droplets, beads and fibers determined during preliminary studies.....	101
<b>Figure 4.33</b> SEM images showing electrospun PLA fibers obtained after nine different Taguchi experiments.....	104
<b>Figure 4.34</b> Main effects plot for the S/N ratios.....	106
<b>Figure 4.35</b> SEM image and the frequency distribution of the electrospun PLA fiber diameters obtained from the confirmation experiment.....	110
<b>Figure 4.36</b> General and closer view SEM images of the PLA/POSS electrospun fibers having generally beaded morphology.....	112
<b>Figure 4.37</b> General and closer view SEM images of the PLA/POSS 1% nanofibers with bead-free uniform morphology after the addition of 3 wt% KCl salt into polymer solution.....	113

## NOMENCLATURE

$\sigma_{TS}$	:	tensile strength
$\sigma_{Flex}$	:	flexural strength
$\varepsilon_f$	:	elongation at break, final strain
$\Delta H_f$	:	heat of fusion of the specimens
$\Delta H_c$	:	heat of crystallization
$\Delta H_m^\circ$	:	melting enthalpy of 100% crystalline PLA
$E$	:	Young's modulus
$E'$	:	storage modulus
$E_{Flex}$	:	flexural modulus
$G_{Ic}$	:	fracture toughness as critical strain energy release rate
$K_{Ic}$	:	fracture toughness as critical stress intensity factor
<b>Adj MS</b>	:	adjusted mean squares
<b>Adj SS</b>	:	adjusted mean squares
<b>ANOVA</b>	:	analysis of variance
<b>ap-POSS</b>	:	aminopropylisobutyl-POSS
<b>ASTM</b>	:	American Society for Testing and Materials
<b>ATR-FTIR</b>	:	attenuated total reflectance fourier transform infrared spectroscopy
<b>CF</b>	:	chloroform
<b>DCP</b>	:	dicumyl peroxide
<b>DMF</b>	:	dimethyl formamide
<b>DOF</b>	:	degrees of freedom
<b>DSC</b>	:	differential scanning calorimetry
<b>ISO</b>	:	International Organization for Standardisation
<b>KCl</b>	:	potassium chloride
<b>MA</b>	:	maleic anhydride
<b>os-POSS</b>	:	octasilane-POSS
<b>PBS</b>	:	phosphate buffered saline

<b>pH</b>	:	potential for hydrogen
<b>PLA</b>	:	poly(lactic acid) or polylactide
<b>PLLA</b>	:	L-enantiomer of polylactide
<b>PDLA</b>	:	D-enantiomer of polylactide
<b>pd-POSS</b>	:	propanediolisobutyl-POSS
<b>PLA-g-MA</b>	:	maleic anhydride grafted polylactide
<b>POSS</b>	:	octaisobutyl-POSS
<b>SEM</b>	:	scanning electron microscopy
<b>S/N</b>	:	signal-to-noise ratio
<b>TGA</b>	:	thermogravimetric analysis
<b><math>T_{5wt\%}</math></b>	:	thermal degradation temperature at 5 wt% mass loss
<b><math>T_{10wt\%}</math></b>	:	thermal degradation temperature at 10 wt% mass loss
<b><math>T_{25wt\%}</math></b>	:	thermal degradation temperature at 25 wt% mass loss
<b><math>T_c</math></b>	:	cold crystallization temperature
<b><math>T_g</math></b>	:	glass transition temperature
<b><math>T_m</math></b>	:	melting temperature
<b><math>T_{max}, T_d</math></b>	:	thermal degradation temperature of maximum mass loss rate
<b><math>X_c</math></b>	:	degree of crystallinity



# CHAPTER 1

## INTRODUCTION

### 1.1 Polylactides

Due to the depletion of petroleum resources, the importance of bio-based polymers over petroleum-based polymers is increasing more and more both in industry and academia. Polylactide or poly(lactic) acid (PLA), which could be synthesized from renewable sources, such as corn starch, is today one of the most significant biopolymer having comparable mechanical, thermal, and chemical properties with traditional thermoplastics. Moreover, due to its biodegradability and biocompatibility characteristics, PLA attracts a lot of attention in the biomedical sector and tissue engineering.

In 1845, Pelouze first produced low molecular weight PLA by condensing L-lactic acid and continuously removing the water of the reaction output. But, this type of production has many disadvantages like high temperature requirement and by-products that need to be constantly removed. Thus, ring opening polymerization is preferred in the industry for the synthesis of PLA. In 2000s, Cargill started the continuous production of renewable lactic acid and produced PLA by direct ring opening polymerization. According to NatureWorks LLC, the production capacity of the PLA is about 140000 tones/year [1].

Lactic acid has two optically active enantiomer structures; L- and D- as shown in Figure 1.1. Crystallinity of PLA depends on the amount of the L- and D-lactic acid enantiomers. Therefore, mechanical, thermal and barrier properties of PLA are influenced by its optical purity. If PLA is composed of greater than ~90% L-enantiomers, then it tends to be crystalline, while lower amounts lead to amorphous

structure. Melting temperature ( $T_m$ ), glass transition temperature ( $T_g$ ) and crystallinity of PLA are reduced by decreasing the L-lactic acid amount; these temperatures for a semicrystalline PLA are typically 180°C and 60°C, respectively [2].

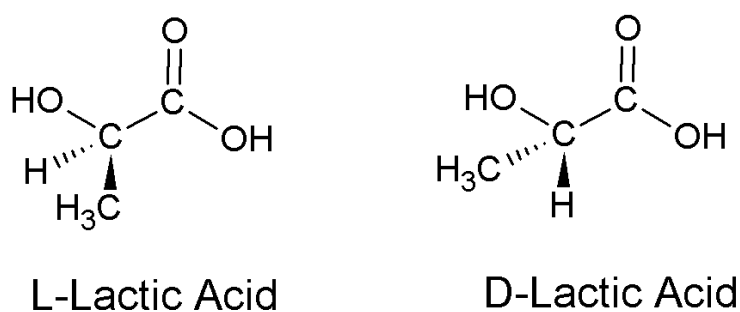


**Figure 1.1** Enantiomers of the lactic acid structure

Lactic acid, the building block of PLA, is obtained by chemical synthesis but mostly by fermentation. The economic production of high molecular weight PLA promotes its widespread use. There are three synthesis routes, such as direct condensation polymerization, polymerization via lactide formation, and azeotropic dehydration condensation as shown in Figure 1.2. Commercially available high molecular weight PLA polymer is produced by ring opening polymerization, while other methods produce only low molecular weight PLA [2].

Typically, PLA has a tensile strength of 50-70 MPa, Young's modulus of 2-3 GPa, elongation at break of 3-4%, and impact toughness of 2-3 kJ/m<sup>2</sup>. However, the level of molecular weight i.e. the processing parameters may influence the mechanical properties. For instance, high level of temperatures used during production or other processing techniques decrease the molecular weight of the polymer due to thermal degradation leading to lower mechanical properties [3]. Solvents used to dissolve polylactide during solution processes are important. For example, water, alcohols and linear hydrocarbons cannot dissolve PLA; dioxane, acetonitrile, chloroform,



methylene chloride, dichloroacetic acid dissolve PLA totally. It is partially soluble in tetrahydrofuran, ethyl benzene, acetone, toluene at their boiling temperatures [4].

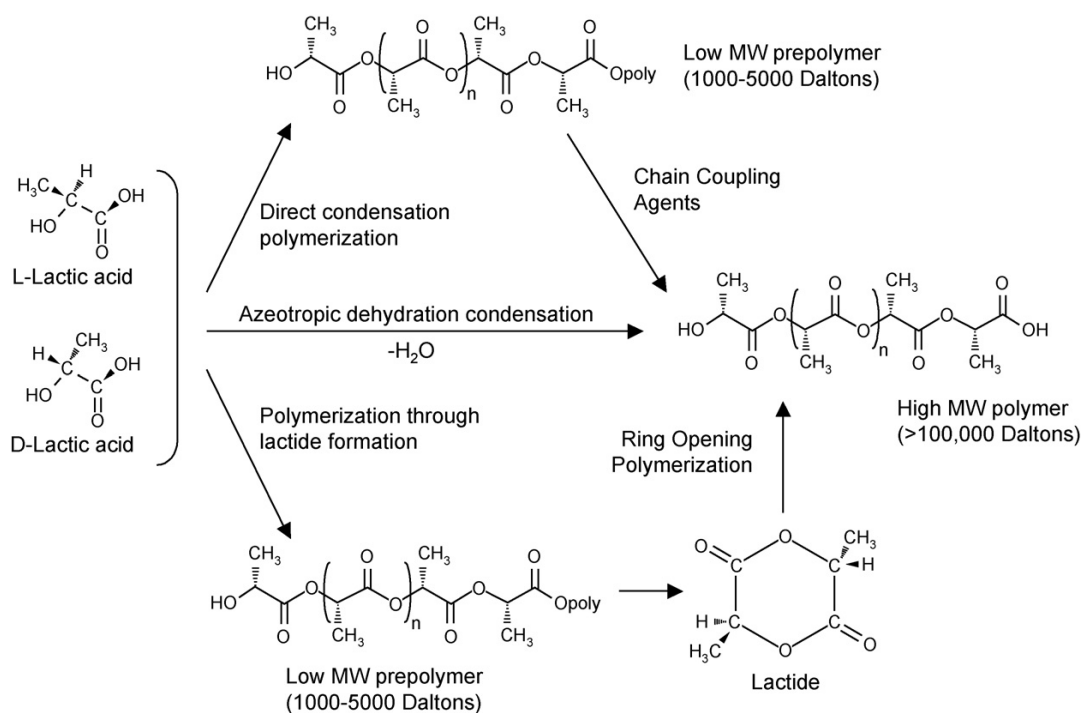


**Figure 1.2** Synthesis routes of PLA from L- and D-lactic acid [2]

Today, PLA has a wide range of use for domestic, engineering, and biomedical applications due to its biodegradability, biocompatibility, low toxicity, and relatively high mechanical performance.

Many home appliances, such as clothing, bottles, cups; and food service ware, food packaging, and also rigid consumer goods and films can be produced from environmentally friendly PLA. Thus, these items made of PLA do not harm the environment when they are garbage due to its biodegradable feature. Clothing made of PLA has low moisture and odor holding property than the conventional polyesters. They do not cause skin irritation and can be blended with various natural or man-

made fibers to obtain multiple other features. Food packages and drink bottles made from PLA instead of conventional polyethylene terephthalate (PET), polyethylene (PE), polystyrene (PS) and polypropylene (PP) would have sufficient clarity, stiffness and printability properties, additionally being compostable and renewable. Diapers, sanitary pads and wet wipes made of PET and PP fibers need tens of years to degrade after their disposal. Therefore, PLA fibers are also a significant alternative for nonwoven products [5].

In the automotive industry, PLA is becoming an environmentally friendly alternative replacing many automobile parts, such as car mats, cushion fabric, car bumper, spare tire cover made from PE, PP, ABS, etc. Moreover, PLA can replace polyvinyl chloride (PVC), frequently used in the production of building materials, such as laminated flooring; and electric wire insulation. While PLA does not contain any toxicity, PVC releases harmful gases during fire. Besides, PLA is very useful in the agricultural industry with its biodegradable feature without harming the soil. Thus, soil protection and fertilizer retention can be provided by using PLA mulch films [5].

Since PLA and its copolymer polylactide-co-glycolide (PLGA) are biocompatible and nontoxic, they are also preferred in various biomedical applications such as screws, scaffolds, artificial bonds, joints, surgical sutures including drug delivery applications [5].

## **1.2 Polylactide Matrix Composites**

Composites include at least two components, the first one being a continuous phase, in other words “the matrix”, and a discontinuous phase called “the reinforcement”. Matrix behaves as a binder and transfers the applied load to the reinforcements. Reinforcements can exist in fiber or particle form depending on their shape. Although reinforcements are generally used to increase the stiffness and strength of

the matrix, they are sometimes used as a filler to reduce the price of the product or change its physical, optical, rheological properties. The interface between both components is very significant to ensure proper transmission between the matrix and reinforcement [6].

Macro-, micro- or nanocomposites can be obtained depending on the size of the reinforcement used. For instance, if at least one dimension of the reinforcement is less than 100 nm then these composites are called as nanocomposites. Micro-scale particles or macro-scale natural and synthetic fibers can be used as reinforcements to obtain macro and micro-composites, respectively. Various natural fibers have been used as reinforcement materials in PLA matrix, such as sisal, flax, kenaf, and agricultural residues, like wheat straw and soy stalks. It was reported that the incorporation of especially sisal and flax natural fibers increase strength and modulus values of PLA matrix. However, their low thermal stability and moisture absorption were considered as disadvantages [6].

Mechanical properties of the natural fiber-reinforced PLA composites could be enhanced by using micro and nano-reinforcements. In this respect, use of cellulose microfibrils, cellulose nanofibrils and cellulose nanocrystals have been investigated. It was shown that they may also act as nucleating agents in the PLA matrix leading to increases in the crystallinity degree [6].

Just like for other polymer matrices, carbon-based reinforcements are another group of reinforcements used to obtain PLA matrix composites with high properties, such as stiffness, strength, thermal stability, electrical conductivity and chemical resistance. The most widely used macro reinforcement was carbon fibers, while carbon nanotubes and graphenes are the effective nano-reinforcements used in different areas, such as aerospace, civil and electrical engineering including military and sports applications. It is known that carbon nanotubes and graphenes with

surface modification might improve many properties of PLA matrix due to their very high surface-area-to-volume ratio [6].

Today, due to their nontoxic, biocompatible and hybrid (organic-inorganic) structures, Polyhedral Oligomeric Silsesquioxane (POSS) particles are becoming an important nano-reinforcement material for the PLA matrix composites especially for biomedical applications [6].

### **1.3 Polyhedral Oligomeric Silsesquioxane (POSS)**

Simple composition representing the chemical structure of the polyhedral oligomeric silsesquioxane is  $(\text{RSiO}_{1.5})_n$ . R includes different functional groups, such as hydrogen, alkyl, alkylene, epoxide, silane, alcohol. While the inorganic cage core provides rigidity to the structure, the organic functional groups ensure the compatibility with the polymer matrix. The molecular architecture of silsesquioxanes can be categorized into two main types as “caged structure” and “non-caged structure”. Non-caged silsesquioxane molecules contain partial cage, ladder and random structures as seen in Figure 1.3 (a,b,c). Cage structures are called as polyhedral oligosilsesquioxane or polyhedral oligomeric silsesquioxane (POSS). These highly symmetrical molecules with a diameter of 1-3 nm, together with functional groups in their corners, are considered one of the smallest silica particles.  $T_8$ ,  $T_{10}$ , and  $T_{12}$  POSS structures in the caged silsesquioxane class can be seen in Figure 1.3 (d,e,f). The most widely investigated structure is the POSS molecules with  $T_8$  inorganic core ( $\text{R}_8\text{Si}_8\text{O}_{12}$ ). POSS nanoparticles are odorless, non-volatile, non-toxic and environmentally friendly [7].

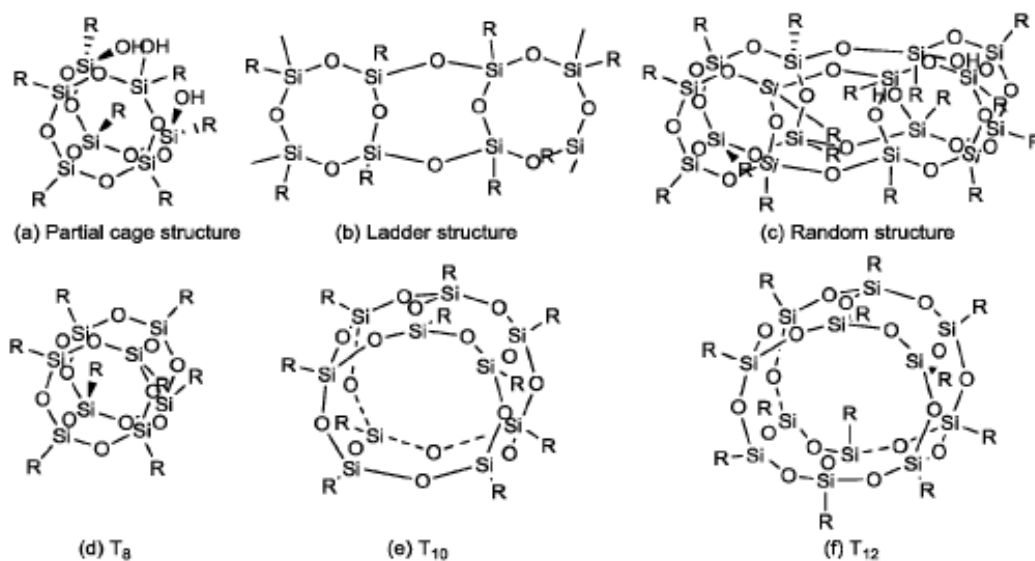


**Figure 1.3** Chemical structures of non-caged (a,b,c) and caged (d,e,f) silsesquioxanes [7]

POSS structures are also divided into three categories in terms of functional groups such as molecular POSS, monofunctional POSS and multifunctional POSS. When all the organic groups are non-reactive, such as methyl, isobutyl, phenyl, cyclohexyl; they are referred to as molecular silica. They can be used as nano-fillers due to their dispersion capability. If one of the organic groups is reactive such as methacrylate, acrylate, styrene, amine, epoxy, alcohol, phenol; these POSS structures are called as monofunctional POSS. These functional groups provide a chance to incorporate POSS into a polymer chain through polymerization or grafting. If more than one of the organic groups are reactive, they are known as multifunctional POSS. POSS molecules whose organic groups are all reactive are frequently encountered in the multifunctional POSS category [8].

## 1.4 Polymer/POSS Nanocomposites

Special features of POSS structures being rigid hybrid cage with an ability to be functionalized by different organic groups make them an important candidate in many structural engineering applications including electronic, optic, energy devices. Figure 1.4 shows examples of various Polymer/POSS nanocomposite systems including typical applications [7].

In biomedical applications, materials should be non-toxic with a significant degree of biocompatibility, which is defined as the ability to give the desired biological response in the natural environment. The silsesquioxane family is among the most studied nanofillers in the development of these nanocomposite materials. Due to their non-toxicity, biocompatibility and ability to be easily incorporated into different polymers, POSS nanoparticles have the potential to be used in a variety of applications such as dentistry, drug delivery, biomedical devices, and tissue engineering. Moreover, POSS structure consisting of Si-O and Si-C is also very similar to the structure of silicone used in the breast implants since the 1960s, being very inert with low inflammatory response [9].

POSS nanoparticles interact with the polymer matrix in three-dimensions like dendrimer structures. While non-reactive POSS particles are investigated as fillers capable of dispersing at the molecular level due to their small size, stronger applications are possible by covalent bonding to the polymer matrix [10]. POSS particles could be incorporated into polymer matrices with four different architectures as shown in Figure 1.5; (i) “POSS with nonreactive groups in a polymer network”; (ii) “monofunctional POSS as a tethering macromolecule to graft onto a polymer backbone”; (iii) “multifunctional POSS as a microinitiator to initiate polymerization from the surface of the POSS obtaining a star-shaped macromolecule”; and (iv) “POSS with multi-reactive groups as a microinitiator to produce a crosslinked polymer network”.

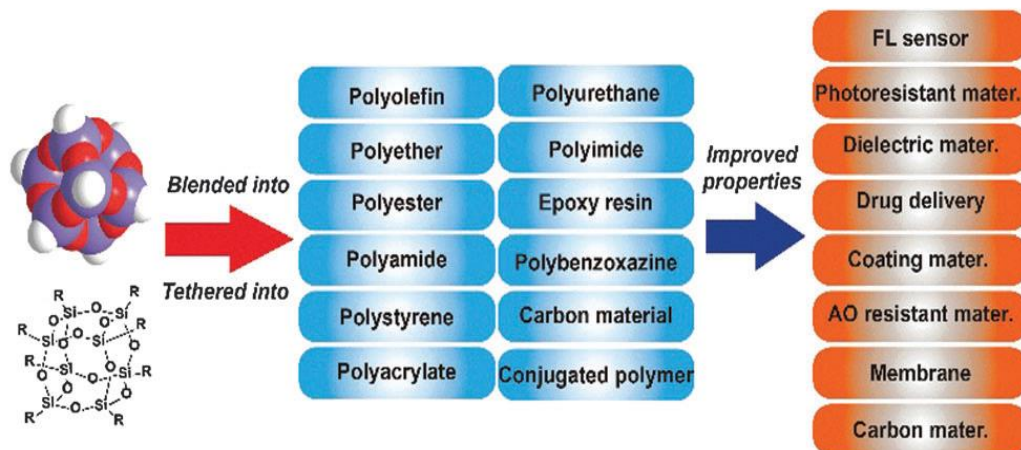


**Figure 1.4** Examples of Polymer/POSS nanocomposites including typical applications [7]

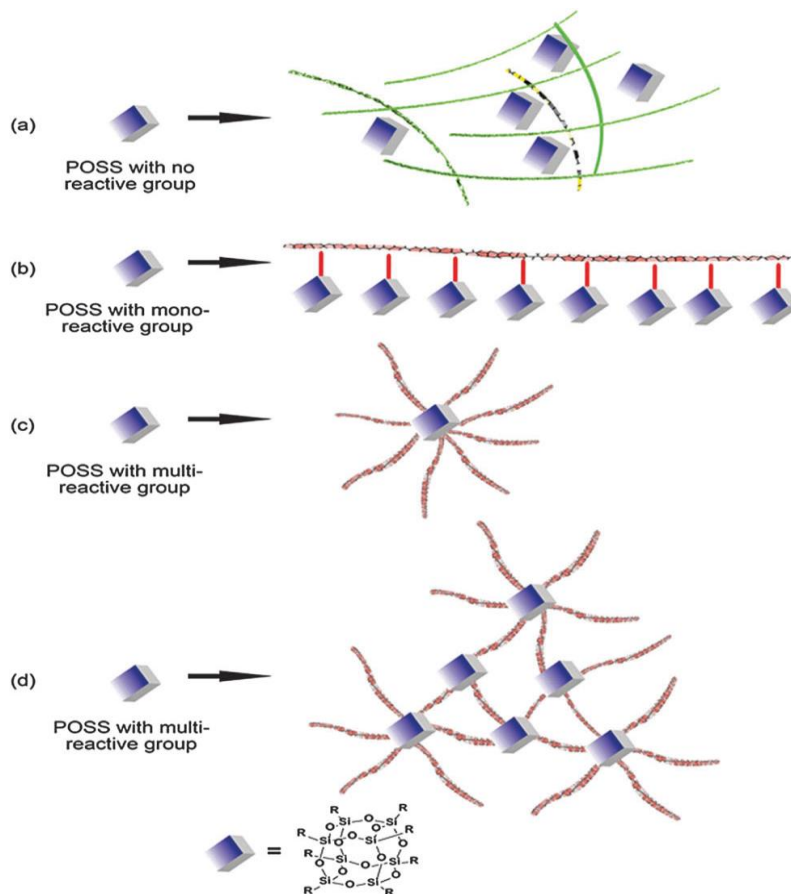


**Figure 1.5** Different Polymer/POSS nanocomposite architectures [7]

The main factor in determining the properties of the nanocomposites is the degree of dispersion and agglomeration of POSS particles in the polymer matrix; which is affected by thermodynamic interactions between them. If the interactions between the polymer matrix and the POSS particles are favorable or mutually unfavorable compared to the interaction between the POSS-POSS nanoparticles, then POSS particles are well dispersed; otherwise, they are aggregated [10].

Researchers generally use two approaches to form Polymer/POSS nanocomposite systems. In the first approach named as “In Situ Polymerization” technique, POSS particles are attached (i.e. chemically cross-linked) from their functional organic groups present on the cage corners to the compatible organic groups present in the macromolecule of the polymer matrix. Although this technique is rather difficult to control, the advantage would be very homogeneous presence of the POSS particles attached to macromolecular backbone of the matrix polymer leading to no phase separation or particle agglomeration.

The second approach is to mix POSS particles with the polymer matrix either in the molten state or solution state; thus named as “melt mixing” or “solution mixing”, sometimes also referred as physical blending. It is known that use of melt mixing has many advantages compared to in situ polymerization, such as simplicity, cost-effectiveness and versatility. In this technique, surface interactions between POSS nanoparticles and polymer matrix would influence the degree of the distribution of POSS nanoparticles. Therefore, various cage corner functional groups can be used to control the degree of POSS distribution in polymer matrices [8].



## 1.5 3D-Printing Techniques

Additive manufacturing (AM), in other words, 3D-printing is a technique that converts digital data into layer by layer production of any prototype. Charles Hull has invented the first model of this technology in 1986 under the name stereolithography (SLA) [11]. SLA-type additive manufacturing basically includes eight steps from product design to finalization: creation of computer-aided design (CAD) file, conversion of CAD file to STL (stereolithography file format), transfer of STL file to additive manufacturing machine, machine set-up, construction, removal, post-processing, and application as shown in Figure 1.6.

First of all, a software model has to be made which demonstrates the external geometry to produce parts with additive manufacturing. Because the machines accept an STL file that shows parts in sliced form, the CAD file type must be converted to the STL file type. Generated STL type files must be then transferred to the additive manufacturing machine. After that, the device has to be set up appropriately before the construction of the parts. Once the process has started, the device can continue with superficial monitoring; however, it must still be checked for reasons such as lack of material or production failure. When the process is completed, the printed part can be carefully removed. Then, printed parts may require additional cleaning or removing any residuals prior to they are ready for use [12].

Today, 3D-printing techniques have many different methods such as powder bed fusion, inkjet printing, stereolithography, direct energy deposition, laminated object deposition, and fused deposition modeling as shown in Figure 1.7.

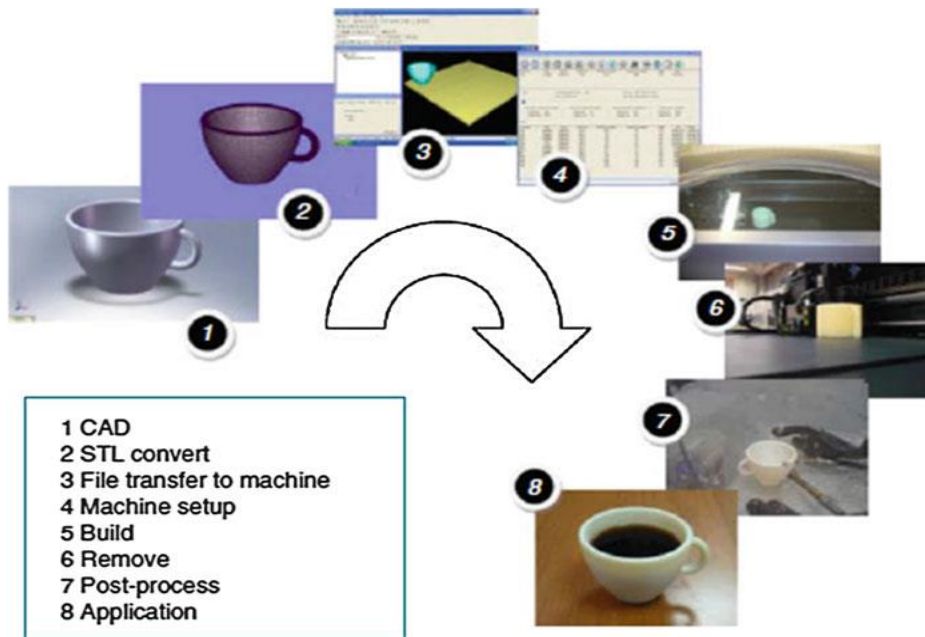


**Figure 1.6** Eight steps of the stereolithography type 3D-printing technique [12]

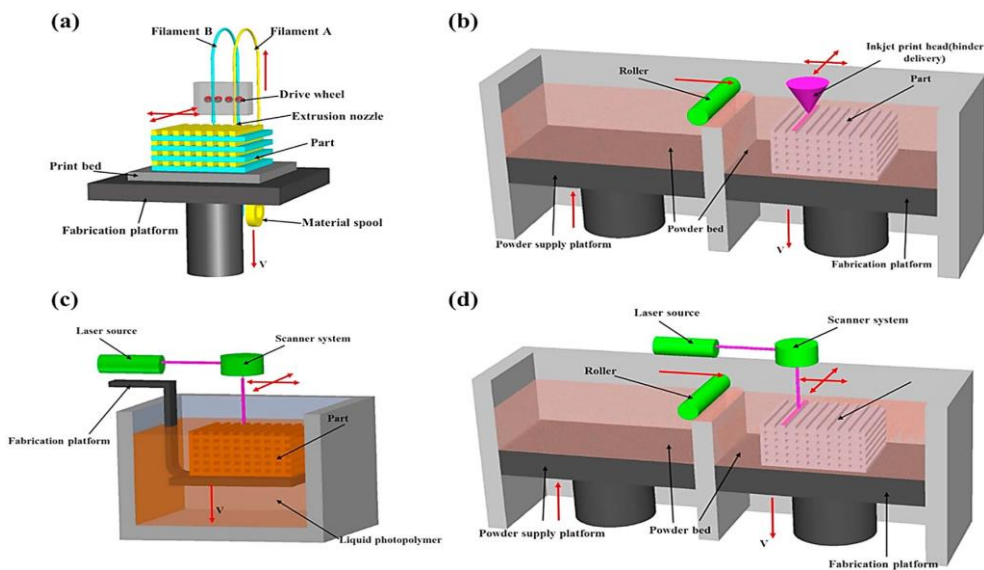


**Figure 1.7** Four principal methods of the 3D-printing techniques: (a) fused deposition modeling (b) inkjet printing (c) stereolithography (d) powder bed fusion

[11]

In the powder bed fusion process, very fine powders are spread in layers onto the build plate and formed firmly. The coalescence of the powders in the layers takes place through a laser beam with a binder. The method used in the additive manufacturing of ceramics is inkjet printing. It can be used for the printing of advanced ceramic structures in scaffolds used in tissue engineering applications. A ceramic solution is deposited on the built plate with the help of a nozzle. Another technique, stereolithography, is the first additive manufacturing method developed. Ultraviolet light is used to induce a chain reaction on the layer of a monomer solution. Acrylic or epoxy-based monomers constitute polymer chains when exposed to UV light. Besides, one of the first additive manufacturing methods in the market was laminated object manufacturing (LOM) based on sheet based cutting and sheet lamination. The successive layers are cut by means of a mechanical cutter or laser before they are connected to each other [11].

Recently, the most widely preferred method for polymer-based materials is the fused deposition modeling (FDM); in which continuous filaments made of thermoplastic polymers are used to obtain printed parts. The filament is first heated to the appropriate temperature to reach a fluid state in the nozzle, and then extruded onto the build plate. In this technique the polymer filaments easily should fuse with each other during printing and become solid at room temperature after printing.

The main factors affecting the mechanical properties of the printed parts are the layer thickness, width, the orientation of the filaments, and the air gap within or between the same layer. Furthermore, inter-layer distortion can be considered as the leading cause of poor mechanical properties. The reasons why FDM is preferred over other methods are low budget, high speed and ease of operation. On the other hand, drawbacks of the FDM method are lower mechanical properties, appearance of the interlayer, poorer surface quality and availability of limited number of thermoplastic filament materials.

In the stereolithography method, ultraviolet light activates photosensitive polymer resins for polymerization. According to Wohlers Associates, prototypes produced using photosensitive polymers cover about 50% of the 3D-printing market. The most widely used thermoplastic filament polymers in the FDM method are acrylonitrile butadiene styrene (ABS), polylactide (PLA) and polycarbonate (PC) [11].

In order to obtain higher mechanical properties various fiber reinforcements can be added into filament polymers. Nevertheless, fiber orientation and lower adhesion between the fiber and the matrix could be problematic in 3D printed fiber-reinforced composite parts [11].

Nowadays, application areas in the additive manufacturing of polymers and composites are biomedical, automotive, aerospace, architecture, and sports. The biomedical market today accounts for 11% of the total additive manufacturing market share and is a driving force for the growth of the additive manufacturing market. Biomedical applications have some essential requirements such as high level of complication, an arrangement to the specific needs of patients, and small manufacturing volumes. Additive manufacturing is capable of responding to these demands. Moreover, drug production and delivery systems are also intended to benefit from additive manufacturing by producing customized medicines. Implants having complex geometries can be produced reliably and inexpensively via additive manufacturing. Recently, bioprinting is a promising additive manufacturing method for tissue engineering. This method allows in-situ rehabilitation of organs and tissues. According to the report of Wohler's, 18% of the total additive manufacturing market includes aerospace industry, while only 3% in the architectural implementation [11].

## 1.6 Electrospinning Techniques

In the conventional polymer spinning techniques such as melt-spinning used in textile industry, fiber diameters are in the micron range. Today, in order to obtain polymer fiber forms with nano-range diameters, electrospinning techniques have been developed. The essential components of a typical electrospinning set-up are a syringe pump delivering polymer solution to the nozzle via polyethylene tubing, a high voltage supply that charges the polymer solution, and a grounded collector where nanofibers are deposited.

As shown in Figure 1.8, electrospinning set-ups can be constructed with a vertical or horizontal design. Vertical set-ups might be constructed in an upward or downward position which would influence the orientation of the electrospun fibers and the number of bead formation. For instance, compared to downward set-up, fibers deposited in the upward set-up would have more uniform pattern with lower number of bead formation. In these set-ups, apart from the stationary collector forms, there are other possibilities such as rotating drum collectors, parallel conducting collectors, rotating thin disk collectors, and two ring collectors [13].

Parameters influencing electrospinning techniques can be divided into three classes: polymer solution properties, process parameters and ambient conditions. Polymer solution parameters include solution concentration, viscosity, conductivity and solvent type; while tip-to-collector distance, applied voltage, feeding rate and needle diameter are the process parameters. The ambient conditions are basically humidity and temperature of the set-up environment.

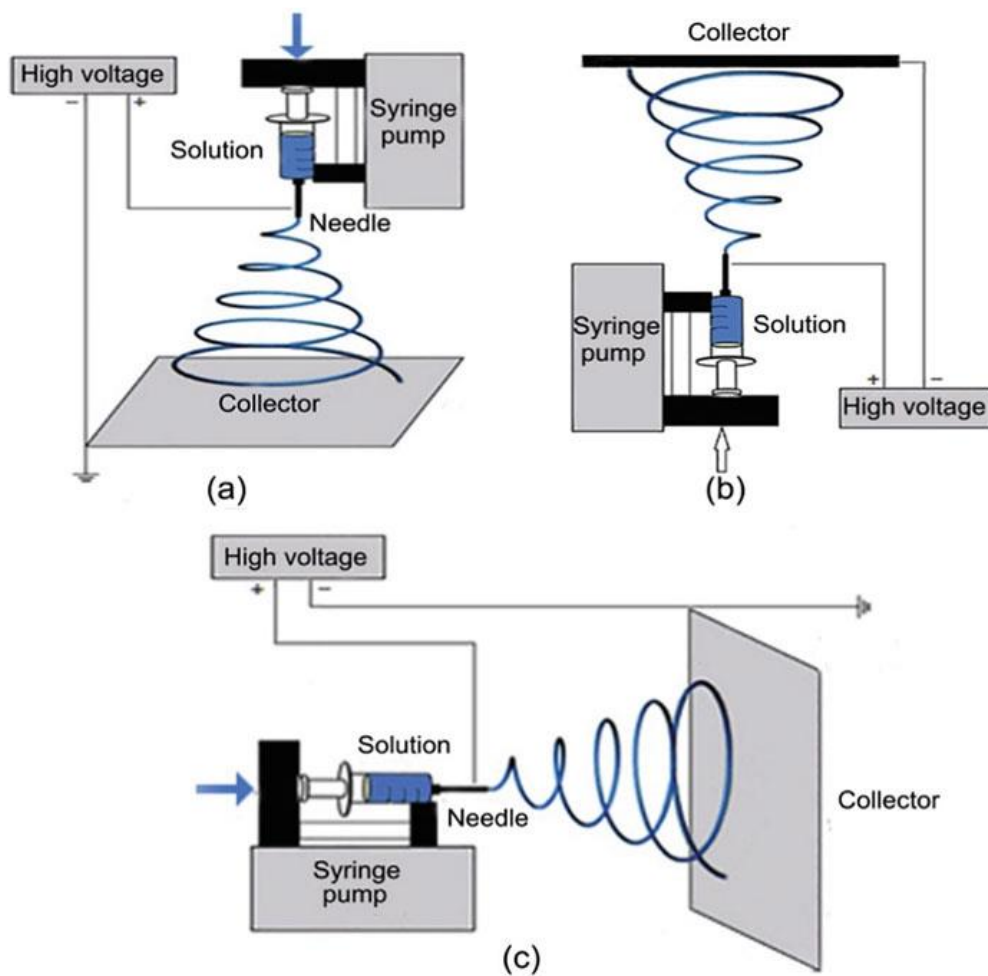


**Figure 1.8** Design schematics of the (a) downward, (b) upward and (c) horizontal electrospinning set-ups [13]

Concentration of the polymer solution is especially important for the structure of the charged polymer jet. For instance, when the concentration of the polymer solution is less than a determined critical value, then the entangled polymer chains in fragments would be deposited at the collector leading to formation of beads or beaded fibers. The degree of polymer chain entanglement would increase when the concentration was increased with sufficient viscosity, so that uniform and beadless nanofibers could be obtained. If the polymer solution concentration exceeds the determined

critical value too much, then clogging of the needles and formation of the defected nanofibers would occur [14].

Type of the solvent selected is also crucial to obtain smooth and bead-free nanofibers. First of all, it should dissolve the polymer used very well; and should have an intermediate boiling point. Because, the degree of volatility of the solvent is very important to have easy vaporization during the electrospinning of nanofibers from the needle tip to the collector. Solvents with low boiling points should be avoided as this may cause drying and clogging of the needle tip during the process. Solvents with high boiling points should be also avoided as they prevent ease of vaporization and drying of nanofibers leading to formation of beaded morphology [14].

Conductivity of the polymer solution is also important to have charges on the droplet surface and the formation of Taylor cone during electrospinning process. In a dielectric polymer solution, electrostatic forces generated by the applied electric field could be not enough for the charges to travel to the solution surface preventing the Taylor cone formation to start. On the other hand, it should be pointed out that very high conductivity of the solution might reduce the tangential electric field, thus adversely affect formation of the Taylor cone. Diameter of the electrospun fibers are influenced by the length of the straight and whipping region of the polymer jet. When the whipping region is stretched with surface charges, then the diameter of the electrospun fibers would decrease. Therefore, sufficient degree of conductivity in the polymer solution can be achieved by adding certain salts to have smooth, bead-free electrospun nanofibers [14].

Another factor affecting the diameter and morphology of the electrospun fibers is the tip-to-collector distance. Because, it influences deposition time, vaporization rate and jet type. It is indicated that diameter of electrospun fibers decreases with increasing this distance, while defective and larger diameter fibers were obtained when this

distance was decreased [14]. Thus, it is important to determine an optimum tip-to-collector distance.

The optimum value for the applied voltage during electrospinning would be different depending on the polymer type used. When the applied voltage increases, the polymer solution would be stretched in relation to the charge repulsion in the polymer jet, leading to lower diameters. If the applied voltage exceeds the determined optimum value, then electrospun fibers will have a beaded morphology [14].

Polymer solution feeding-rate is also a critical parameter to get uniform and bead-free electrospun fibers. Use of high feeding rates above the determined optimum value may result in higher diameters and bead formation. Because, the polymer jet would not have sufficient time to dry completely from the needle tip to the collector [14].

Electrospun nanofibers have a wide range of applications in biomedical sector, environmental protection, electronics, sensors and protective clothing textiles. Biomedical applications include production of fibrous scaffolds for tissue engineering, wound dressing and drug delivery mechanisms. Electrospun nanofibers are considered to be promising scaffold materials because of their unique features such as their morphology, porous structures, high surface area to volume ratio. In terms of environmental protection; porous nanofilters and microfilters can be produced to remove targeted contaminants. Protective clothes have to be lightweight and breathable, and they should have high resistance to chemicals or biological threats. Electrospun fibers with high porosity and small size pores meet these requirements.

For tissue regeneration, biocompatible and biodegradable fibrous scaffolds are usually used instead of conventional scaffolds due to their unique properties and



ability to mimic the extracellular matrix. Chitosan, collagen and starch can be used as natural electrospun polymer fibers due to their perfect biocompatibility and biodegradability. Synthetic polymers such as PLGA are also used for the regeneration of cartilage, dermal tissue and bones due to their adjustable and biodegradable nature with ease of processing. Electrospun nanofibers can also be used to deliver anticancer agents, antibiotics and proteins to the targeted site. Drug delivery can be provided by introducing the drug into the nanofibers, or by coating the drug on the surface of the nanofibers. The wound dressing is essential for protecting the wound area, removing efflux and preventing the growth of microorganisms. Electrospun nanofibers might excite response of the cells with their high surface area, pores on their surfaces and pores in between them [14].

## **1.7 Taguchi Optimization Method**

In those manufacturing techniques having so many different process parameters, such as electrospinning, it is very crucial to determine the optimum process parameters for the effective use of time and money. Although there are other methods cited in the literature [15] such as Simplex Optimization and Response Surface Methodology; Taguchi optimization technique is the most suitable method that can be used to determine optimum electrospinning parameters. In this method, Dr. Genichi Taguchi aims to produce high-quality products at low cost and labor. Because, after World War II, Japan has low-quality raw materials, improper labor and tools in poor condition. Hence, that optimization technique is used for highly effective design, progress and production [16].

Noise factors are uncontrollable factors such as external or manufacturing imperfection. External factors are related to environment, equipment or human error,

such as temperature, humidity, dust, and vibrations. Manufacturing imperfection results in uneven properties in each unit of the sample which is inevitable in every production [17].

The Signal-to-Noise (S/N) ratio is an indication of robustness, and its higher value means, there would be less damage during variations in the system. The origin of the S/N ratio comes from the communications sector. This ratio is important to the elasticity and repeatability of technology improvement. Nowadays, S/N ratio is used in all technology fields. Maximizing the S/N ratio by regulating the system parameters is also called as parameter design in quality engineering. S/N ratios can be defined in three ways as “smaller is better”, “larger is better” and “nominal is best” [16], that can be calculated by the following equations:

$$\text{“Smaller is better”}: \quad S/N = -10 \log \frac{1}{n} \sum_{i=1}^n y_i^2 \quad (1.1)$$

$$\text{“Larger is better”}: \quad S/N = -10 \log \frac{1}{n} \sum_{i=1}^n \frac{1}{y_i^2} \quad (1.2)$$

$$\text{“Nominal is best”}: \quad S/N = 10 \log \frac{\bar{y}^2}{s^2} \quad (1.3)$$

where “y” is the measurement result, “n” is the experiment repeat number, and “s<sup>2</sup>” is the variance [18, 19].

The orthogonal array is prepared for data analysis and prediction of optimal results, ensuring well-balanced and minimal experimentation. The number of experimental combinations can be significantly reduced by using the orthogonal array. Using the orthogonal array experimental design proposed by Dr. Taguchi, the influence of many different parameters on the performance characteristics of a process can be

investigated. The parameters affecting the process should be decided, and then the variable levels of these parameters should be determined [20].

There are eight steps to apply the Taguchi methodology in any manufacturing process [20]:

- Determine the fundamental function, side reactions and breakdown mode
- Determine the quality characteristics, test conditions and noise factors
- Determine the target function to be optimized
- Determine the control factors and their levels for the manufacture
- Choose the orthogonal array matrix for experimental combinations
- Perform the experiment matrix
- Analyze the experimental data, estimate the optimum levels and the performance

These steps can be followed by “*Analysis of Variance (ANOVA)*” test which was developed by Fisher in the 1930s in order to indicate the difference between performance factors and experimental data comments in Taguchi experiments. Additionally, this test could be used to determine efficiency of the controlled parameters.

The degrees of freedom (*DOF*), the adjusted sum of squares (*Adj SS*), the adjusted mean square (*Adj MS*), the F test (*F*), and the percentage contribution (*PC*) can be calculated for each controlled parameter. In this analysis, *DOF* for each parameter is the number of levels minus one. *Adj SS* for each parameter is the square of deviation from the grand mean, while *Adj MS* is determined by dividing the *Adj SS* with the respective *DOF* value [21] as given in the following equations;

$$Adj SS_p = \left( \sum_{i=1}^m \frac{P_i^2}{n_{pi}} \right) - \frac{T^2}{N} \quad (1.4)$$

$$Adj SS_{Total} = \sum_{i=1}^m y_i^2 - \frac{T^2}{N} \quad (1.5)$$

$$DOF_p = m - 1 \quad (1.6)$$

$$Adj MS_p = \frac{Adj SS_p}{DOF_p} \quad (1.7)$$

$$Contribution (\%) = \frac{Adj SS_p}{Adj SS_T} \quad (1.8)$$

where  $m$  is number of the level of the any parameter,  $P$  represents any parameter,  $n_{pi}$  is the number of the experimental results on the level  $i$  for any parameter,  $T$  is the sum of all experimental results, and  $N$  refers sum of the all levels [18].

## **CHAPTER 2**

### **LITERATURE SURVEY AND AIMS OF THE THESIS**

#### **2.1 Literature Survey on the Effects of Filler Content, Functional Group and Copolymer Compatibilization on the Behavior of PLA/POSS Nanocomposites**

Poly(lactide) (PLA) is today a well-known biopolymer having aliphatic thermoplastic polyester structure polymerized from renewable sources especially from corn starch. In the last decade it has been particularly used for biomedical, agricultural and food packaging applications due to its inherent biodegradable and compostable nature. Today, PLA has been considered for many other engineering applications; in which its mechanical and thermal properties should be improved. In this respect, there is tremendous number of works especially using micro or nanocomposite approach; for example reinforcing PLA structure with montmorillonite [22-24] and halloysite [25-27] nanoclays, carbon nanotubes [28-30] and graphene [28, 29, 31-33], nanosilica [24, 34-36] and nanotitania [37-40] particles.

From this point of view, Polyhedral Oligomeric Silsesquioxane (POSS) particles could be also considered as an important candidate with their inorganic-organic nanosized cage structures. When incorporated into polymer matrices, the inorganic core of the cage may provide molecular reinforcement while the organic groups may increase compatibility with the polymer matrices. Depending on the application area, the chemistry of POSS can be changed by altering the organic groups attached to the cage corners. In order to prepare polymer nanocomposites, POSS particles can be

mixed with the matrix directly, or attached to the macromolecules during polymerization.

Literature survey revealed that PLA/POSS nanocomposites have been produced by different techniques for certain purposes. For instance, some studies [41-44], especially investigated effects of POSS content on the certain properties of PLA matrix nanocomposites as follows:

Pan and Qiu [41] prepared PLA/POSS nanocomposites with 1, 5, 10 wt% basic POSS particles (having only isobutyl groups) via solution mixing method. SEM analysis indicated that POSS particles were dispersed in the matrix forming sub-micrometer aggregates of 100-200 nm. They indicated that crystallization amount of the PLA matrix increased with increasing POSS loading; and use of 1 wt% POSS increased the storage modulus ( $E'$ ) value of the neat PLA at 20°C by 35%; the increase was slight with further increasing POSS loading from 1 to 10 wt%.

Turan *et al.* [42] produced PLA nanocomposites with POSS contents of 1, 3, 10 wt% via melt mixing. One of the corner of their POSS was functionalized by aminopropyl, other corners having only isobutyl. Their SEM analyses revealed that compared to 10 wt%; use of 1 and 3 wt% POSS particles had more uniform distribution leading to certain level of improvements in the properties of especially elastic modulus, percent strain at break and matrix crystallinity degree. On the other hand, no improvements were observed in the yield and tensile strength values.

Guo and Wang [43] investigated effects of POSS content (0.5, 1, and 3 % mass fractions) especially on the crystallization kinetics of the PLA matrix. Before production of the nanocomposites by melt mixing, they functionalized all corners of the POSS cage by attaching epoxy vinyl groups. Their DSC analyses and POM examinations revealed that POSS particles acted as nucleation agents for the

formation of PLA spherulites. Determination of the kinetic parameters also revealed that especially use of 3% POSS increased the crystallization rate of PLA matrix.

Liu *et al.* [44] prepared PLA nanocomposite films with incorporation of 2, 4, 6 and 8 wt% POSS content via solution mixing and casting method. Before that, they attached PLA oligomers to the eight corners of the POSS cage structure. They revealed that use of 2 and 4% POSS particles resulted in improved mechanical properties, beyond these contents the properties declined. For instance, when POSS content increased from 0 to 4 wt%, the Young's modulus increased from 1.10 to 1.56 GPa, the tensile strength increased from 33.7 to 41.8 MPa, elongation at break enhanced from 9% to 56%, and the fracture energy increased from 206 to 2360 MJ/m<sup>2</sup>.

Another group of studies in the literature [45-50] investigated effects of having different functional groups at the corners of the POSS cage on certain properties of neat or blended PLA matrix nanocomposites as follows:

Fernandez *et al.* [45] prepared PLA/POSS nanocomposites by using three different POSS molecules; two amino-POSS derivatives with different nonreactive organic substituents attached to the corner silicon atoms (aminopropylheptaisobutyl-POSS, APIBPOSS, and aminopropylheptaisooctyl-POSS, APIOPOSS) and a PLA-g-POSS organic-inorganic hybrid (PIOPOSS-PLA).

In the studies of Kodal *et al.* [46, 47], the matrix was highly plasticized PLA with poly(ethylene glycol) (PEG). They compared use of three reactive POSS structures as aminopropylisobutyl-POSS (A-POSS), trisilanolisobutyl-POSS (T-POSS), glycidylisobutyl-POSS (G-POSS) and one nonreactive basic structure as octaisobutyl-POSS (O-POSS).

In the study of R. Wang *et al.* [48] the matrix was 70:30 blend of PLA with poly(butylene succinate-co-adipate) (PBSA). Their functional POSS structures were octavinyl POSS (vPOSS) and epoxyhexyl POSS (ePOSS). In the study of B. Wang *et al.* [49] the matrix was a copolymer of PLA with rigid segments of poly(butylene terephthalate) (PBT). Their functional POSS structures were POSS-NH<sub>2</sub> and POSS-PEG.

Gardella *et al.* [50] compared two different POSS molecules as trans-cyclohexanediolisobutyl POSS (POSS-OH) and aminopropyl heptaisobutyl POSS (POSS-NH<sub>2</sub>). Moreover, they also used 5 g of maleic anhydride-grafted polylactic acid (PLA-g-MA) copolymer in the production of PLA matrix nanocomposites.

Due to the different chemical interactions between the functional groups of POSS structures and PLA based matrices, they [45-50] generally revealed that there were certain differences in the mechanical properties (elastic modulus, yield strength, tensile strength, toughness, ductility, etc.); thermal behavior (transition temperatures, enthalpies, crystallinity amounts, etc.) and morphology of the nanocomposites.

## **2.2 Literature Survey on the Behavior of 3D-Printed PLA Matrix Composites**

Just like other conventional thermoplastic based materials, products made from PLA and its micro and nanocomposites are normally shaped by traditional molding processes such as injection and compression molding. On the other hand, these conventional molding techniques require very high initial cost for tooling and machinery, so that they would be only feasible for the very high rates of mass production. In this respect, especially for the small batch size productions, “additive manufacturing techniques” are becoming significant alternatives against traditional molding techniques. For instance, “Fused Deposition Modeling” (FDM) type 3D-printing technologies are today important candidates for not only small batch size



production of engineering components, but also for many biomedical parts such as scaffolds, artificial organs, vascular stents, etc. [51].

Consequently, the number of academic studies on the use of FDM type 3D-printing of PLA based composites are just started to rise. Examples of these studies cited in the literature are; PLA matrix composites reinforced with carbon fibers (CF) [51-54], glass fibers (GF) [55-57], titania (TiO<sub>2</sub>) microparticles [58], carbon nanotubes (CNT) [59-61], graphene (Gr) [62-65], and hydroxyapatite (HA) nanoparticles [66]. These studies especially investigated effects of the “filler content” and “3D-printing process parameters”, such as layer thickness, infill percentage, infill pattern, etc., on the various properties of 3D-printed specimens.

Of course it is very important for the 3D-printed parts to have the same level of mechanical and other properties compared to their traditionally molded counterparts. From this point of view, it would be crucial to compare properties of the PLA based materials shaped by 3D-printing and conventional molding processes. In the literature, there are limited number of studies comparing the properties of 3D-printed neat PLA [67-72] and PLA-based composites [57, 73, 74] with their injection molded counterparts. These studies generally indicated that depending on the type of the properties, there could be certain level of differences.

### **2.3 Literature Survey on the Electrospinning of Neat PLA and PLA/POSS Nanofibers**

When polymer based materials are produced in the form of “nanofiber” structure, they might have unique properties such as high surface area, high porosity, superior mechanical, chemical and electrical properties leading to a wide range of applications. Although there are other techniques to form polymer based nanofibers,

such as drawing, self-assembly, phase separation, template synthesis, etc. “electrospinning” method has been accepted as the most practical technique [75].

Electrospinning set-ups generally composed of three components: (i) a high voltage power supply to charge the polymer solution, (ii) a syringe to pump the solution to the needle, and (iii) a grounded collector to deposit nanofibers [75]. The droplet of the charged polymer solution, pumped to the tip of the needle, would be under two opposite forces: (i) electrostatic repulsion and (ii) surface tension. When the repulsive charges start to exceed the surface tension, the droplet transforms to a conical form, known as “Taylor cone”. These two forces stretch the polymer solution jet stream to have a kind of “whipping” motion resulting in also evaporation of the solvent. Then, the polymer jet stream solidifies in the form of continuous nanofibers to be deposited on the stationary grounded collector [75].

Of course, in order to obtain smooth and uniform nanofiber structures, determination of the optimum electrospinning parameters for each polymer solution would be extremely critical. In their comprehensive review, Haider et al. [14] pointed out that electrospinning parameters can be categorized into three groups: (i) solution parameters (solvent, polymer concentration, viscosity and solution conductivity), (ii) electrospinning set-up parameters (applied voltage, distance between the needle and collector and flow rate), and (iii) environmental parameters (humidity and temperature).

Literature survey indicated that there are certain number of studies on the electrospinning of neat PLA [76-85] and PLA/POSS [86-90] nanofibers. These works especially investigated mechanical, thermal, chemical and other properties of the electrospun nanofibers; some of them also investigated effects of only one or two process parameters on the structure of these nanofibers. Because, consideration of the so many different process parameters listed above would be extremely difficult and

time consuming. That is, use of a certain statistical optimization technique in the design of experiments would be necessary.

In this manner, the Taguchi method for robust design of experiment appears to be a useful approach to determine the optimum levels of processing parameters with minimum sensitivity against different causes of variations. In this method generally two basic tools are necessary: (i) an Orthogonal Array (OA) to accommodate several experimental design factors and (ii) Signal to Noise (S/N) ratio to measure the most robust set of operating conditions from variations within the results [91].

Moreover, Analysis of Variance (ANOVA) could be also used to conclude the statistical significance of the electrospinning parameters. Thus, use of S/N ratios and ANOVA determine the optimum electrospinning parameters. Finally, the Confirmation Experiment can be performed to validate the Taguchi optimization method [92].

In the literature, although the Taguchi technique has been used to optimize electrospinning parameters of various polymer nanofibers [21, 91-100]; the number of the studies for the PLA based materials are extremely limited. There are only two studies for the neat PLA and one study for the halloysite nanotube (HNT) filled PLA, as summarized below.

In the first work, Patra *et al.* [101] investigated selection of optimum process parameters for the electrospinning of PLA nonwoven mats (for membrane applications) via Taguchi method. Their aim was to obtain a robust set of parameters that would minimize the variation in product quality (i.e. fiber diameter and bead area) with minimum number of experiments. They pointed out that low concentration of polymer solution, low feeding rate, high applied voltage, and longer distance between the needle and the collector would be a desirable combination of process

parameters. They also indicated that S/N ratio and ANOVA approaches have converged on the same type of parameter selection.

In the second work, Su *et al.* [102] used the Taguchi method (both S/N ratio and ANOVA) to design the optimal electrospinning parameters of PLA continuous nanofibrous yarns. The parameters investigated were the concentration of the solution, nozzle size, flow rate, and take-up velocity of the rotating collector. After considering the quality characteristics of fiber diameter, fiber uniformity, and fiber arrangement, they concluded that the experimental results obtained by the method were more accurate and objective than one-factor-at-a-time experiments.

In the third work, Dong *et al.* [103] used Taguchi method, both S/N ratio and ANOVA approaches, to determine optimum electrospinning process parameters of PLA filled with 1.5, 5, 10 wt% halloysite nanotube (HNT) particles. They investigated effects of applied voltage, feed rate of solution, collector distance and HNT concentration both on the fiber diameter, and also on the level of distribution of HNTs and their nucleation effects in the PLA matrix. It was revealed that electrospinning process do not facilitate the distribution of HNT particles in the PLA matrix, but it was observed that HNTs could act as nucleation agents increasing the cold crystallization level of PLA matrix. They also concluded that the reduction in the composite fiber diameter could be achieved by controlling the parameters of feed rate, collector distance, and applied voltage.

## **2.4 Purposes of the Dissertation**

- (i) Literature survey summarized in section 2.1 above indicated that there were very limited number of publications on the effects of POSS content, POSS functional groups and maleic anhydride compatibilization on the performance of PLA matrix nanocomposites. Therefore, the main purpose of the first part of

this thesis was, as the first time in the literature, to investigate PLA/POSS nanocomposites by emphasizing the effects of these three parameters (filler content, functional groups, MA compatibilization). For this purpose, mechanical and thermal properties of the PLA matrix nanocomposites were compared first by reinforcing with 1, 3, 5, 7 wt% basic POSS structure having only isobutyl groups, and then POSS structure having three different functional groups (aminopropyl, propanediol, dimethylsilane), and finally using PLA-g-MA copolymer for each specimen groups.

- (ii) Literature survey summarized in Section 2.2 above revealed that there is no published work studying the 3D-printing of PLA filled with POSS nanoparticles. Therefore, the main purpose of the second part of this thesis was, first to investigate 3D-printability of PLA/POSS nanocomposites, and then to evaluate their mechanical and thermal properties by comparing with the compression molded PLA/POSS specimens. Since PLA/POSS nanocomposites would be a significant alternative for biomedical parts, it would be important to follow their especially mechanical performance in the human body fluid. In this respect, although there are very limited number of studies for the conventionally molded PLA-based specimens [25,104-107] and only two studies for PLA/POSS specimens [87, 108], no work has been cited for the 3D-printed specimens, yet. Consequently, secondary aim in this part was, as the first time in the literature, to observe whether there would be changes or not in the physical structure and mechanical properties of the 3D-printed PLA/POSS specimens after keeping them at least 120 days in the plain PBS (phosphate buffered saline) solution having human body temperature of 37°C.
- (iii) As discussed in Section 2.3, use of the Taguchi optimization method for the electrospinning of neat PLA was applied only in two studies and there is no reported one for the PLA/POSS nanocomposite structure; hence the main purpose of the third part of this thesis was to determine the optimum

electrospinning parameters by applying the Taguchi technique first to neat PLA and then to reveal the applicability of these parameters for the electrospinning of PLA/POSS nanofibers.

## CHAPTER 3

### EXPERIMENTAL WORK

#### 3.1 Experimental Procedures Used in the First Part of the Thesis

##### (i) Materials Used

In this thesis, PLA matrix material used was commercial L-lactic acid type polylactide supplied from NaturePlast (France) with an extrusion grade (PLE 001). The general chemical structure of PLA is shown in Figure 3.1. As it is indicated in its technical data sheet, it melts between 145°-155°C and degrades in the range of 240°-250°C; its melt flow index range at 190°C under 2.16 kg is 2-8 g/10 min, as well as a density of 1.25 g/cm<sup>3</sup>. Gel permeation chromatography analysis indicated that its weight average molecular weight was 101 100 g/mol.

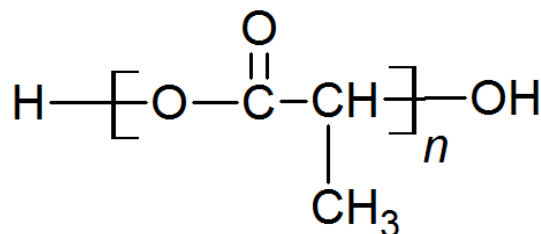


**Figure 3.1** Chemical structure of PLA

As the nano-reinforcement material, in all parts of the thesis, a basic Polyhedral Oligomeric Silsesquioxane (POSS) particles with non-reactive isobutyl corner groups (as shown in Figure 3.2) were used. Additionally, in this first part, in order to investigate effects of functional groups apart from the basic structure, three different functionalized structures were also used. Details of these functional POSS structures

will be given in Section 4.1.2. These four different POSS structures were purchased from Hybrid Plastics Inc. (USA).

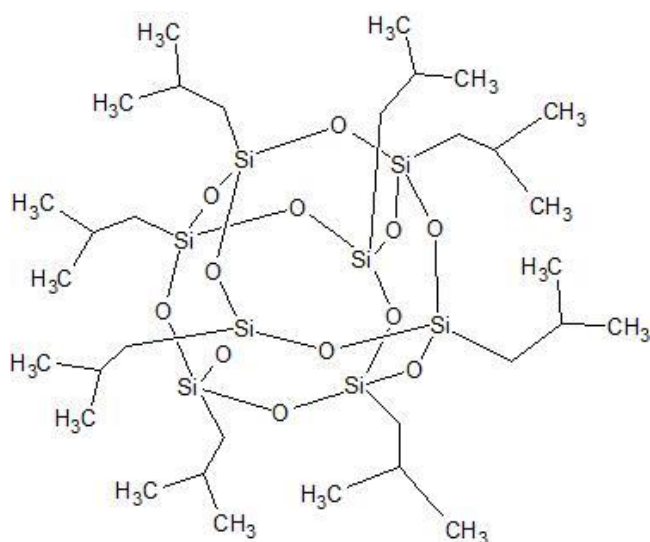


**Figure 3.2** Chemical structure of the basic POSS nanoparticles used

During copolymer compatibilization studies maleic anhydride (MA) (Sigma Aldrich, purity 99%) used for grafting of PLA has a molecular weight of 98.06 g/mol, a melting temperature range of 51-56°C, and a boiling temperature of 200°C. The initiator used for MA grafting reaction was dicumyl peroxide (DCP) (Sigma Aldrich, purity 99%) with melting temperature of 39°C.

## (ii) Production of PLA/POSS Nanocomposites

PLA granules were first pre-dried overnight in a vacuum oven at 60°C and then pre-mixed with certain amounts of POSS particles manually. This mixture was melt compounded via Rondol Microlab 300 laboratory size (D=10 and L/D=20) twin-screw extruder (Rondol Technology Ltd., UK). Typical temperature profile from feeder to die used was 115°-170°-180°-175°-150°C while the typical screw speed used was 75 rpm.



Before shaping of the test specimens by compression molding; continuous strands coming out from the twin-screw extruder die were cut into 2-3 mm granules by using a four-blade cutter. Then, pellets were again allowed to re-dry for 15 h in a vacuum oven at 60°C. Standard size specimens required for testing and analyses were melt shaped via laboratory scale compression molding (MSE Press Series, LP-M2SH05, Turkey) at 160°C under 25 kN with 5 minutes of melting and then pressing time.

Effects of copolymer compatibilization in this part was investigated via MA grafted PLA (PLA-g-MA) copolymer which was produced by using reactive extrusion technique via twin-screw melt mixing of PLA and 2 wt% MA including 0.5 wt% dicumyl peroxide (DCP) as the free radical initiator. By using titration method, the amount of grafted MA on PLA was found as 2.67%. Details of these procedures are explained in our former study [109].

### **(iii) Structural and Morphological Characterization**

Fourier transform-infrared (FTIR) spectroscopy was used in order to reveal possible interfacial interactions between PLA, MA and POSS nanoparticles. At least 32 scans were signal-averaged by the attenuated total reflectance (ATR) unit of Bruker ALPHA IR spectrometer (Bruker Optik GmbH, Germany) in the wavenumber range of 400 to 4000  $\text{cm}^{-1}$  with a resolution of 4  $\text{cm}^{-1}$ . In order to observe fracture surface morphology and distribution of the POSS nanoparticles in the PLA matrix of the specimens shaped by 3D-printing and compression molding, scanning electron microscopy (SEM) (FEI Nova Nano 430) analysis was conducted on the gold sputtered fracture surfaces of the fracture toughness test specimens with secondary electron detector.

#### **(iv) Mechanical Tests and Thermal Analysis**

In order to determine mechanical properties of the PLA/POSS nanocomposites in terms of strength, modulus and ductility, tension and flexural tests were performed. Tension tests were applied according to ISO 527-2 standard while three-point-bending flexural tests were carried out according to ISO 178 standard. These tests were performed under 5 kN Instron 5565A universal testing system (Instron Engineering Co., USA). Fracture toughness tests were also carried out to determine the  $K_{IC}$  and  $G_{IC}$  values of the nanocomposites. These tests were conducted by using single-edge-notched-bending specimens according to ISO 13586 standard again under Instron 5565A system. Ceast Notchvis device (Instron Engineering Co., USA) was used to form the notches and pre-cracks on these specimen edges as described in the standard. All these mechanical tests were repeated 5 times for each specimen group, and the average values including their standard deviations were determined.

Two different thermal analyses were carried out to determine the thermal behavior of all PLA/POSS nanocomposite specimens. First of all, differential scanning calorimetry analyses (DSC) (SII X-DSC 700 Exstar, Japan) were used to determine the important transition temperatures and enthalpies of melting and crystallization of the samples during a heating profile from  $-80^{\circ}$  to  $220^{\circ}\text{C}$  at a rate of  $10^{\circ}\text{C}/\text{min}$  under nitrogen flow. Then, thermogravimetric analyses (TGA) (SII TG/DTA 7300 Exstar, Japan) were conducted to determine the thermal degradation temperatures of the specimens under a heating rate of  $10^{\circ}\text{C}/\text{min}$  from  $30^{\circ}$  to  $550^{\circ}\text{C}$  under nitrogen flow.

### **3.2 Experimental Procedures Used in the Second Part of the Thesis**

In this part, matrix (PLA) and reinforcement (POSS) materials, conventional compression molding, SEM analysis, mechanical tests (tension, flexural, fracture

toughness) and thermal analyzes (DSC, TGA) used were all the same as explained in Section 3.1 above. Other procedures used in this part of the thesis are as follows:

**(i) Production of the PLA/POSS and PLA Filaments**

Before shaping of the specimens by 3D-printing, first their filament forms must be obtained. In the second part of this thesis PLA/POSS nanocomposite filaments were produced with two different contents, i.e. having 1 wt% and 3 wt% POSS nanoparticles, designated as PLA/POSS 1 and PLA/POSS 3.

These PLA/POSS nanocomposite structures were formed by melt-mixing technique with a laboratory scale twin-screw extruder (Rondol Microlab 300, D=10, L/D=20). Initially, powdered PLA were pre-dried overnight in a vacuum oven at 60°C, and then pre-mixed with 1 and 3 wt% POSS nanoparticles manually. The temperature profile used from feeder to die was 115°-170°-180°-175°-150°C, while the screw speed was 75 rpm. Filaments in the form of continuous threads coming out from the twin-screw extruder die were carefully air cooled to dry and then wound on empty filament spools keeping their diameter 1.80±0.2 mm. Neat PLA filaments were produced in the same manner without any filler.

**(ii) 3D-Printing of the Specimens**

Specimen shaping via 3D-printing was performed with an FDM-type commercial 3D-printer by using neat PLA, PLA/POSS 1 and PLA/POSS 3 nanocomposite filaments produced as described above. For the designation of these 3D-printed specimens, an italic suffix of “3D” was used as; PLA - *3D*, PLA/POSS 1 - *3D* and PLA/POSS 3 - *3D*. Here, it should be pointed out that, in order to differentiate the designation of the Compression Molded specimens, the italic suffix of “CM” was used as; PLA - *CM*, PLA/POSS 1 - *CM* and PLA/POSS 3 - *CM*.

The table-top model 3D-printer (Ultimaker 2+) (Figure 3.3) used in this part of the thesis was an open-source code equipment with replaceable nozzles and multiple process parameters. Build chamber size of the printer is 223x223x205 mm, whereas the temperature ranges of the nozzle and built plate are 180°-260°C and 50°-100°C, respectively. Before using the Cura 2.3.1 slicing software of the printer to generate the G-code, geometries of the test samples, according to the related ISO standards having 2 mm thickness, were drawn with a CAD software (SolidWorks).

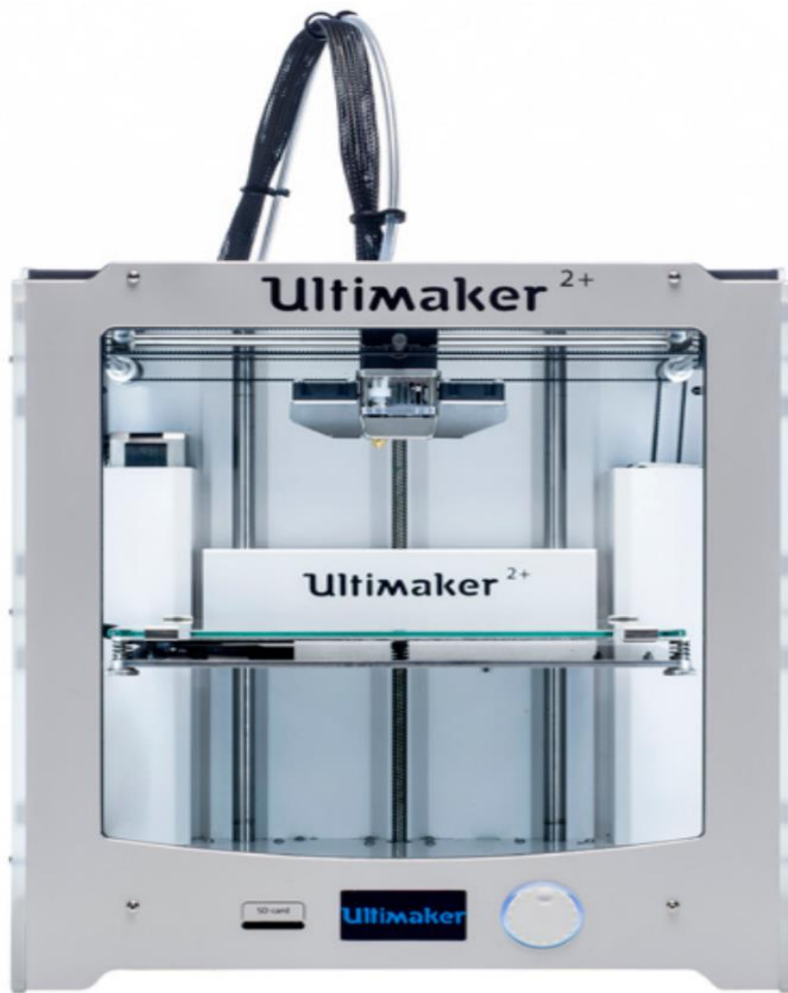


**Figure 3.3** Front view of the 3D-printer used

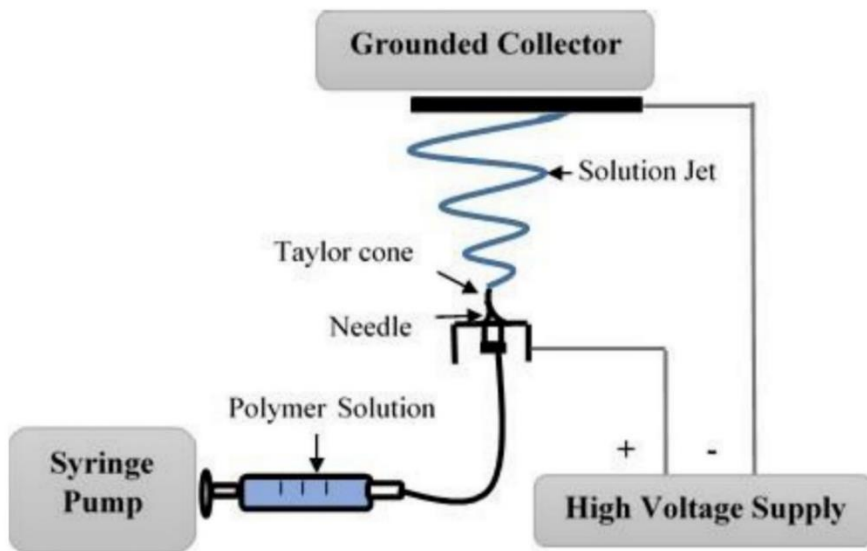
Important hardware and software parameters were determined after several trials. As the hardware parameters; the built plate was set as 70°C whereas the nozzle diameter and temperature were selected as 0.4 mm and 190°C, respectively. Specimens were printed as “laying down” position with alternating  $\pm 45^\circ$  raster orientation. Software parameters used were; layer height of 0.06 mm, wall thickness of 0.6 mm, the thickness of the top and bottom layers of 0.72 mm, infill density of 100%, and print speed of 50 mm/s.

### **3.3 Experimental Procedures Used in the Third Part of the Thesis**

In this part, matrix (PLA) and reinforcement (POSS) materials used were again the same as explained in Section 3.1 above. Solvents used for the preparation of electrospinning solution were chloroform (CF) (purity>99%, Sigma Aldrich) and dimethylformamide (DMF) (purity>99%, Fluka). Other procedures used in this part of the thesis are as follows:

#### **(i) Electrospinning Equipment**

In the third part of this thesis, electrospinning experiments were conducted by using a single nozzle, bottom-up vertical configuration commercial set-up (Nanospinner Ne100, Inovenso Inc.) as shown in Figure 3.4. The range of its high voltage power supply is 0-40 kV, while the capacity of the 10 mL syringe polymer solution pump system (New Era Pump System Inc.) is 0.01-1000 mL/h. A polyethylene capillary tube connects the syringe and the needle having inner diameter of 0.8 mm. To collect electrospun fibers, the set-up has a stationary type earth-grounded round aluminum plate collector covered with aluminum foil.



(a)



(b)

**Figure 3.4** (a) Three basic components of a typical electrospinning set-up, and (b) General view of the electrospinning equipment used

During the experiments, air-ventilation of the system was kept running to maintain the temperature of the cabin around 30°C and the relative humidity around 40%. In order to collect similar amount of electrospun fibers in the form of web, a total of 10 minutes electrospinning period was applied during each experiment.

## **(ii) SEM and Image Analysis**

In order to observe surface morphology and size distribution of the electrospun fibers, field emission scanning electron microscopy (FEI Nova Nano 430, FEI Inc.) was conducted under an accelerating voltage of 20 kV with the working distance of 5-7 mm as mentioned before. Nanofibers collected on the aluminum foil were sputtered with a thin gold layer to provide conductive surfaces. After SEM analysis, in order to determine electrospun fiber diameter size and distributions, micrographs were also evaluated by using an image analysis software (ImageJ). Measurements in the image analysis software were conducted for at least three different locations of each SEM micrograph, so that the number of individual fibers evaluated for each case were around 350.





## CHAPTER 4

### RESULTS AND DISCUSSION

As stated before, since this dissertation has three different parts, their results are presented and discussed successively in the following three subsections.

#### **4.1 Effects of Filler Content, Functional Group and Copolymer Compatibilization on the Behavior of PLA/POSS Nanocomposites**

Behavior of PLA/POSS nanocomposites in terms of morphological, mechanical and thermal properties were investigated by revealing the influences of three different parameters. The first one was the effects of using different POSS contents, the second one was effects of having different functional groups on the POSS structure, and the third one was effects of using maleic anhydride grafted copolymer compatibilization.

##### **4.1.1 Effects of POSS Content**

The basic POSS structure used had only isobutyl (a rather non-polar organic group) attached to each eight corner of the inorganic cage. Effects of the filler content was studied by reinforcing the PLA matrix with 1, 3, 5 and 7 wt% POSS nanoparticles. These specimens were designated by using the format of PLA/POSS  $x$ , where  $x$  denotes the amount of the nanoparticles used.

Since distribution and agglomeration level of the nanoparticles in the matrix has significant influences on the mechanical and other properties of the nanocomposites, SEM studies were conducted on the fracture surface of the fracture toughness test

specimens of all compositions. SEM images taken at a magnification of 40000X given in Figure 4.1 show that lower POSS contents, i.e. 1 and 3 wt%, resulted in rather uniform distribution with lower degree of agglomeration in PLA matrix. For instance, for the 1 wt% POSS content, the average size range of the agglomerates were not more than 100 nm. On the other hand, the level of agglomeration for the higher POSS contents i.e. 5 and 7 wt%, were much larger.

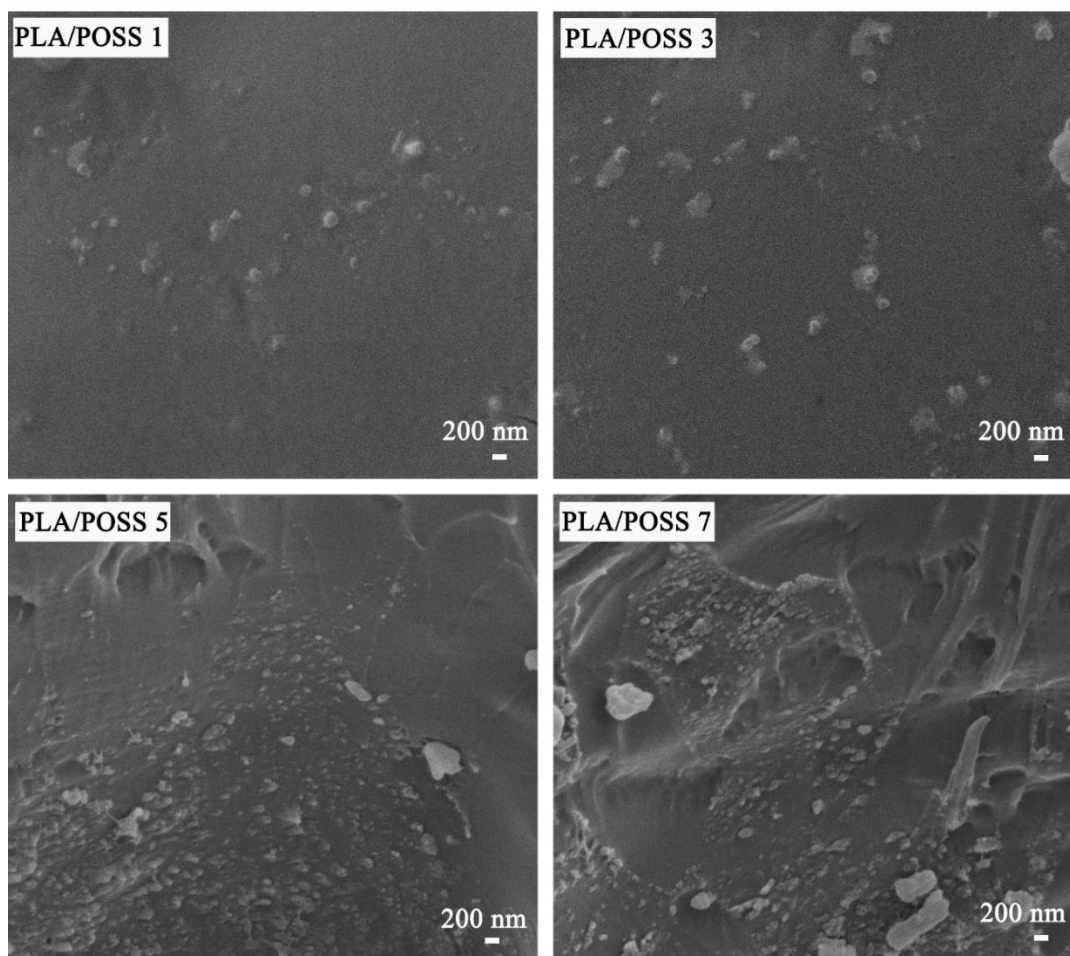


**Figure 4.1** SEM fractographs showing effects of POSS content on the distribution and agglomeration level of particles in the PLA matrix

Effects of POSS content on the mechanical properties were first evaluated by conducting tension tests and three-point-bending tests to determine the influences on the strength and elastic modulus values of PLA. While “tensile stress-strain” curves and “flexural stress-strain” curves of specimens are given separately in Figure 4.2, the values of “Tensile Strength ( $\sigma_{TS}$ )” and “Tensile Modulus ( $E$ )” determined by tension tests; and the values of “Flexural Strength ( $\sigma_{Flex}$ )” and “Flexural Modulus ( $E_{Flex}$ )” determined by bending tests are all tabulated in Table 4.1. Moreover, influences of increasing POSS content on the strength and elastic modulus values of PLA/POSS nanocomposites were compared in Figure 4.3.

Due to the basic strengthening and stiffening mechanisms of “load transfer from the matrix to the reinforcement” and “decreased mobility of the macromolecular chains of matrix”, Table 4.1, Figures 4.2 and 4.3 simply show that use of 1 wt% POSS content could improve strength and modulus values of PLA matrix slightly; which was for instance around 3% in Flexural Strength ( $\sigma_{Flex}$ ) and 6% in Flexural Modulus ( $E_{Flex}$ ). However, beyond 1 wt% POSS content, due to the higher degree of agglomeration, the effectiveness of the basic strengthening and stiffening mechanisms started to decrease gradually.

Effects of POSS content on the ductility and fracture toughness values of PLA were also evaluated in Table 4.1 and Figure 4.4. Ductility values were taken as “% Strain at Break” ( $\% \epsilon_f$ ) values obtained from the tension tests. It is known that ductility is the ability of materials to have permanent plastic deformation up to fracture. Fracture toughness, i.e. ability of the materials to withstand crack initiation and propagation, values of the specimens were evaluated in terms of both “Critical Stress Intensity Factor ( $K_{IC}$ )” and “Critical Strain Energy Release Rate ( $G_{IC}$ )” values.

**Table 4.1** Tensile strength ( $\sigma_{TS}$ ), flexural strength ( $\sigma_{Flex}$ ), tensile modulus ( $E$ ), flexural modulus ( $E_{Flex}$ ); % strain at break (%  $\varepsilon_f$ ) and fracture toughness ( $K_{IC}$  and  $G_{IC}$ ) values of the specimens with different POSS contents

<b>Specimens</b>	<b><math>\sigma_{TS}</math> (MPa)</b>	<b><math>\sigma_{Flex}</math> (MPa)</b>	<b><math>E</math> (GPa)</b>	<b><math>E_{Flex}</math> (GPa)</b>	<b><math>\varepsilon_f</math> (%)</b>	<b><math>K_{IC}</math> (MPa<math>\sqrt{m}</math>)</b>	<b><math>G_{IC}</math> (kJ/m<sup>2</sup>)</b>
<b>PLA</b>	56.04±0.57	94.80±1.5	2.71±0.07	3.16±0.07	5.11±0.05	3.75±0.04	6.28±0.41
<b>PLA/POSS 1</b>	56.80±0.89	97.43±2.3	2.87±0.01	3.36±0.11	5.64±0.90	3.92±0.10	8.92±1.17
<b>PLA/POSS 3</b>	54.24±0.27	91.76±2.9	2.87±0.01	3.19±0.09	6.64±0.47	4.16±0.06	11.14±0.94
<b>PLA/POSS 5</b>	46.76±1.29	82.62±1.2	2.77±0.04	3.03±0.14	6.55±0.38	3.89±0.19	9.02±0.46
<b>PLA/POSS 7</b>	43.44±1.25	80.60±2.7	2.76±0.08	2.99±0.12	6.41±0.49	3.39±0.13	8.66±0.39

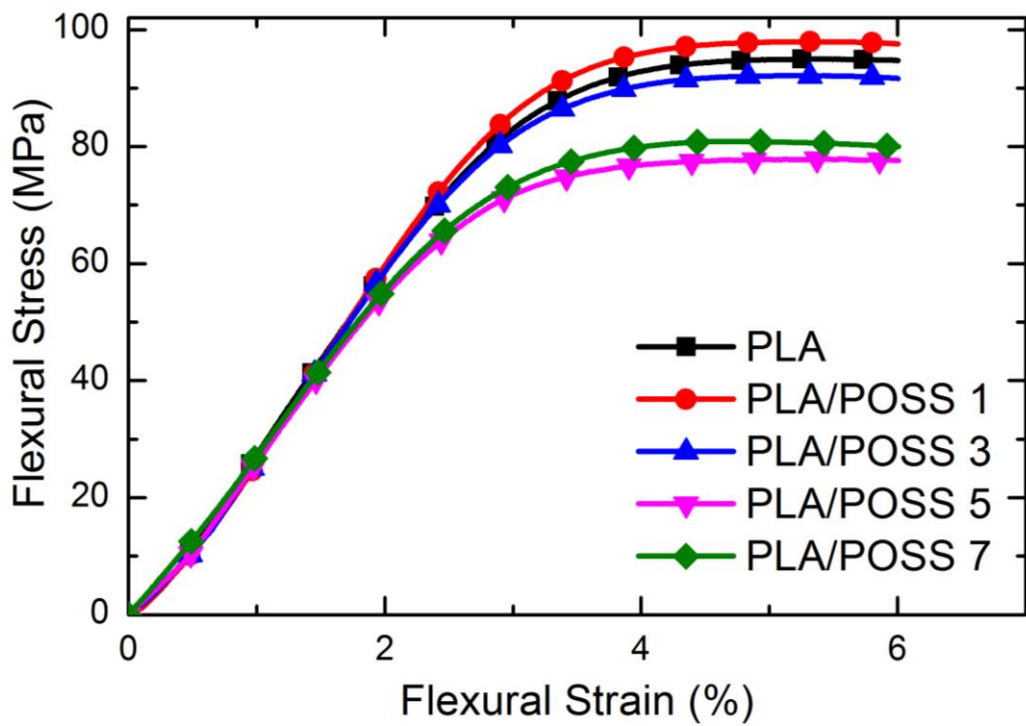
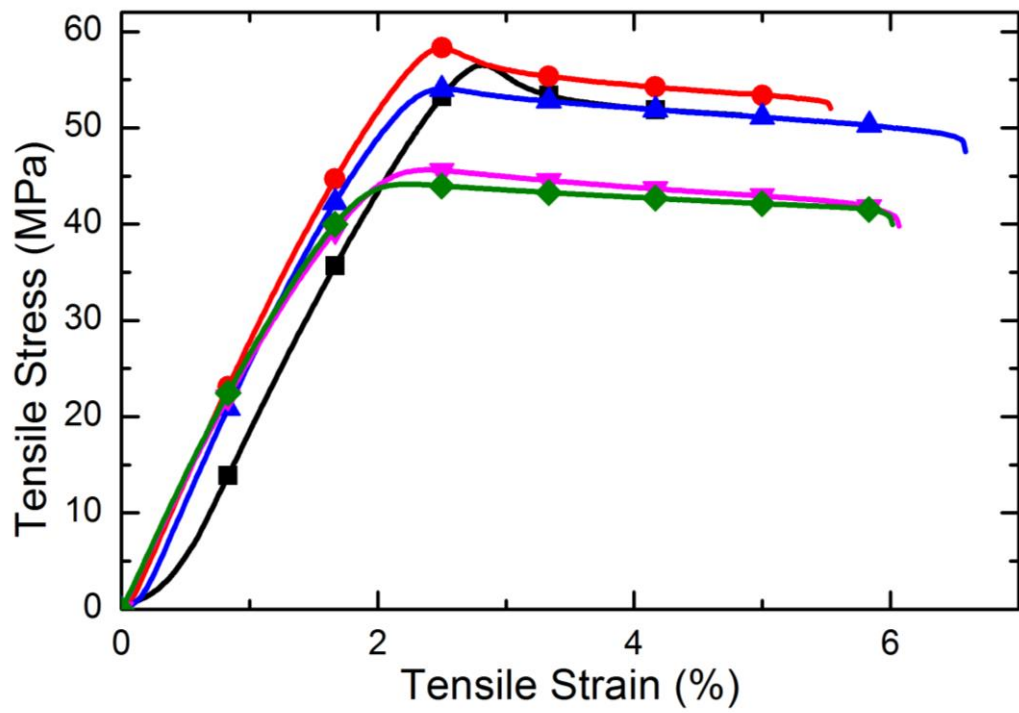


**Figure 4.2** Stress-Strain curves of the specimens with different POSS contents obtained during tensile and 3-point-bending flexural tests

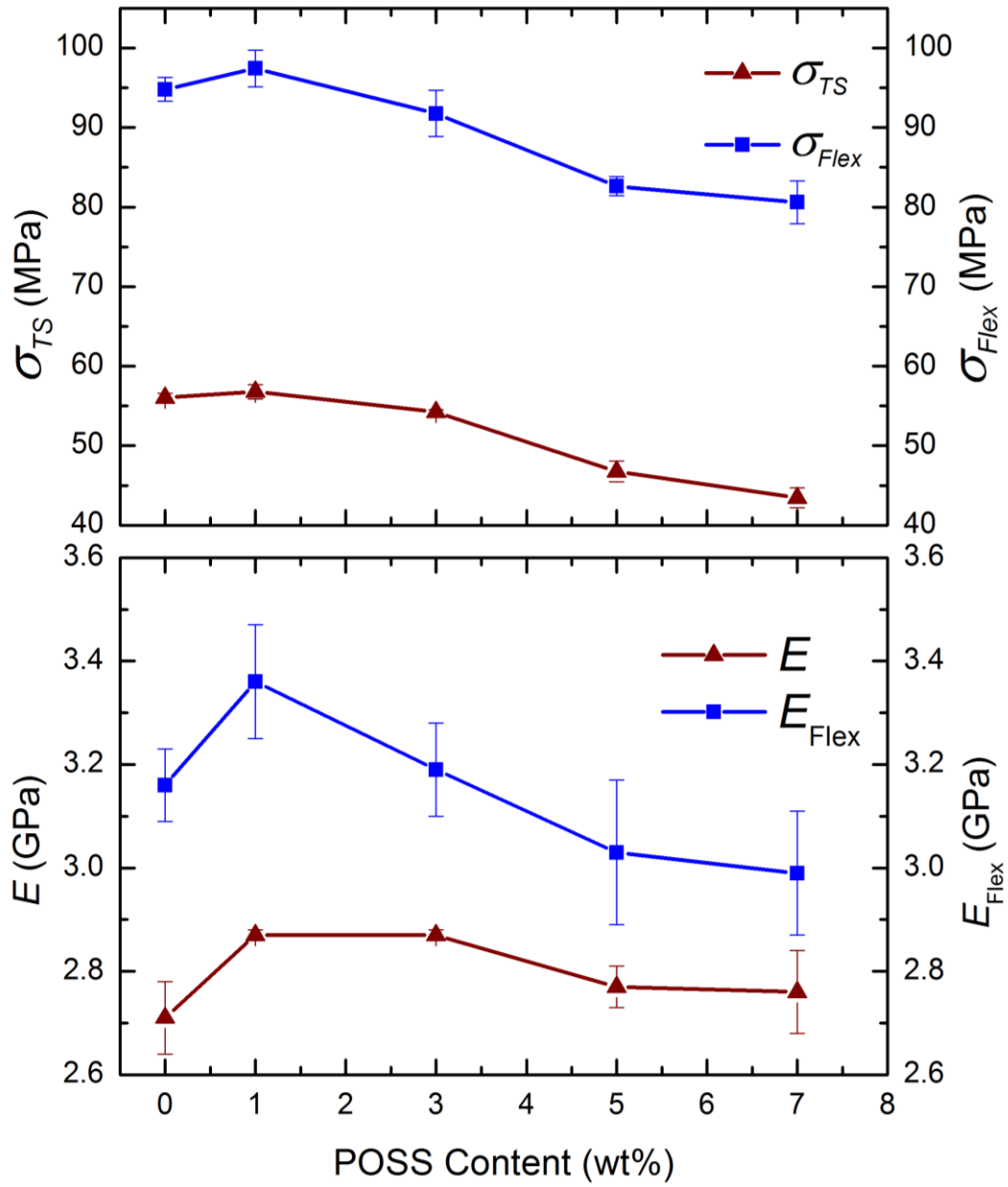


**Figure 4.3** Effects of POSS content on the strength ( $\sigma_{TS}$  and  $\sigma_{Flex}$ ) and modulus ( $E$  and  $E_{Flex}$ ) values of the specimens

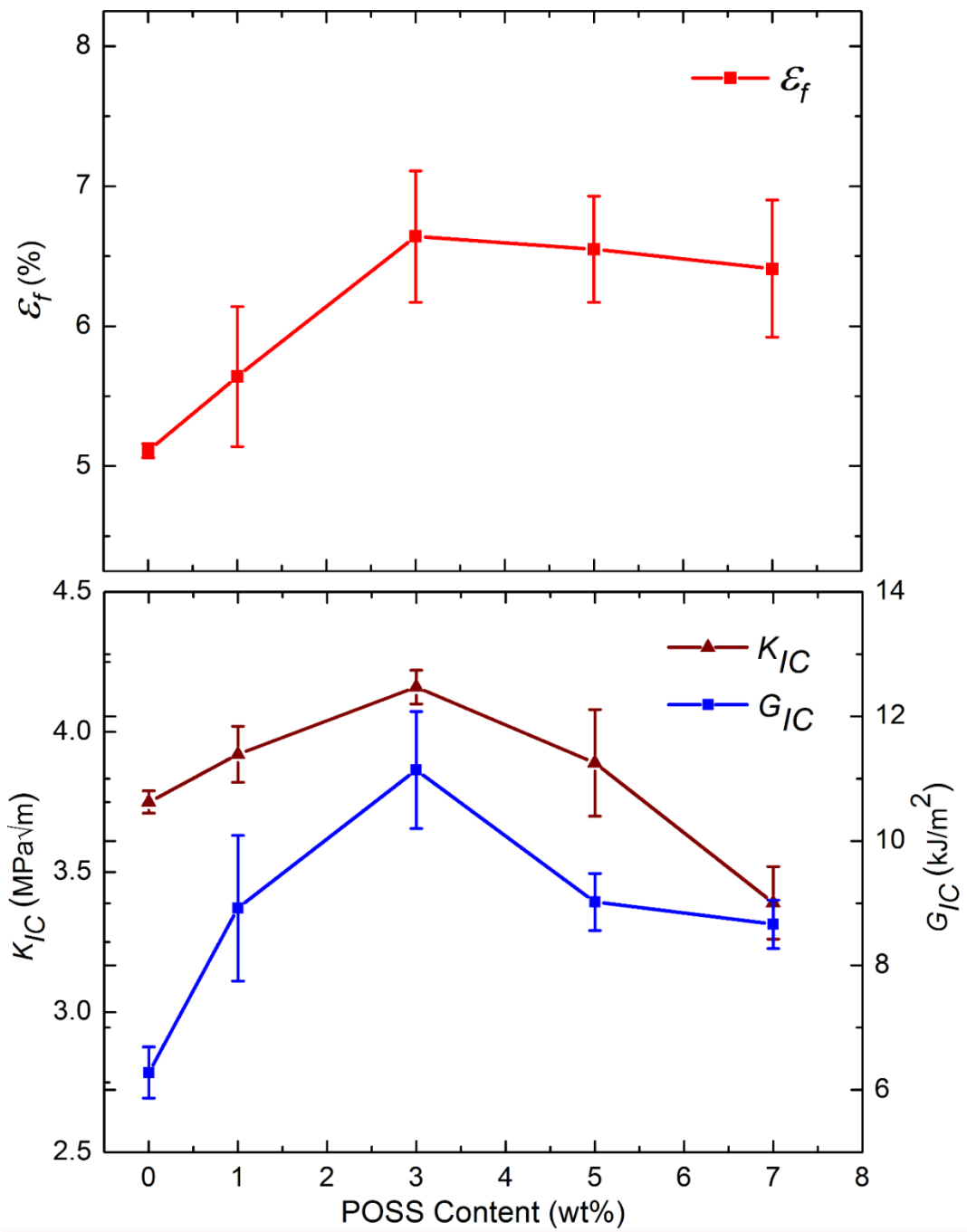


**Figure 4.4** Effects of POSS content on the ductility ( $\epsilon_f$ ) and fracture toughness ( $K_{IC}$  and  $G_{IC}$ ) values of the specimens

Due to the effectiveness of the POSS nanoparticles on the basic toughening mechanisms of “crack deflection”, “shear band formation”, “debonding and pull out”, etc.; Table 4.1 and Figure 4.4 show that the increases in the ductility and fracture toughness values of the PLA matrix continue beyond 1 wt%, reaching maxima at 3 wt% POSS content. At this composition, the increase in % Strain at Break ( $\% \varepsilon_f$ ) value was 30%, while the increases in  $K_{IC}$  and  $G_{IC}$  fracture toughness values were as much as 11% and 77%, respectively. Beyond 3 wt% content, ductility and fracture toughness values started to decrease gradually, again due to the same reason mentioned before.

Effects of POSS content on the thermal behavior of the specimens were studied by DSC and TGA analyses. First heating DSC thermograms of the specimens were given in Figure 4.5, while the important transition temperatures such as glass transition ( $T_g$ ), cold crystallization ( $T_c$ ) and melting ( $T_m$ ) temperatures were tabulated in Table 4.2 together with the enthalpy of melting ( $\Delta H_m$ ) and enthalpy of crystallization ( $\Delta H_c$ ) including percent crystallinity ( $X_c$ ) of the PLA matrix. The relation used in calculation of percent crystallinity is given below;

$$X_c = \frac{\Delta H_m - \Delta H_c}{w_{PLA} \Delta H_m^o} \times 100 \quad (4.1)$$

where  $w_{PLA}$  is the weight fraction of the PLA matrix and  $\Delta H_m^o$  is the melting enthalpy of 100% crystalline PLA determined as 93 J/g in literature [110].

It was observed that use of POSS nanoparticles resulted in no significant influences on the glass transition temperature ( $T_g$ ) and melting temperature ( $T_m$ ) of the PLA matrix. On the other hand, due to the nucleation agent effect of the nanoparticles, increasing POSS content resulted in significant increases in the crystallinity amount. For instance, the increase in crystallinity amount ( $X_c$ ) was more than 2 times with only 1 wt% POSS, while this increase was more than 3 times with 5 wt% POSS.



**Table 4.2** Transition temperatures ( $T_g$ ,  $T_c$ ,  $T_m$ ), enthalpies ( $\Delta H_m$ ,  $\Delta H_c$ ) and crystallinity percent ( $X_C$ ) of the specimens with different POSS contents during DSC first heating profile

<b>Specimens</b>	$T_g$ (°C)	$T_c$ (°C)	$T_m$ (°C)	$\Delta H_m$ (J/g)	$\Delta H_c$ (J/g)	$X_C$ (%)
<b>PLA</b>	60.1	124.6	150.2	17.2	13.7	3.76
<b>PLA/POSS 1</b>	60.0	121.0	150.0	14.7	6.82	8.56
<b>PLA/POSS 3</b>	62.2	120.9	150.0	15.3	6.40	9.87
<b>PLA/POSS 5</b>	62.0	114.7	149.8	14.2	2.23	13.5
<b>PLA/POSS 7</b>	61.2	116.8	149.3	18.3	9.34	10.36

**Table 4.3** Thermal degradation temperatures ( $T_{5\%}$ ,  $T_{10\%}$ ,  $T_{25\%}$ ) of the specimens with different POSS contents at 5, 10 and 25 wt% mass losses, the maximum mass loss temperature ( $T_{max}$ ) and %Residue at 550°C

<b>Specimens</b>	$T_{5\%}$ (°C)	$T_{10\%}$ (°C)	$T_{25\%}$ (°C)	$T_{max}$ (°C)	<b>%Residue at 550°C</b>
<b>PLA</b>	332	342	353	362	0.16
<b>PLA/POSS 1</b>	327	337	349	365	0.36
<b>PLA/POSS 3</b>	321	334	349	368	0.49
<b>PLA/POSS 5</b>	314	330	347	364	0.62
<b>PLA/POSS 7</b>	315	327	345	362	0.95

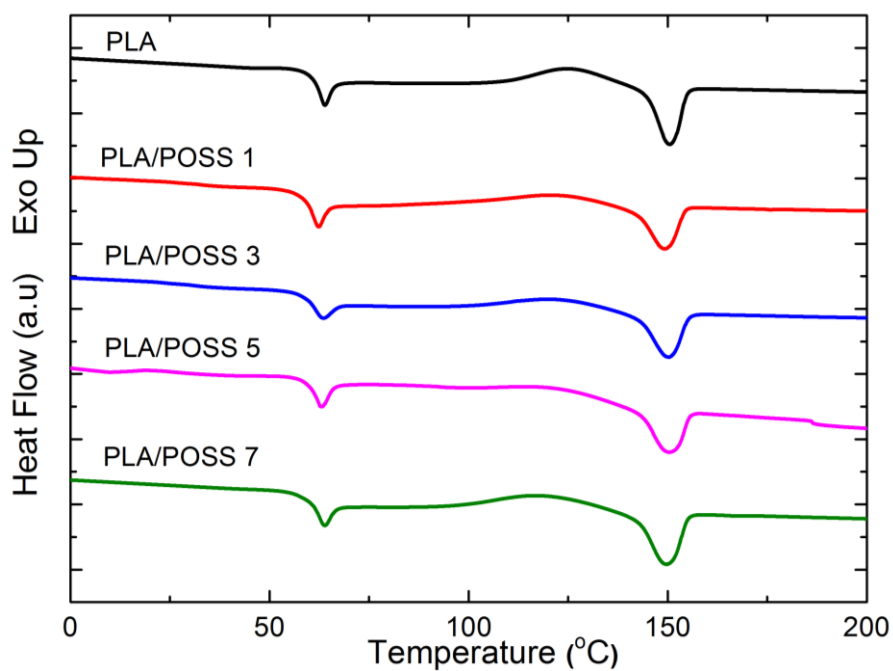


**Figure 4.5** First heating DSC thermograms of the specimens with different POSS contents

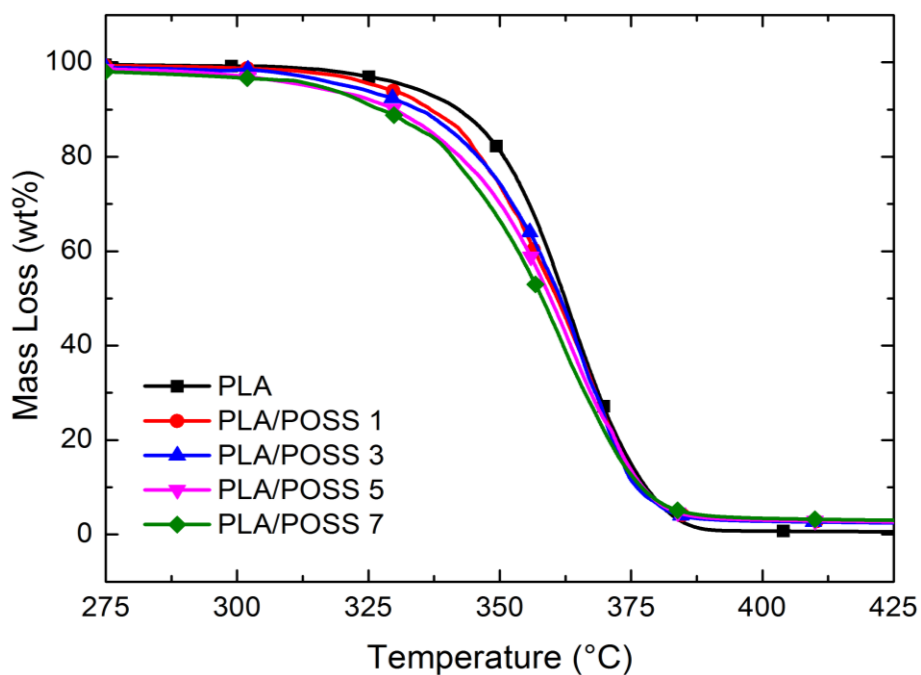


**Figure 4.6.** Thermogravimetric curves of the specimens with different POSS contents

Thermogravimetric (TGA) curves indicating the thermal degradation temperatures and %residue of each specimen were given in Figure 4.6, while the data determined were tabulated in Table 4.3 as  $T_{5\%}$ ,  $T_{10\%}$  and  $T_{25\%}$  representing the degradation temperatures at 5%, 10% and 25% mass losses; and  $T_{max}$  representing the temperature at maximum mass loss. It was generally seen that use of POSS nanoparticles resulted in slight decreases in the  $T_{5\%}$ ,  $T_{10\%}$  and  $T_{25\%}$  thermal degradation temperatures of the PLA matrix. There were a few degrees of increase only in the  $T_{max}$  degradation temperature. Table 4.3 also indicates that inorganic residue% increases parallel to the POSS content in the matrix.

#### 4.1.2 Effects of the Functional Groups on the POSS Structure

Depending on the application, corners of the inorganic cage structure of POSS could be functionalized by attaching different organic groups. The basic POSS structure used had only “isobutyl” (a rather non-polar group) attachment at each eight corners. That structure simply designated as **POSS** is actually named as **OctaIsobutyl-POSS**.

Influences of having different organic functional groups on the corners of the POSS structure were explored by comparing the performances of the three more POSS structures with each other. In the second POSS structure, one of the corner was functionalized by “aminopropyl” group; it is named as **AminopropylIsobutyl-POSS** and simply designated as **ap-POSS**. In the third POSS structure, one of the corner was this time functionalized by “propanediol” group; it is named as **PropanediolIsobutyl-POSS** and simply designated as **pd-POSS**. In the fourth POSS structure, all eight corners were functionalized by “dimethylsilane” groups; it is named **OctaSilane-POSS** and simply designated as **os-POSS**. Figure 4.7 shows these commercially available four different POSS structures compared in this thesis.

Note that in the previous section, since use of 1 wt% POSS resulted in lowest degree of agglomeration in PLA matrix, performance comparison of the four different POSS structures were evaluated by using this optimum POSS content for each. Therefore, in the designation of each nanocomposite specimen group in this section, 1 wt% filler contents were not indicated.

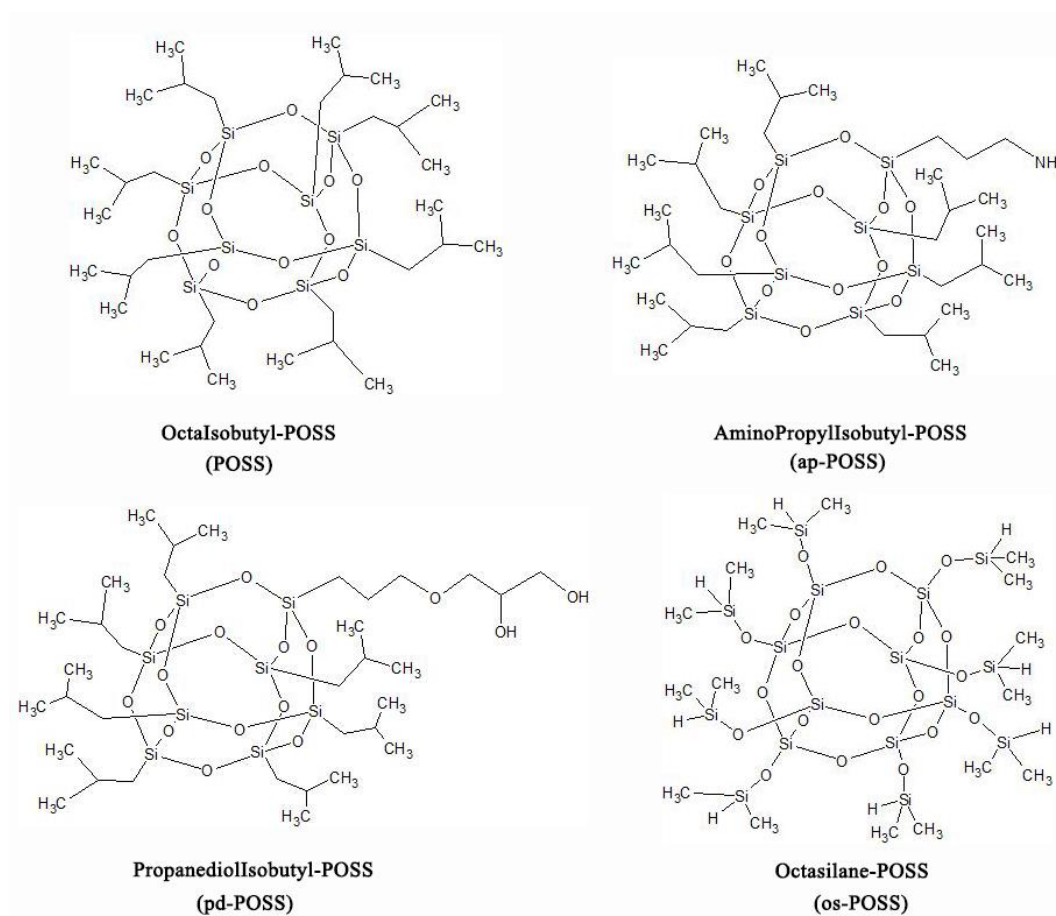


**Figure 4.7** Functional groups of the four different POSS structures compared in the thesis

ATR-FTIR analyses were conducted in order to reveal different functionalities of each POSS structures and their PLA nanocomposites (Figure 4.8).

In the literature [10, 110, 111] distinctive IR bands for the basic POSS structure were reported as; stretching vibration peaks of siloxane (Si-O-Si) between 1050-1150  $\text{cm}^{-1}$ , Si-C vibration peak at 1250  $\text{cm}^{-1}$ , C-H stretching vibrations between 2800-3000  $\text{cm}^{-1}$ , and C-H bending vibration in the band of 1295-1365  $\text{cm}^{-1}$ . Figure 4.8 (a) indicated that, Si-O-Si and Si-C peaks were observed at 1085  $\text{cm}^{-1}$  and 1229  $\text{cm}^{-1}$ , respectively; while C-H stretching vibrations were at around 2870 and 2952  $\text{cm}^{-1}$ , including the C-H bending vibration in the band of 1332-1366  $\text{cm}^{-1}$ .

For the ap-POSS structure the expected additional IR bands should be due to the N-H stretching and bending present in the aminopropyl group. For the pd-POSS structure the additional IR bands could be due to the -OH stretching present in the propanediol group. However, since these functional groups were attached to only one corner of the basic POSS structure, it is difficult to recognize these additional bands from the IR spectra given in Figure 4.8 (a).

For the os-POSS structure, the additional IR bands reported in the literature [113-114] were Si-H stretching vibrations at 900 and 2140  $\text{cm}^{-1}$  due to the silane groups present. Since eight corners of the structure was functionalized with silane groups, it was very easy to recognize these additional Si-H peaks at 890 and 2140  $\text{cm}^{-1}$  on the last IR spectrum given in Figure 4.8 (a).

The first IR spectrum given in Figure 4.8 (b) indicates typical six distinctive bands observed for the neat PLA matrix, which is consistent with the literature [115]; i.e. C-C stretching peak at 868  $\text{cm}^{-1}$ , C-O stretching peaks at 1089  $\text{cm}^{-1}$  and 1185  $\text{cm}^{-1}$ , C-H deformation peak at 1325  $\text{cm}^{-1}$ ,  $\text{CH}_3$  bending absorption peak at 1480  $\text{cm}^{-1}$ ; ester carbonyl C=O stretching peak at 1753  $\text{cm}^{-1}$ , and C-H stretching at 2995  $\text{cm}^{-1}$ .

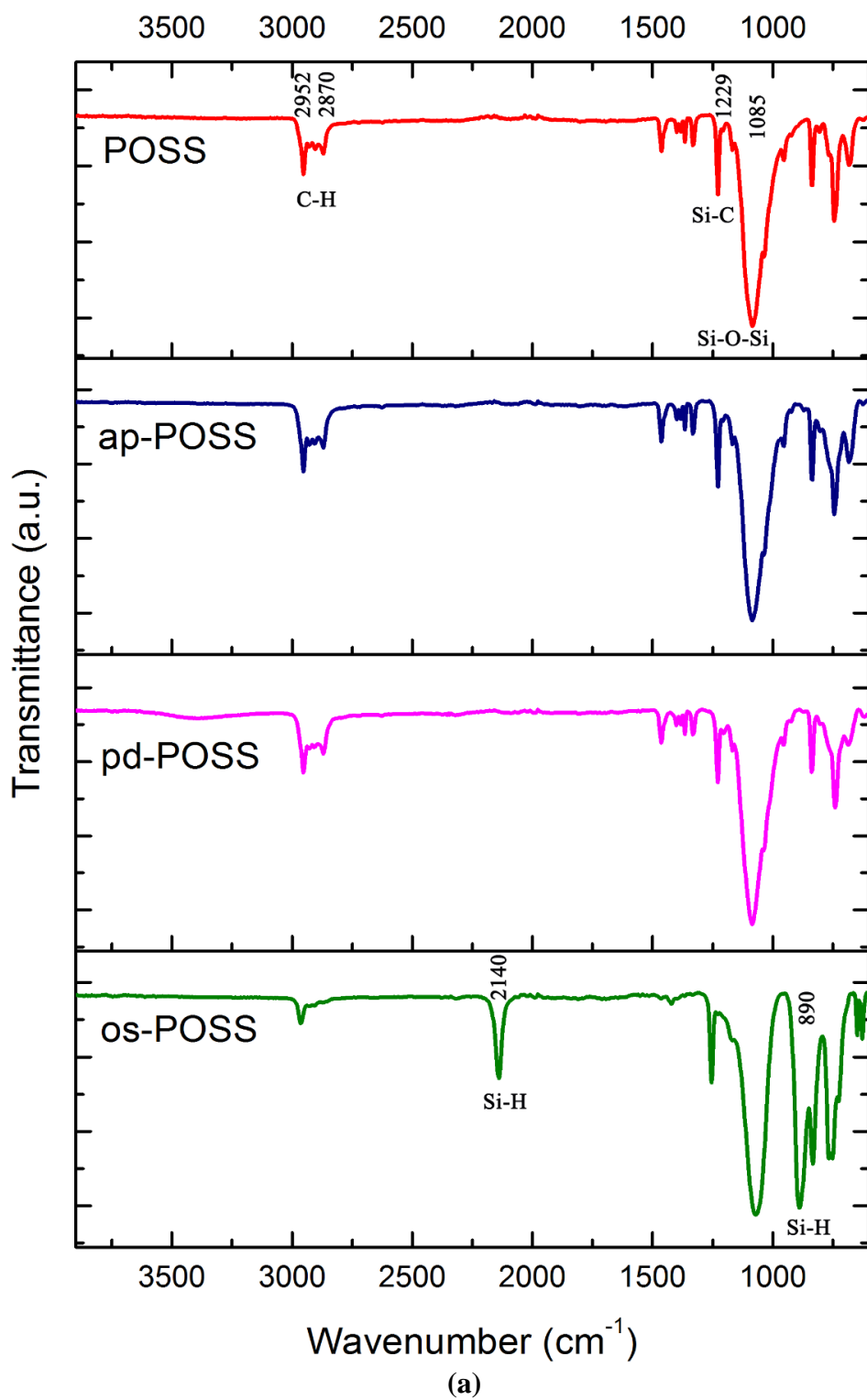
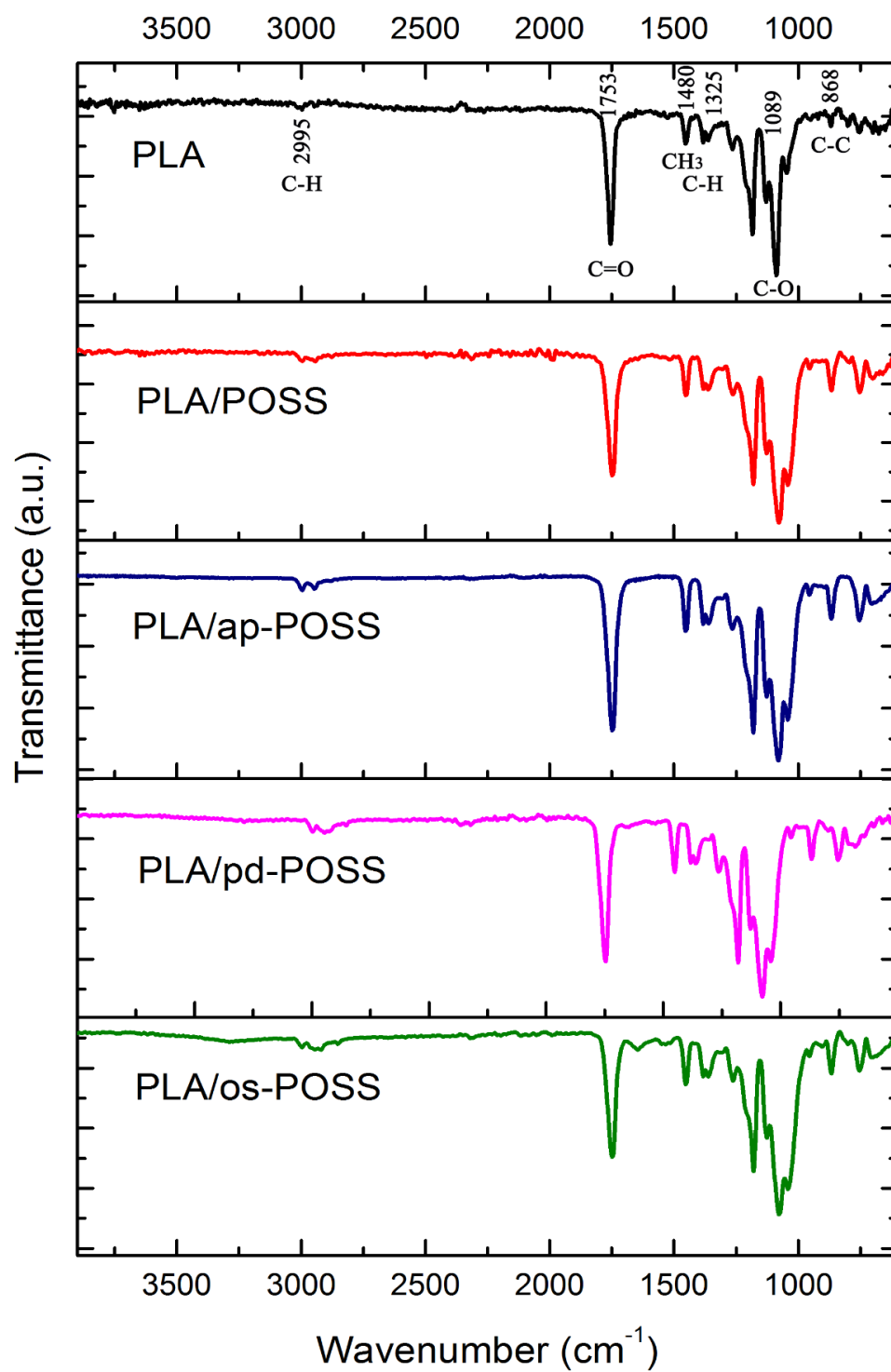


**Figure 4.8** ATR-FTIR spectra of the (a) four different POSS structures and (b) their PLA matrix nanocomposites including neat PLA



(b)

Figure 4.8 (continued)

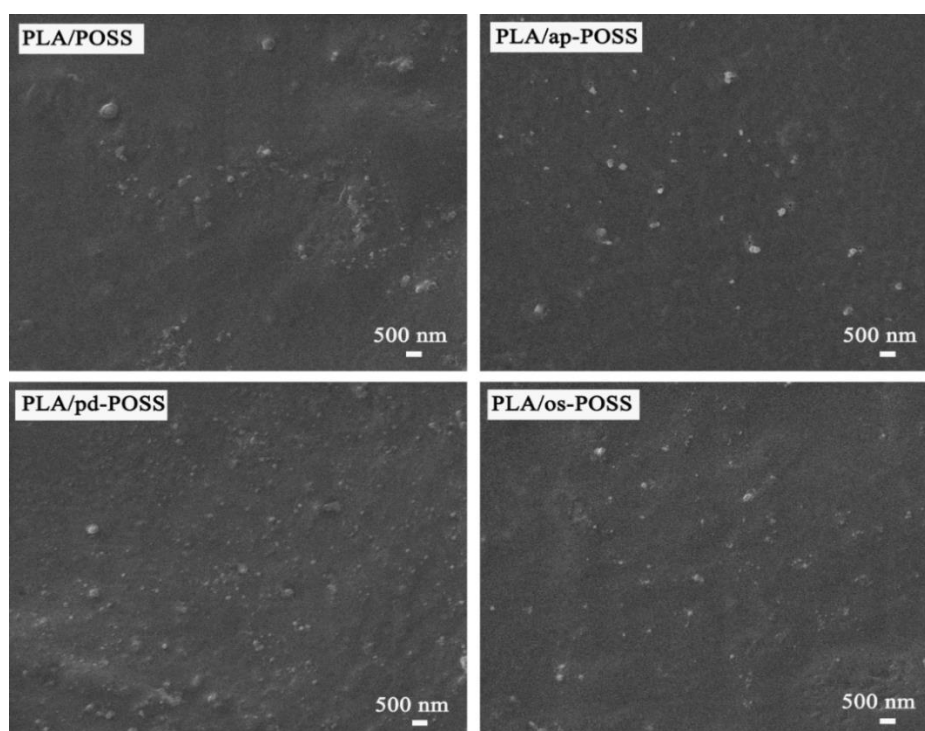
In the rest of the Figure 4.8 (b), IR spectra for each PLA matrix nanocomposites were given. However, due to the very low amount (only 1 wt%) POSS particles and due to the overlapping with typical PLA peaks, it was not easy to recognize differences in the IR spectrum of the nanocomposite specimens.

On the other hand, certain slight differences observed from Figure 4.8 (b) might be mentioned. For instance; when POSS particles were incorporated, there was broadening of the typical C-O stretching peaks ( $1080\text{ cm}^{-1}$ ) of PLA matrix. Another difference observed was the increased intensities of the C-H stretching peaks ( $2950\text{ cm}^{-1}$ ) of PLA matrix. These changes could be speculated that certain level of interfacial interactions between the PLA matrix and functionalized POSS structures were achieved.

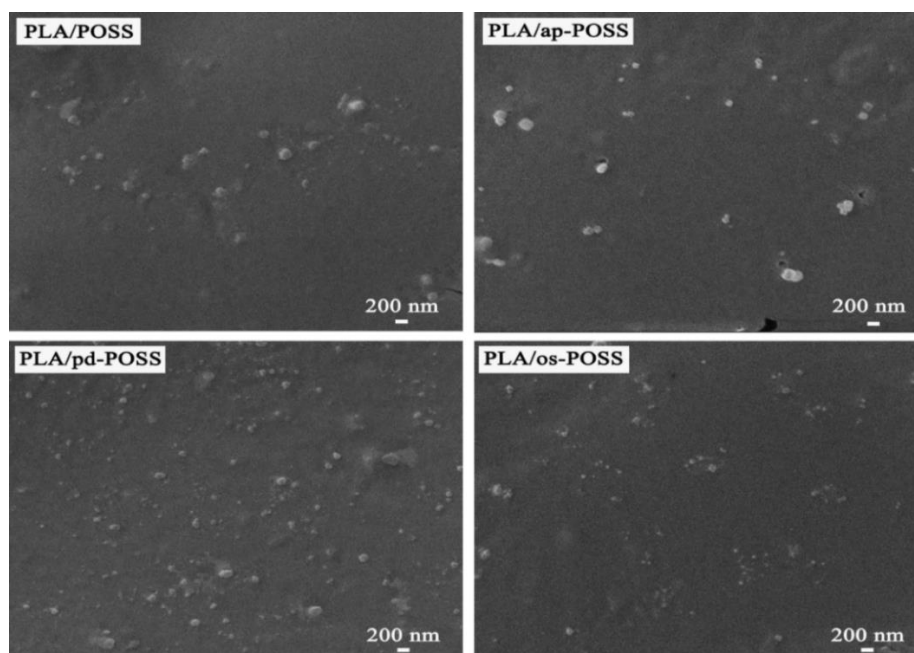
SEM examinations conducted on the fracture surfaces of each specimen group indicated that replacement of the at least one of the rather nonpolar (isobutyl) group on the corners of the POSS structure by functional groups (such as aminopropyl, propanediol, dimethylsilane) might improve the interfacial interactions between the PLA matrix. Thus, Figure 4.9 shows that, compared to basic POSS structure; ap-POSS, pd-POSS and os-POSS particles had rather more homogeneous distribution with lower degrees of agglomeration.

In order to reveal effects of POSS functional groups on the mechanical properties of the PLA matrix nanocomposite specimens; tension, bending and fracture toughness tests were conducted. Tensile and flexural stress-strain curves are given Figure 4.10, while all the mechanical properties; Tensile Strength ( $\sigma_{TS}$ ), Flexural Strength ( $\sigma_{Flex}$ ), Young's Modulus ( $E$ ), Flexural Modulus ( $E_{Flex}$ ), % Strain at Break ( $\% \epsilon_f$ ), Fracture Toughness ( $K_{IC}$  and  $G_{IC}$ ) values were compared in Figures 4.11 and 4.12. The data with standard deviations were tabulated in Table 4.4.





(a)



(b)

**Figure 4.9** SEM fractographs showing effects of POSS functional groups on the distribution and agglomeration level of the particles in PLA matrix, under magnifications of (a) 20000X and (b) 40000X

It was generally observed that due to the certain interfacial interactions between the PLA matrix and the organic functional groups of POSS structure, there were different levels of improvement in the mechanical properties of the PLA/POSS nanocomposites.

In terms of strength ( $\sigma_{TS}$  and  $\sigma_{Flex}$ ) and elastic modulus ( $E$  and  $E_{Flex}$ ) values, Figure 4.11 and Table 4.4 show that “propanediol” functional group on one of the corner of POSS structure resulted in slightly higher improvements compared to other POSS functional groups. This could be due to the higher efficiency of the pd-POSS structure on the strengthening and stiffening mechanisms of “load transfer” and “decreased chain mobility”. For this nanocomposite (i.e. PLA/pd-POSS) the increases in  $\sigma_{TS}$  and  $\sigma_{Flex}$  were 11% and 6%; while in  $E$  and  $E_{Flex}$  the increases were 5% and 16%, respectively.

On the other hand, in terms of fracture toughness ( $K_{IC}$  and  $G_{IC}$ ) values, Figure 4.12 and Table 4.4 indicate that the basic POSS structure having rather nonpolar “isobutyl” on its eight corner resulted in slightly higher improvements compared to other POSS structures having functional groups. This behavior could be due to the lower degree of interfacial interactions between the PLA matrix and the basic POSS structure having only “isobutyl” groups on its corners. Having lower degree of interfacial interactions lead to higher efficiency in the well-known toughening mechanisms of “debonding” and “pull-out”. For this nanocomposite (i.e. PLA/POSS) the increases in the values of  $K_{IC}$  and  $G_{IC}$  were 5% and 42%, respectively.

**Table 4.4** Tensile strength ( $\sigma_{TS}$ ), flexural strength ( $\sigma_{Flex}$ ), tensile modulus ( $E$ ), flexural modulus ( $E_{Flex}$ ); % strain at break (%  $\epsilon_f$ ) and fracture toughness ( $K_{IC}$  and  $G_{IC}$ ) values of the specimens with 1 wt% POSS having different functional groups

<b>Specimens</b>	<b><math>\sigma_{TS}</math> (MPa)</b>	<b><math>\sigma_{Flex}</math> (MPa)</b>	<b><math>E</math> (GPa)</b>	<b><math>E_{Flex}</math> (GPa)</b>	<b><math>\epsilon_f</math> (%)</b>	<b><math>K_{IC}</math> (MPa<math>\sqrt{m}</math>)</b>	<b><math>G_{IC}</math> (kJ/m<sup>2</sup>)</b>
<b>PLA</b>	56.04±0.57	94.80±1.5	2.71±0.07	3.16±0.07	5.11±0.05	3.75±0.04	6.28±0.41
<b>PLA/POSS</b>	56.80±0.89	97.43±2.3	2.87±0.01	3.36±0.11	5.64±0.90	3.92±0.10	8.92±1.17
<b>PLA/ap-POSS</b>	58.44±1.88	97.03±2.4	2.81±0.04	3.65±0.13	6.99±0.73	3.88±0.19	7.54±1.07
<b>PLA/pd-POSS</b>	62.11±1.24	100.78±4.6	2.84±0.02	3.67±0.18	6.20±0.50	3.80±0.04	6.86±0.08
<b>PLA/os-POSS</b>	60.02±0.80	99.11±1.7	2.79±0.01	3.56±0.10	5.45±0.01	3.90±0.08	8.73±1.12

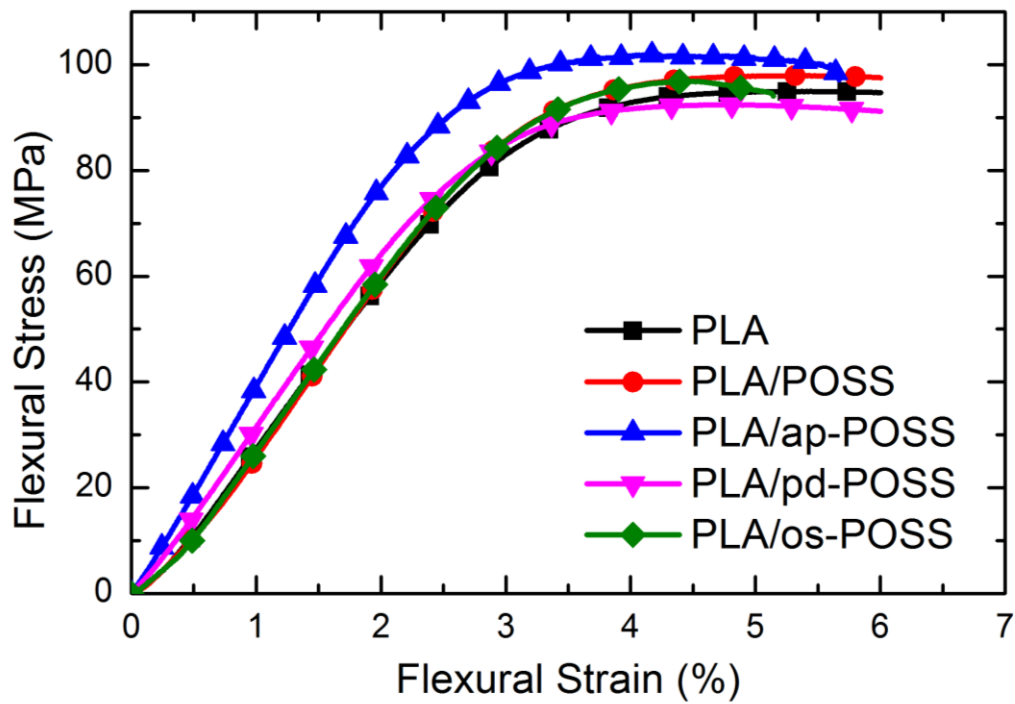
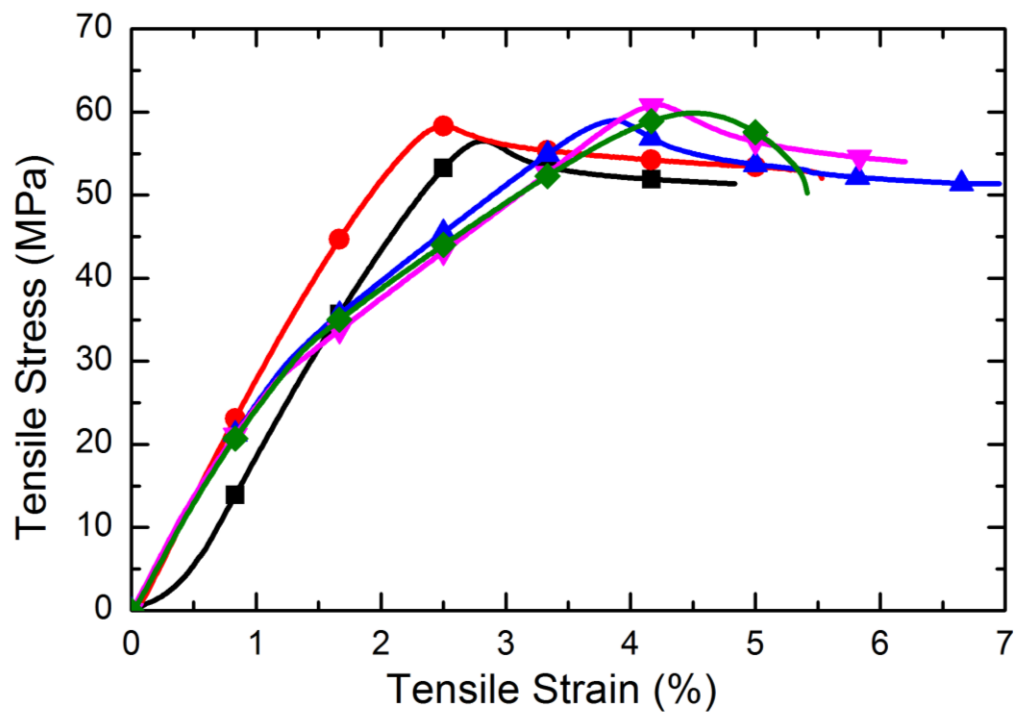


**Figure 4.10** Stress-Strain curves of the specimens, with 1 wt% POSS having different functional groups, obtained during tensile and 3-point bending flexural tests

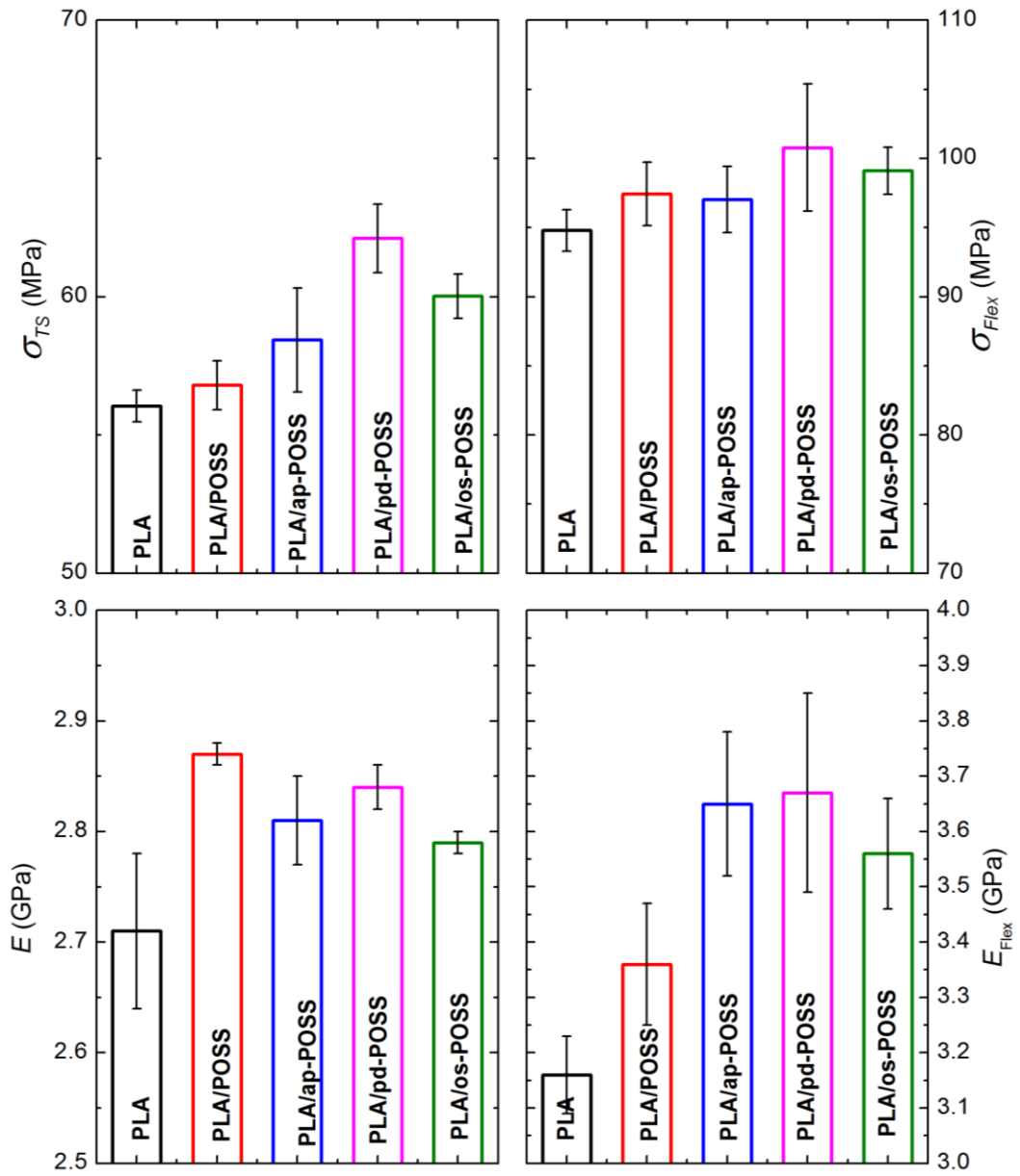


**Figure 4.11** Effects of POSS functional groups on the strength ( $\sigma_{TS}$  and  $\sigma_{Flex}$ ) and modulus ( $E$  and  $E_{Flex}$ ) values of the specimens

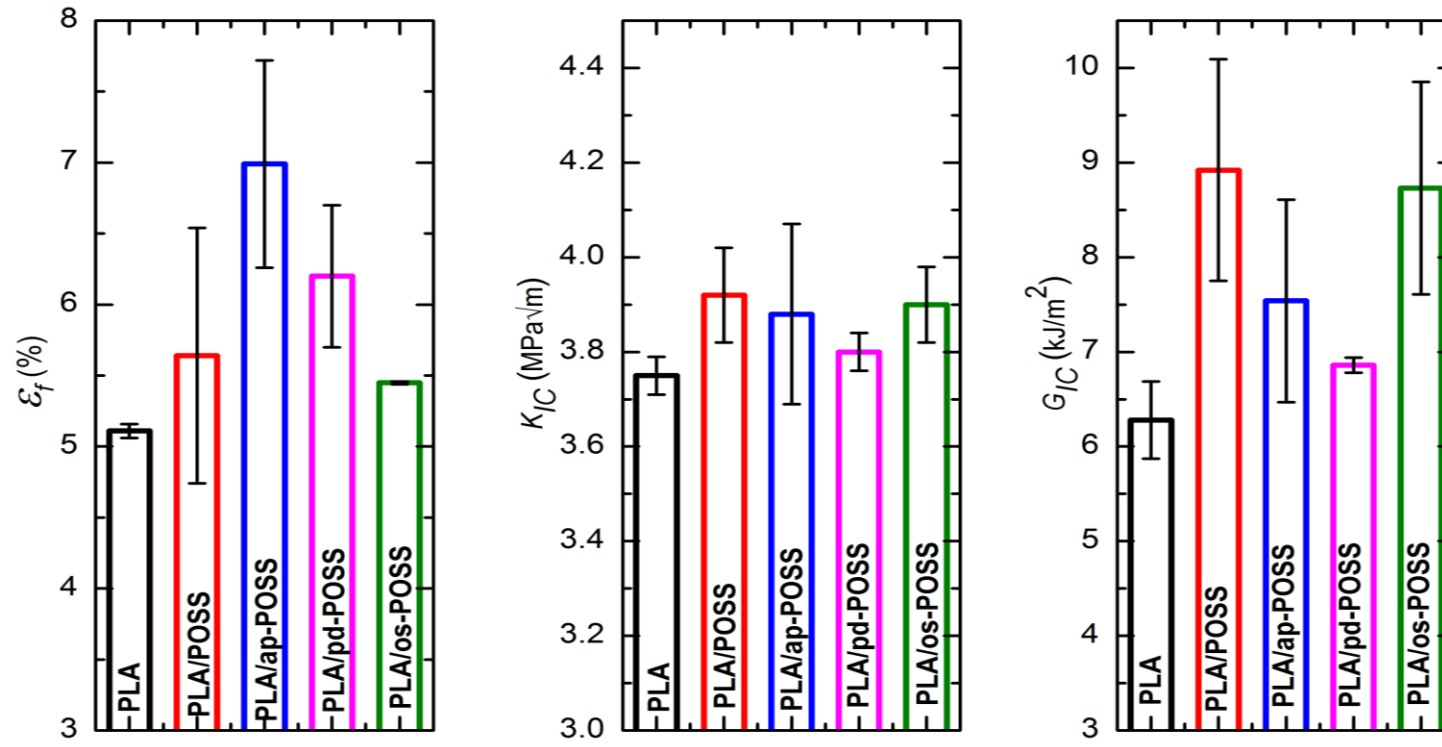


**Figure 4.12** Effects of POSS functional groups on the ductility ( $\% \epsilon_f$ ) and fracture toughness ( $K_{IC}$  and  $G_{IC}$ ) values of the specimens

Effects of POSS functional groups on the thermal behavior of the specimens were evaluated via first heating DSC curves and TG curves given in Figures 4.13 and 4.14, respectively. Data obtained from these curves are tabulated in Tables 4.5 and 4.6.

Figure 4.13 and Table 4.5 show that the most significant influence of using 1 wt% POSS having functional groups was the higher amounts of crystallinity (%  $X_C$ ). For instance, crystallinity amount of neat PLA increases as much as 3 times when filled with 1 wt% pd-POSS or os-POSS; this increase was 2 times when filled with basic POSS structure. Because, efficiency of the “nucleation agent” action of POSS particles would be higher when their at least one corner was functionalized leading to more homogeneous distribution in the PLA matrix.

Figure 4.14 and Table 4.6 reveal that, compared to basic POSS structure use of functionalized POSS structures (ap-POSS, pd-POSS, os-POSS) resulted in similar influences on the thermal degradation temperatures of the specimens.

**Table 4.5** Transition temperatures ( $T_g$ ,  $T_c$ ,  $T_m$ ), enthalpies ( $\Delta H_m$ ,  $\Delta H_c$ ) and crystallinity percent ( $X_C$ ) of the specimens with 1 wt% POSS having different functional groups, during DSC first heating profile

<b>Specimens</b>	$T_g$ (°C)	$T_c$ (°C)	$T_m$ (°C)	$\Delta H_m$ (J/g)	$\Delta H_c$ (J/g)	$X_C$ (%)
<b>PLA</b>	60.1	124.6	150.2	17.2	13.7	3.76
<b>PLA/POSS</b>	60.0	121.0	150.0	14.7	6.82	8.56
<b>PLA/ap-POSS</b>	61.7	117.0	148.0	27.9	19.0	9.67
<b>PLA/pd-POSS</b>	61.0	121.8	150.5	16.4	6.25	11.02
<b>PLA/os-POSS</b>	62.3	118.5	149.7	22.9	12.5	11.30

**Table 4.6** Thermal degradation temperatures ( $T_{5\%}$ ,  $T_{10\%}$ ,  $T_{25\%}$ ) of the specimens with 1 wt% POSS having different functional groups, at 5, 10 and 25 wt% mass losses, the maximum mass loss temperature ( $T_{max}$ ) and %Residue at 550°C

Specimens	$T_{5\%}$ (°C)	$T_{10\%}$ (°C)	$T_{25\%}$ (°C)	$T_{max}$ (°C)	%Residue at 550°C
PLA	332	342	353	362	0.16
PLA/POSS	327	337	349	365	0.36
PLA/ap-POSS	329	338	351	365	0.69
PLA/pd-POSS	331	340	353	369	0.45
PLA/os-POSS	329	336	347	362	0.78

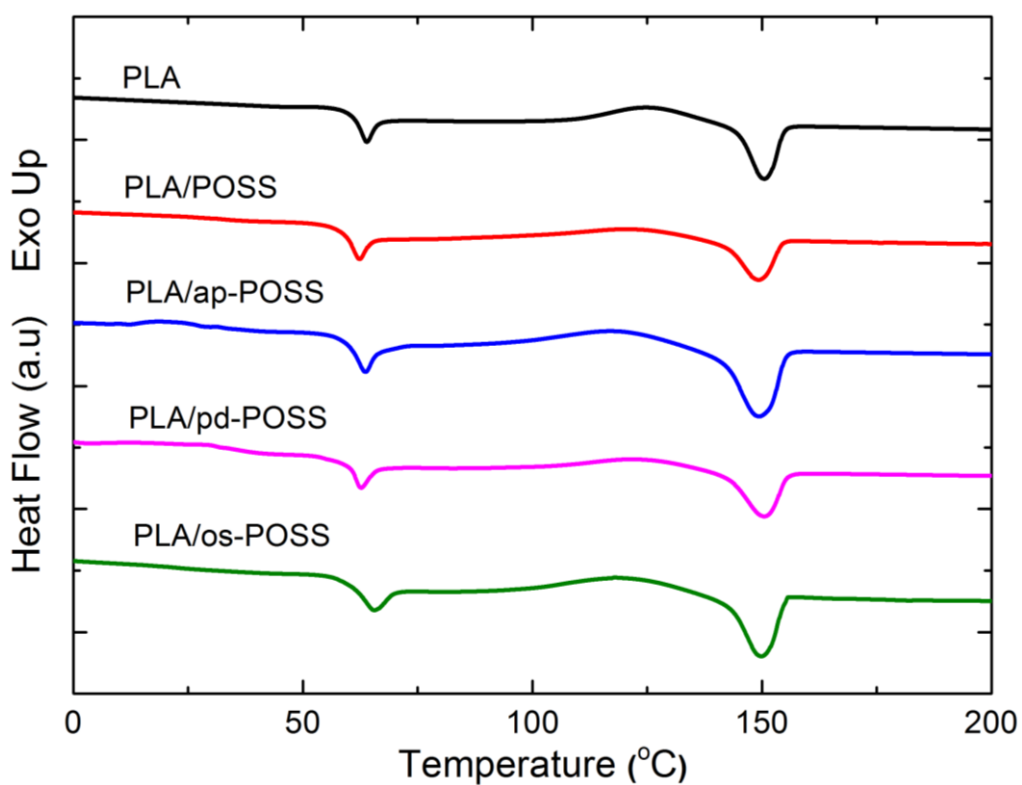


**Figure 4.13** First heating DSC thermograms of the specimens with 1 wt% POSS having different functional groups



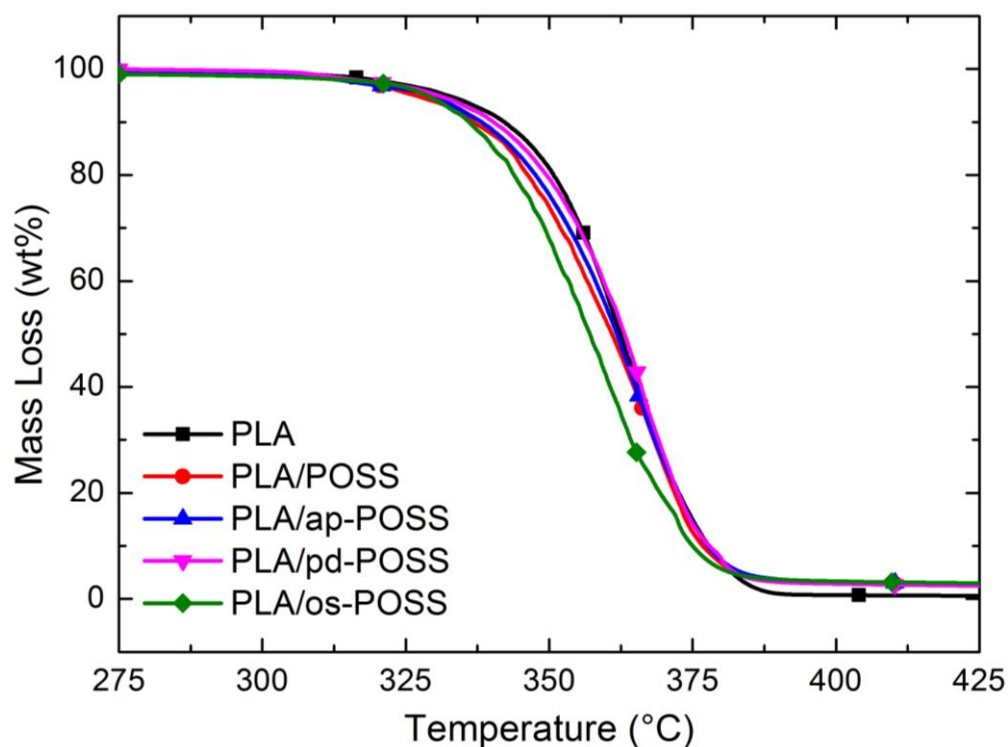


**Figure 4.14** Thermogravimetric curves of the specimens with 1 wt% POSS having different functional groups

#### 4.1.3 Effects of MA Compatibilization

It is known that interfacial interactions between polymer matrix chains and inorganic or organic fillers could be improved by using a suitable graft copolymer structure; in which their graft groups are attracted to the filler surfaces. This technique, which can be named as “graft copolymer compatibilization” is especially applied by using “Maleic Anhydride” (MA) grafts for many polymer matrices and for many fillers.

Thus, use of MA grafted PLA (PLA-g-MA) copolymer compatibilization technique for each specimen group was also conducted in order to reveal whether there would be further interfacial interaction improvement between the PLA matrix and basic and functionalized POSS structures.

For simplicity, “PLA-g-MA” copolymer is designated as “gMA”. Details of the production method of this gMA copolymer was explained in our former study [109]. Since PLA matrix nanocomposites were produced again using only 1 wt% of each POSS structures and 2 wt% of gMA copolymer, these wt%’s are not indicated in the designation of the specimens.

In order to reveal possible interfacial interactions between MA and other groups, ATR-FTIR analyses were conducted first for the PLA-g-MA copolymer (i.e. gMA) and then for all nanocomposite groups having gMA compatibilization, as given in Figure 4.15.

It is known that [116] the distinctive IR bands for MA structure are cyclic C=C stretching peak at  $1590\text{ cm}^{-1}$ , asymmetric C=O stretching vibration at  $1774\text{ cm}^{-1}$  and symmetric C=O stretching vibration at around  $1850\text{ cm}^{-1}$ . As discussed in detail in our former study [109] and indicated in the first spectrum of Figure 4.15, when PLA was grafted with MA, the most significant evidence is the absence of the cyclic C=C stretching peak of MA structure at  $1590\text{ cm}^{-1}$  due to chemical interaction between PLA and MA structure.

Other spectrums in Figure 4.15 belong to PLA matrix nanocomposites filled with 1 wt% four different POSS particles and 2 wt% gMA copolymer. Unfortunately, due to the very low amounts of the ingredients and overlapping of the common IR bands in these nanocomposites, it was very difficult to speculate those possible interfacial interactions between MA and functional groups of the POSS structures.

Since it was difficult via ATR-FTIR analyses, the second analyses conducted to reveal the effects of MA compatibilization on the interfacial interactions was SEM examination of the fracture surfaces of all specimen groups. Compared to the SEM fractographs of the previous section (i.e. Figure 4.9); it is seen in Figure 4.16 that use

of MA compatibilization had no detrimental effects on the interfacial morphology between PLA matrix and basic POSS and os-POSS particles.

On the other hand, it was very obvious in Figure 4.16 that, there were certain levels of “debonding” and “pull-out” when PLA matrix was filled with ap-POSS and pd-POSS particles. As will be seen in the following paragraphs, there was also substantial reductions in the mechanical properties of these specimens. Therefore, it could be speculated that use of MA compatibilization resulted in no additional interfacial interactions between PLA matrix and ap-POSS and pd-POSS particles.

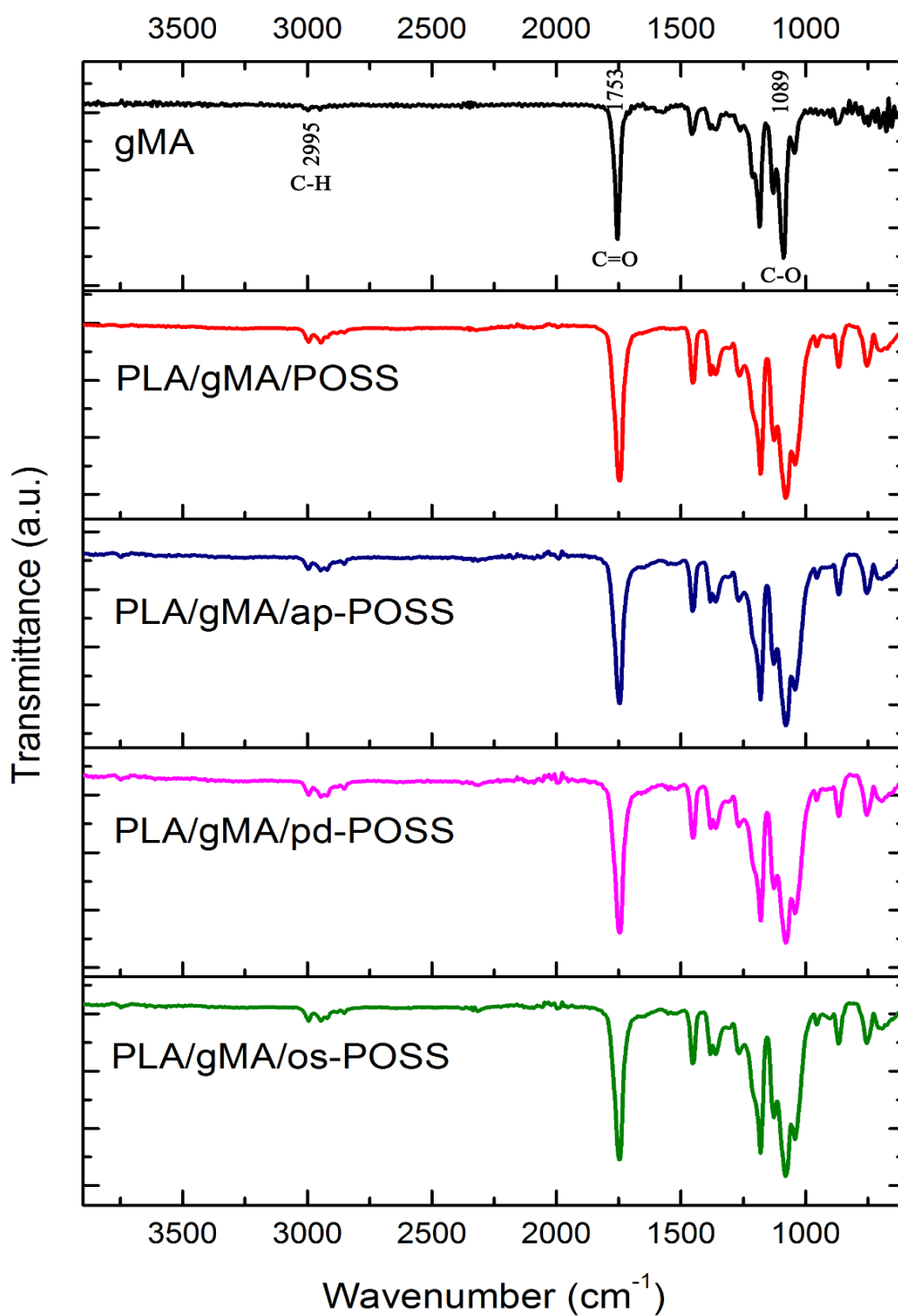
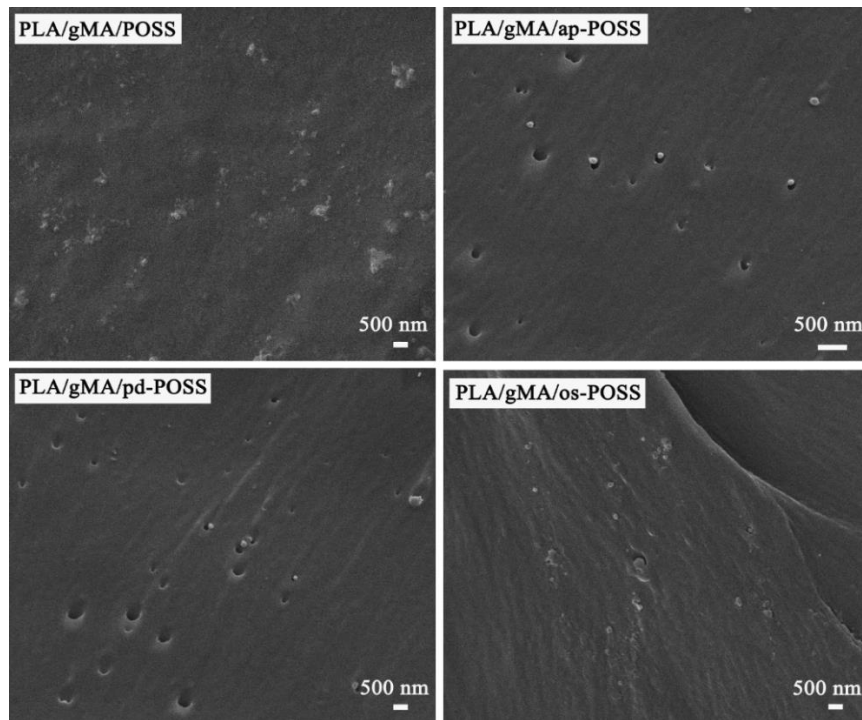
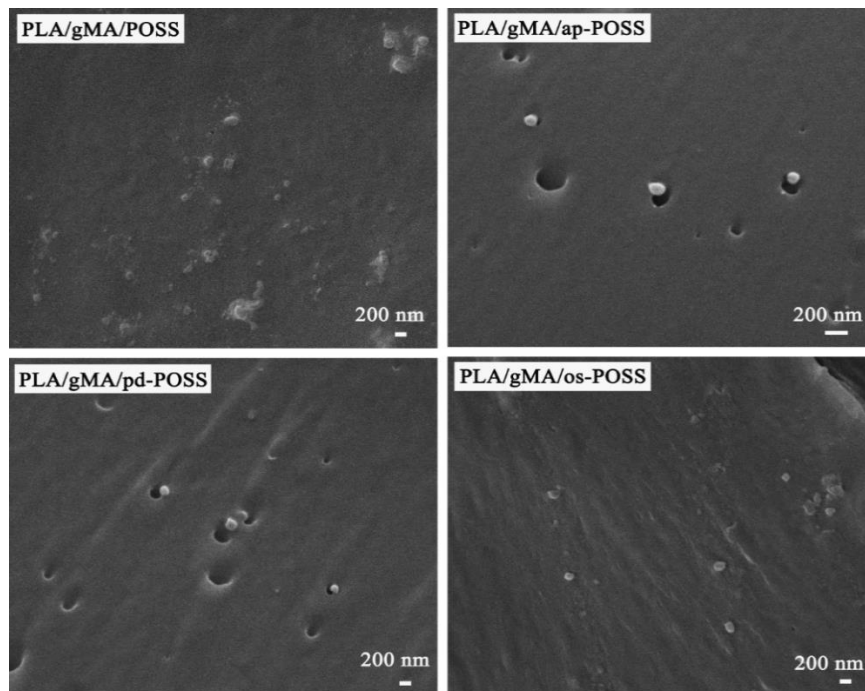


**Figure 4.15** ATR-FTIR spectra of the PLA-g-MA (i.e. gMA) copolymer and all PLA matrix nanocomposites with MA compatibilization



(a)



(b)

**Figure 4.16** SEM fractographs showing effects of MA compatibilization on the interfacial morphology between PLA matrix and all POSS structures, under the magnifications of (a) 20000X and (b) 40000X

Then, the same mechanical tests mentioned before were applied for all nanocomposite specimen groups after their MA compatibilization. Stress-Strain curves of these specimens were compared in Figure 4.17, while values of all mechanical properties (strength, modulus, ductility, fracture toughness) of the specimens before and after MA compatibilization were compared in Figures 4.18 and 4.19; and tabulated in Table 4.7 with standard deviations.

Generally, it was seen in these figures and table that, due to the improved interfacial interactions, all mechanical properties of the nanocomposites filled with 1 wt% basic POSS and functionalized os-POSS particles were increased after their MA compatibilization.

For instance, because of the higher efficiency in strengthening and stiffening mechanisms, Figure 4.18 and Table 4.7 indicate that, compared to neat PLA the increase in flexural strength ( $\sigma_{Flex}$ ) was 3% when filled with 1 wt% basic POSS particles; in which after MA compatibilization this increase was risen to 8%. Similarly, the increase in flexural modulus ( $E_{Flex}$ ) was 13% when filled with 1 wt% os-POSS particles; in which after MA compatibilization this increase was risen to 19%.

Again, due to the further improvements in the toughening mechanisms, Figure 4.19 and Table 4.7 show that the increase in  $K_{IC}$  fracture toughness for the PLA/POSS was 5%, while that increase was risen to 7.5% for the PLA/gMA/POSS specimen. Similarly, the increase in  $G_{IC}$  fracture toughness for PLA/os-POSS was 39%, while that increase was risen to 58% for the PLA/g-MA/os-POSS specimen.

**Table 4.7** Tensile strength ( $\sigma_{TS}$ ), flexural strength ( $\sigma_{Flex}$ ), tensile modulus ( $E$ ), flexural modulus ( $E_{Flex}$ ); % strain at break ( $\% \epsilon_f$ ) and fracture toughness ( $K_{IC}$  and  $G_{IC}$ ) values of the specimens before and after MA compatibilization

Specimens	$\sigma_{TS}$ (MPa)	$\sigma_{Flex}$ (MPa)	$E$ (GPa)	$E_{Flex}$ (GPa)	$\epsilon_f$ (%)	$K_{IC}$ (MPa $\sqrt{m}$ )	$G_{IC}$ (kJ/m <sup>2</sup> )
<b>PLA</b>	56.04±0.57	94.80±1.5	2.71±0.07	3.16±0.07	5.11±0.05	3.75±0.04	6.28±0.41
<b>PLA/POSS</b>	56.80±0.89	97.43±2.3	2.87±0.01	3.36±0.11	5.64±0.90	3.92±0.10	8.92±1.17
<b>PLA/gMA/POSS</b>	58.08±0.95	102.41±5.24	2.92±0.19	3.59±0.22	6.18±0.65	4.03±0.08	9.54±1.11
<b>PLA/ap-POSS</b>	58.44±1.88	97.03±2.4	2.81±0.04	3.65±0.13	6.99±0.73	3.88±0.19	7.54±1.07
<b>PLA/gMA/ap-POSS</b>	46.69±4.05	90.00±2.91	2.80±0.05	3.31±0.14	3.48±1.32	3.63±0.05	7.02±0.32
<b>PLA/pd-POSS</b>	62.11±1.24	100.78±4.6	2.84±0.02	3.67±0.18	6.20±0.50	3.80±0.04	6.86±0.08
<b>PLA/gMA/pd-POSS</b>	51.36±3.67	92.66±4.53	2.81±0.03	3.33±0.22	4.35±1.86	3.37±0.17	5.91±0.94
<b>PLA/os-POSS</b>	60.02±0.80	99.11±1.7	2.79±0.01	3.56±0.10	5.45±0.01	3.90±0.08	8.73±1.12
<b>PLA/gMA/os-POSS</b>	61.25±1.25	102.57±5.76	3.02±0.05	3.75±0.26	5.51±1.23	4.14±0.14	9.93±1.14

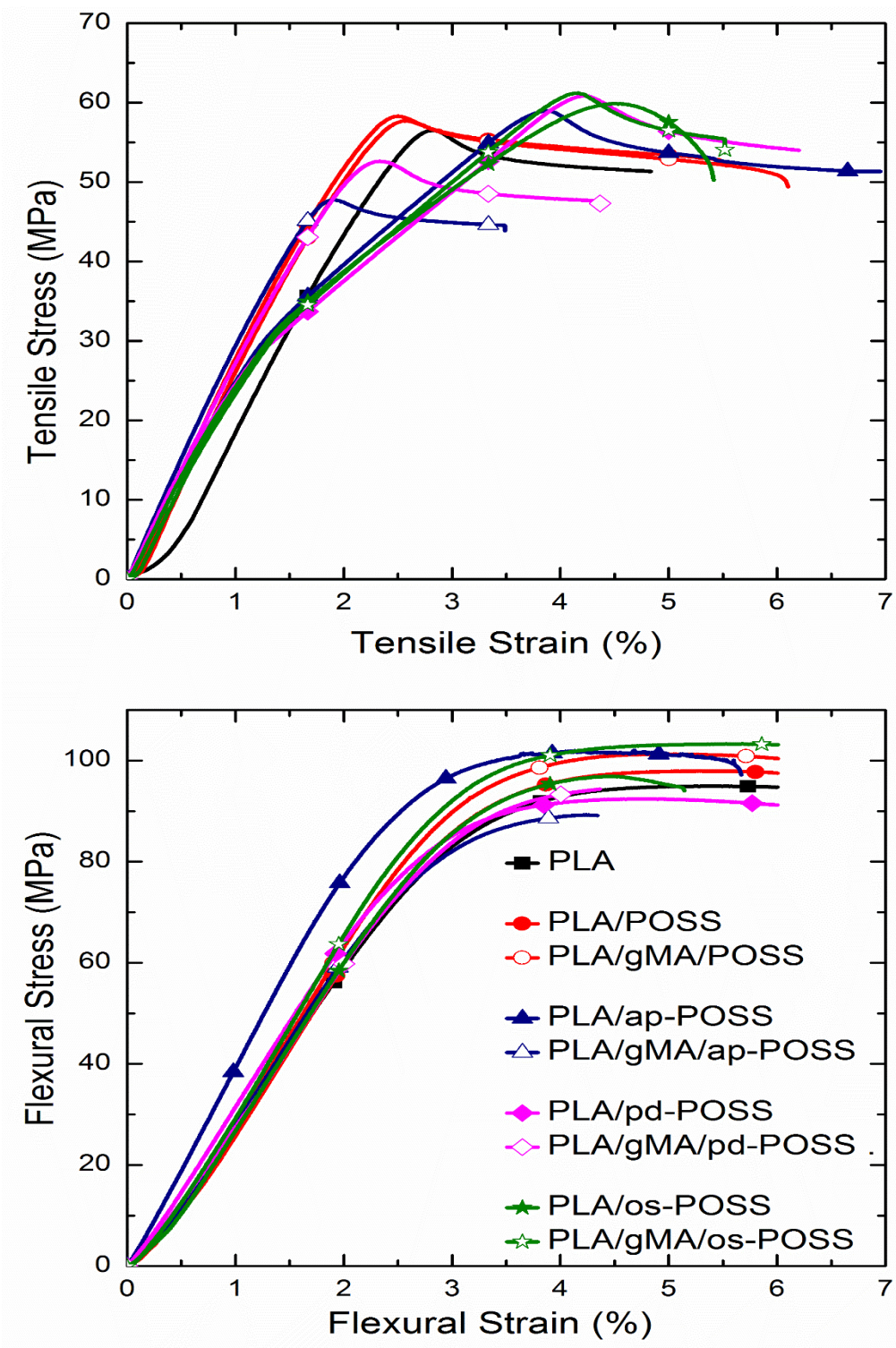


**Figure 4.17** Stress-Strain curves of the specimens, before and after MA compatibilization, obtained during tensile and 3-point bending flexural tests



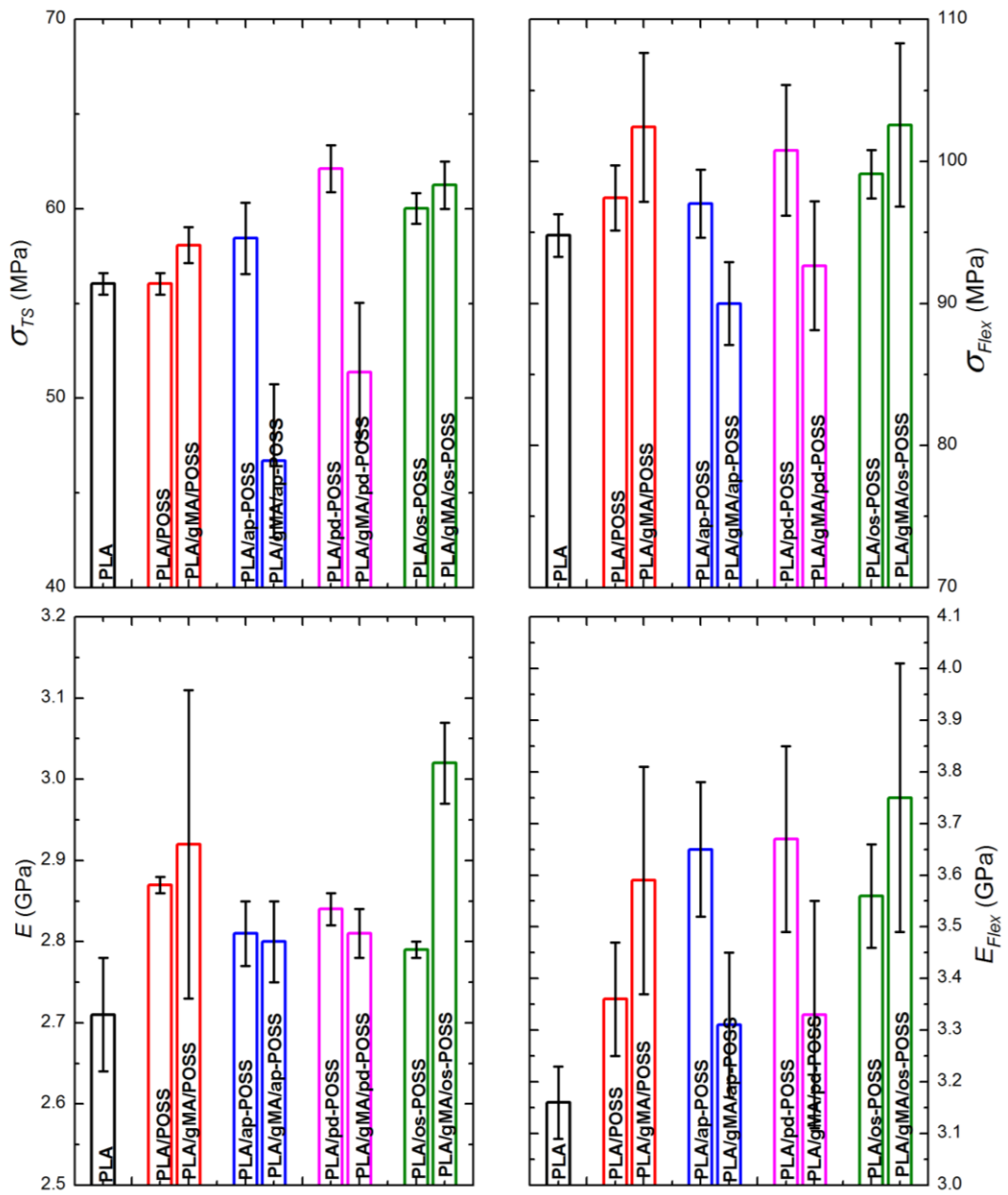


**Figure 4.18** Effects of MA compatibilization on the strength ( $\sigma_{TS}$  and  $\sigma_{Flex}$ ) and modulus ( $E$  and  $E_{Flex}$ ) values of the specimens

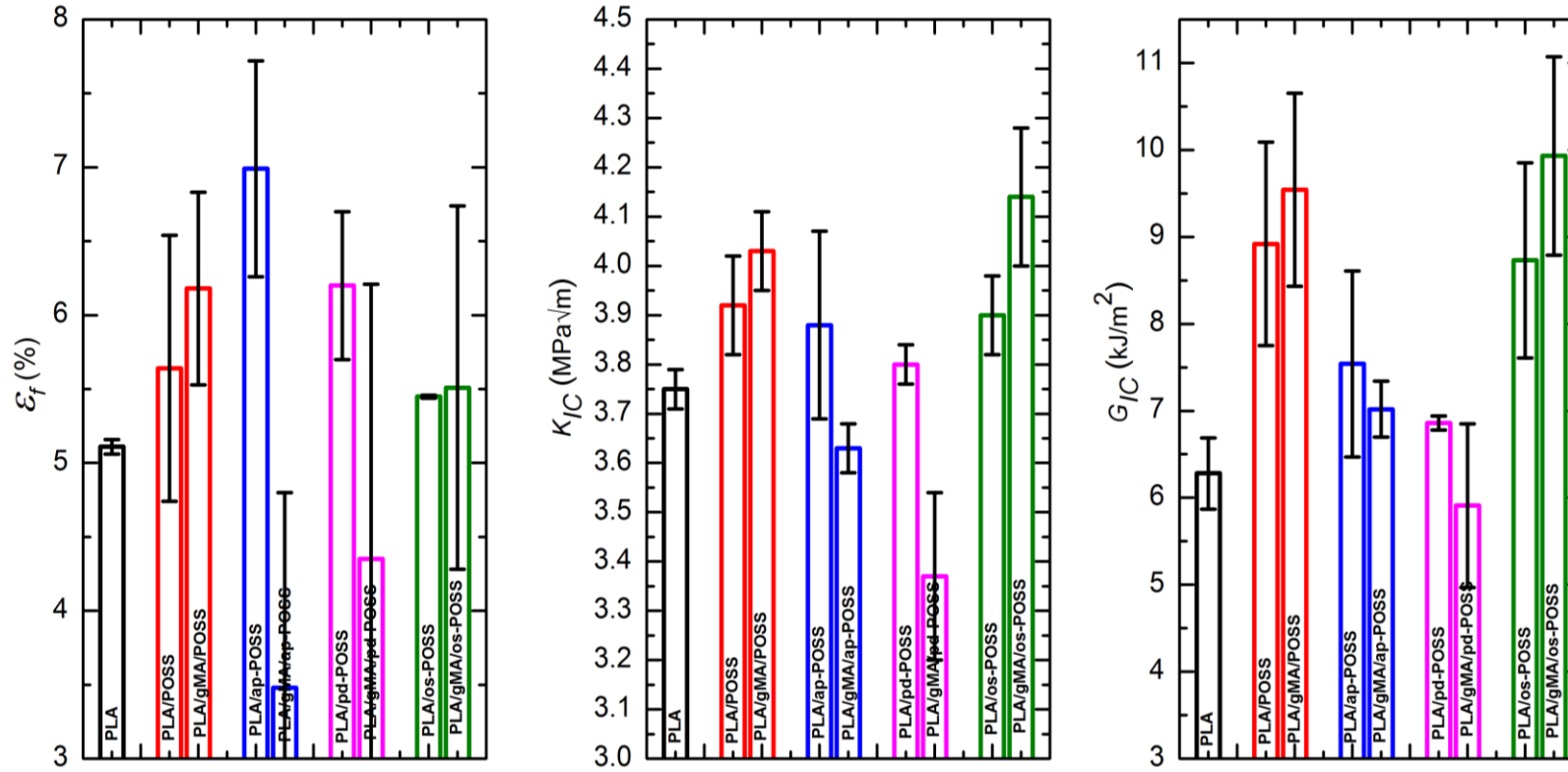


**Figure 4.19** Effects of MA compatibilization on the ductility ( $\epsilon_f$ ) and fracture toughness ( $K_{IC}$  and  $G_{IC}$ ) values of the specimens

On the other hand, Figures 4.18, 4.19 and Table 4.7 indicate that, due to the no further improvements in the strengthening, stiffening and toughening mechanisms, all mechanical properties of the PLA matrix composites filled with ap-POSS and pd-POSS particles decreased substantially after their MA compatibilization.

Changes in the thermal behavior of the PLA matrix nanocomposites before and after MA compatibilization were evaluated by DSC and TG analyses as shown in Figures 4.20 and 4.21, respectively; while the data obtained were tabulated in Tables 4.8 and 4.9.

Figure 4.20 and Table 4.8 reveal that the most significant change in the DSC analyses was the reductions in the crystallinity amounts ( $\%X_C$ ) of the PLA matrix nanocomposites after their MA compatibilization. It can be speculated that the reason for these reductions might be due to the reduced conformational mobility of the matrix chains required for crystallization.

TGA results in Figure 4.21 and Table 4.9 show that all thermal degradation temperatures ( $T_{5\%}$ ,  $T_{10\%}$ ,  $T_{25\%}$ ,  $T_{max}$ ) including %Residue values of the nanocomposite specimens increased substantially after their MA compatibilization.

**Table 4.8** Transition temperatures ( $T_g$ ,  $T_c$ ,  $T_m$ ), enthalpies ( $\Delta H_m$ ,  $\Delta H_c$ ) and crystallinity percent ( $\%X_C$ ) of the specimens, before and after MA compatibilization, during DSC first heating profile

<b>Specimens</b>	<b><math>T_g</math> (°C)</b>	<b><math>T_c</math> (°C)</b>	<b><math>T_m</math> (°C)</b>	<b><math>\Delta H_m</math> (J/g)</b>	<b><math>\Delta H_c</math> (J/g)</b>	<b><math>X_C</math> (%)</b>
<b>PLA</b>	60.1	124.6	150.2	17.2	13.7	3.76
<b>PLA/POSS</b>	60.0	121.0	150.0	14.7	6.82	8.56
<b>PLA/gMA/POSS</b>	62.5	120.6	151.2	12.1	5.35	7.48
<b>PLA/ap-POSS</b>	61.7	117.0	148.0	27.9	19.0	9.67
<b>PLA/gMA/ap-POSS</b>	60.7	116.4	150.6	17.7	11.1	7.32
<b>PLA/pd-POSS</b>	61.0	121.8	150.5	16.4	6.25	11.02
<b>PLA/gMA/pd-POSS</b>	60.8	115.7	149.1	18.3	13.1	5.76
<b>PLA/os-POSS</b>	62.3	118.5	149.7	22.9	12.5	11.30
<b>PLA/gMA/os-POSS</b>	61.2	121.2	150.5	9.02	4.53	4.98

**Table 4.9** Thermal degradation temperatures ( $T_{5\%}$ ,  $T_{10\%}$ ,  $T_{25\%}$ ) of the specimens, before and after MA compatibilization, at 5, 10 and 25 wt% mass losses, the maximum mass loss temperature ( $T_{max}$ ) and %Residue at 550°C

<b>Specimens</b>	<b><math>T_{5\%}</math> (°C)</b>	<b><math>T_{10\%}</math> (°C)</b>	<b><math>T_{25\%}</math> (°C)</b>	<b><math>T_{max}</math> (°C)</b>	<b>%Residue at 550°C</b>
<b>PLA</b>	332	342	353	362	0.16
<b>PLA/POSS</b>	327	337	349	365	0.36
<b>PLA/gMA/POSS</b>	331	343	354	368	0.59
<b>PLA/ap-POSS</b>	329	338	351	365	0.69
<b>PLA/gMA/ap-POSS</b>	329	339	352	368	0.75
<b>PLA/pd-POSS</b>	331	340	353	369	0.45
<b>PLA/gMA/pd-POSS</b>	335	345	356	369	0.76
<b>PLA/os-POSS</b>	329	336	347	362	0.78
<b>PLA/gMA/os-POSS</b>	333	342	354	369	1.13

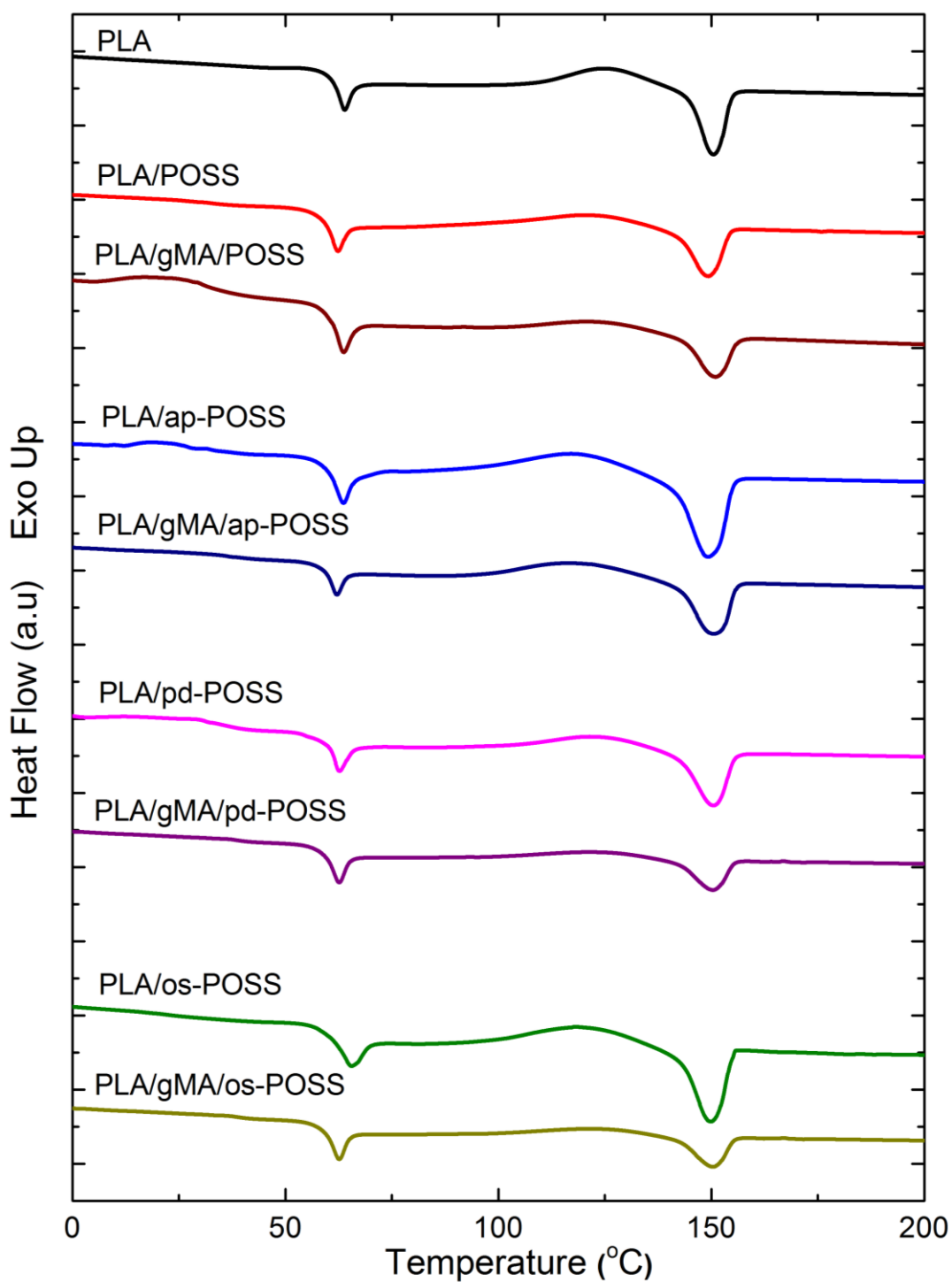


**Figure 4.20** First heating DSC thermograms of the specimens before and after MA compatibilization

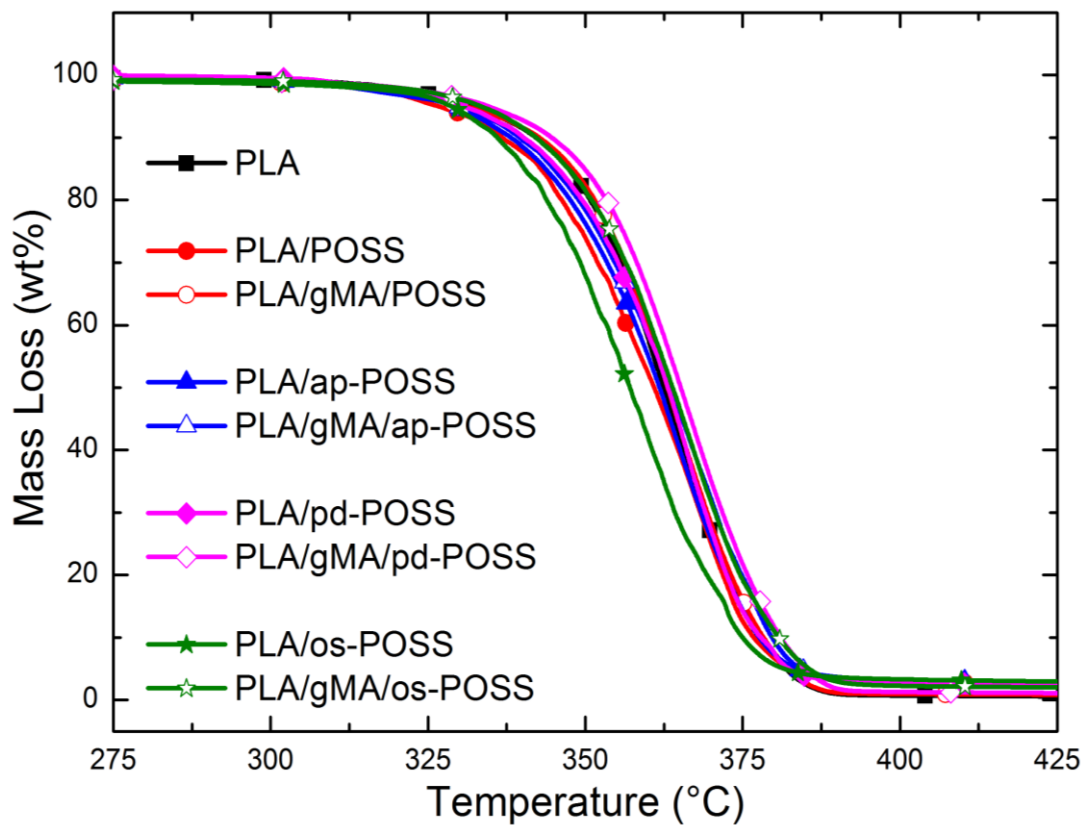


**Figure 4.21** Thermogravimetric curves of the specimens before and after MA compatibilization

#### **4.2 Effects of 3D-Printing on the Behavior of PLA/POSS Nanocomposites Compared with Their Compression Molded Counterparts**

In the following three sub-sections, comparison of the 3D-printed and compression molded specimens were evaluated first in the form of appearances, and then in terms of mechanical properties and thermal behavior. In the fourth sub-section, behavior of the only 3D-printed specimens in a physiological (PBS) solution was also discussed.

#### **4.2.1 Appearances of the 3D-Printed and Compression Molded Specimens**

In order to observe whether there would be certain differences or not in the physical appearances of the 3D-printed and compression molded mechanical test (tension, flexural, fracture toughness) specimens, they were first examined physically and photographically. It was generally observed that there were no significant differences in the physical appearances of the specimens. It should be mentioned that, compared to the smooth surfaces of the compression molded specimens, 3D-printed specimen surfaces were rather textured slightly due to  $\pm 45^\circ$  raster orientation used during printing. Figure 4.22 compares appearances of only flexural and fracture toughness test specimens.

Then, in order to observe possible differences on the fracture surface morphology and particle distribution degree of the 3D-printed and compression molded specimens, SEM analysis (under 40000X magnification) were conducted on the fracture surfaces of the fracture toughness test specimens (Figure 4.23).

It was very clear in Figure 4.23 that, both 3D-printed and compression molded neat PLA specimens have very smooth fracture surface morphology which represents inherently very brittle PLA structure. In terms of the degree of the particle distribution in PLA matrix, Figure 4.23 also shows that, POSS nanoparticles in the 3D-printed specimens were distributed rather more uniformly compared to the compression molded specimens. Thus, as will be discussed in the following subsection, 3D-printed PLA/POSS specimens had rather higher mechanical properties compared to compression molded ones.

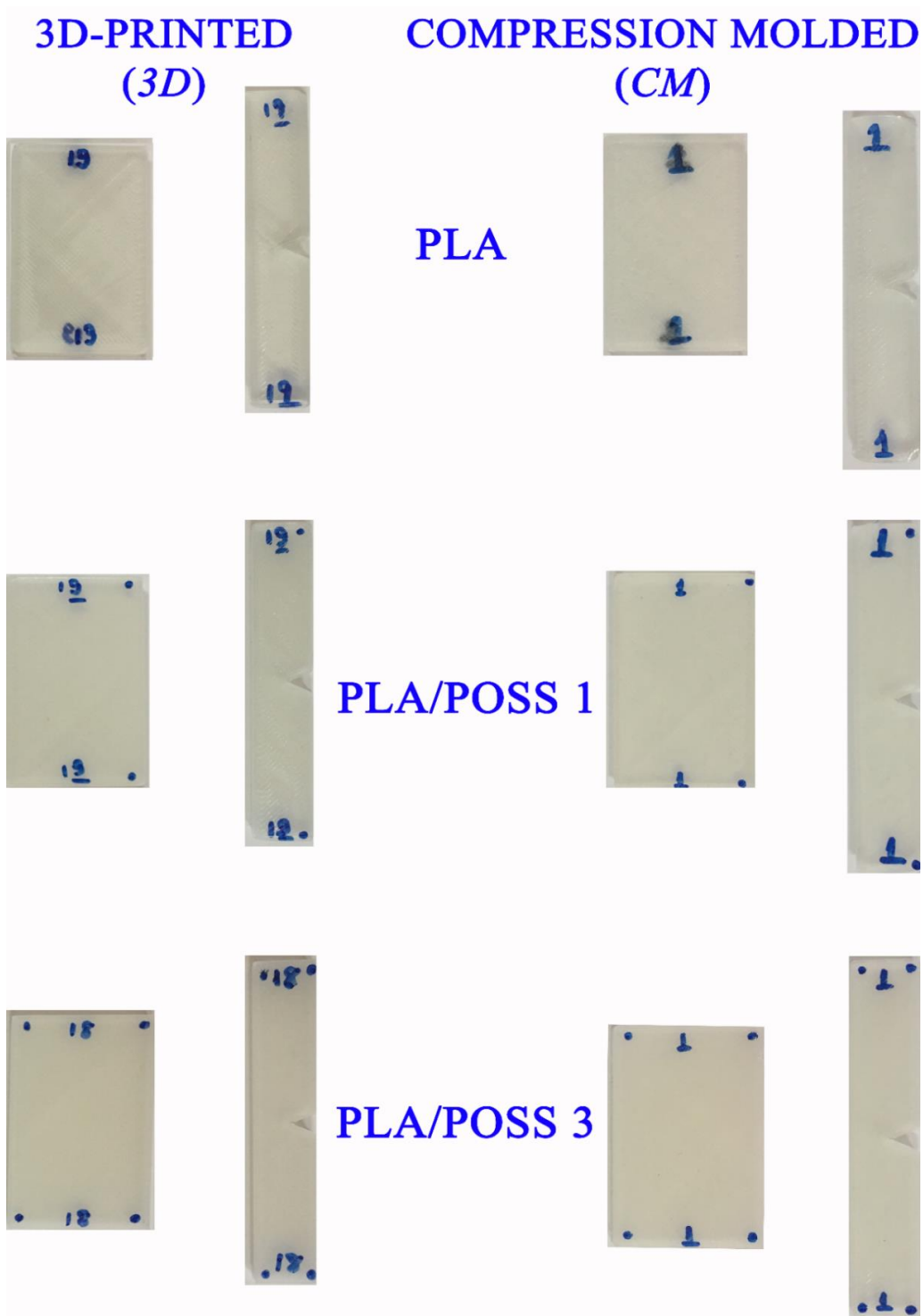


**Figure 4.22** Images of the 3D-printed and compression molded specimens shaped for flexural and fracture toughness tests



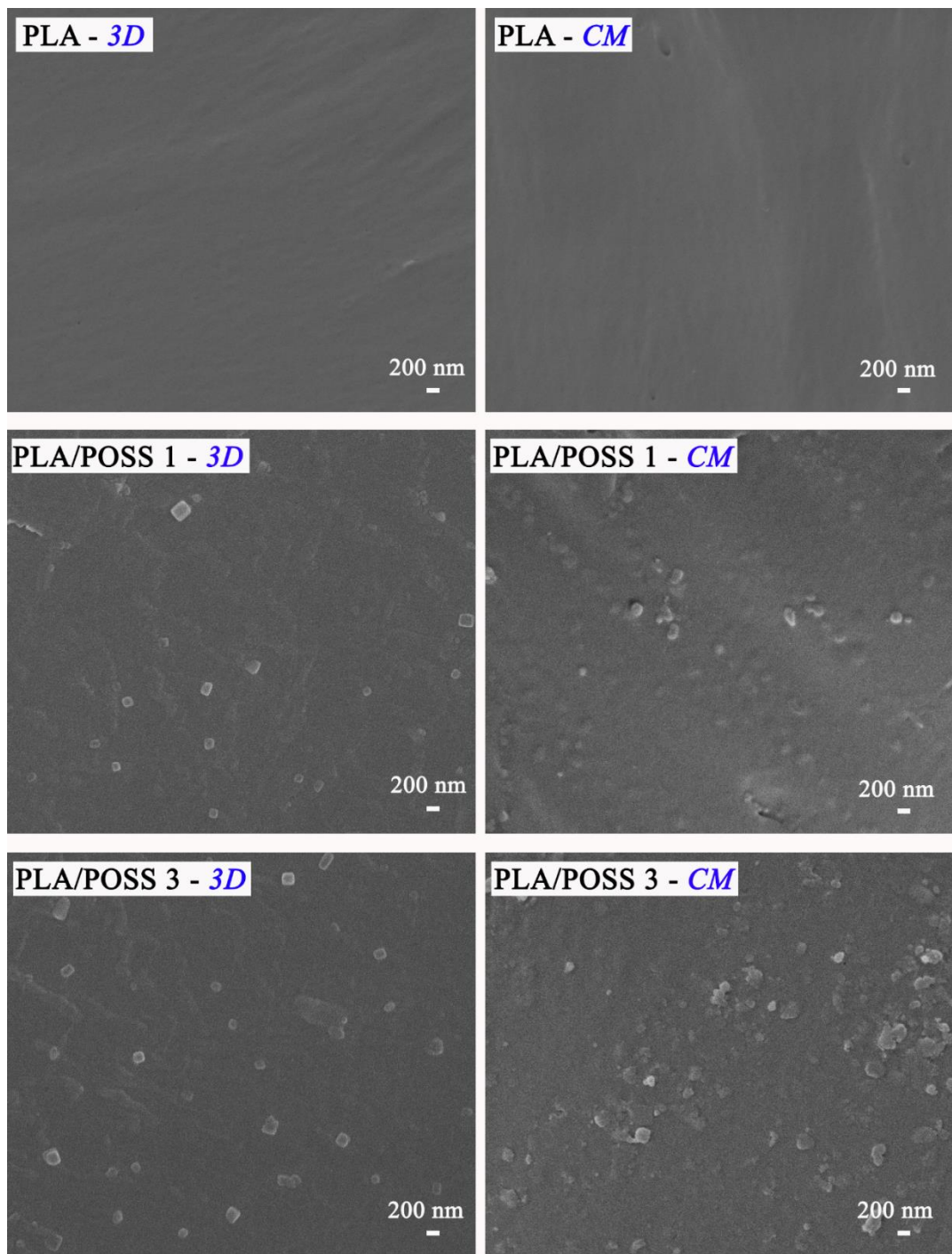


**Figure 4.23** SEM fractographs of the 3D-printed and compression molded specimens

**4.2.2 Mechanical Properties of the 3D-Printed and Compression Molded Specimens**

In order to determine the differences in the mechanical performance of the 3D-printed PLA/POSS nanocomposite (1 and 3 wt% filled) specimens compared to their compression molded counterparts, including their neat PLA specimens, various mechanical tests were conducted. First of all, to compare “strength” and “stiffness” (i.e. elastic modulus) of the specimens under two different loading conditions; both “Tension Tests” and three-point bending type “Flexural Tests” were performed. Figures 24 and 25 show “tensile stress-strain curves” and “flexural stress-strain curves” obtained from the 3D-printed and compression molded specimens, respectively. Then, values of “Tensile Strength ( $\sigma_{TS}$ )”, “Flexural Strength ( $\sigma_{Flex}$ )”, “Tensile Modulus ( $E$ )”, and “Flexural Modulus ( $E_{Flex}$ )” determined from these curves are tabulated in Table 4.10, as average values with standard deviations.

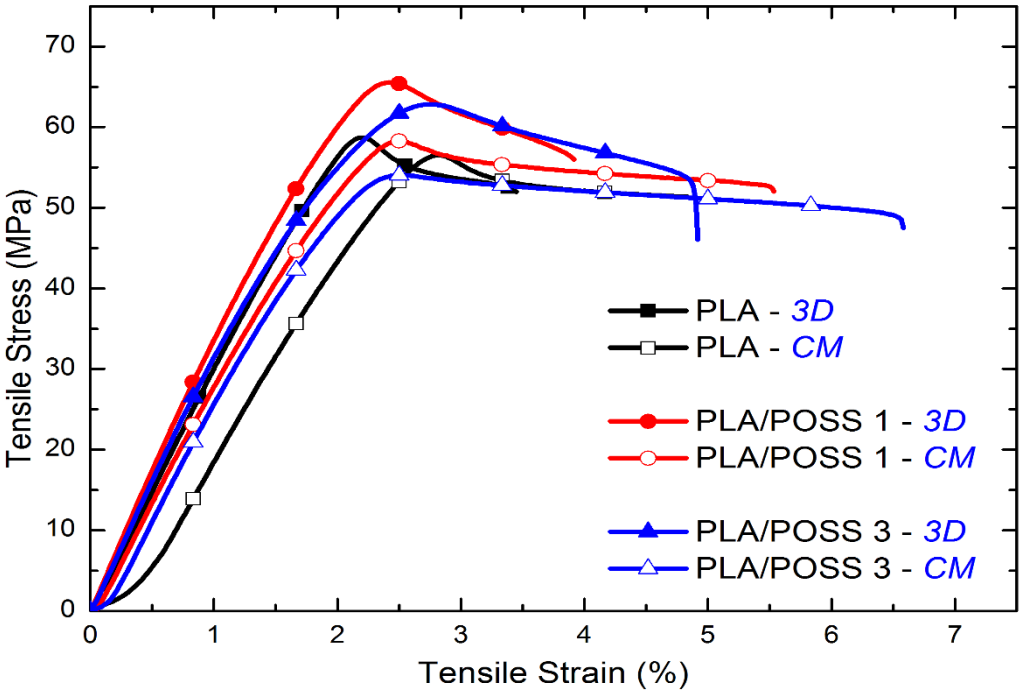


**Figure 4.24** Tensile stress-strain curves of the 3D-printed and compression molded specimens

**Table 4.10** Tensile strength ( $\sigma_{TS}$ ), flexural strength ( $\sigma_{Flex}$ ), tensile modulus ( $E$ ), flexural modulus ( $E_{Flex}$ ), and fracture toughness ( $K_{IC}$  and  $G_{IC}$ ) of the 3D-printed and compression molded specimens

<b>Specimens</b>	<b><math>\sigma_{TS}</math> (MPa)</b>	<b><math>\sigma_{Flex}</math> (MPa)</b>	<b><math>E</math>(GPa)</b>	<b><math>E_{Flex}</math> (GPa)</b>	<b><math>K_{IC}</math>(MPa<math>\sqrt{m}</math>)</b>	<b><math>G_{IC}</math> (kJ/m<sup>2</sup>)</b>
<b>PLA - 3D</b>	58.40±0.30	97.20±1.4	3.11±0.03	3.93±0.21	5.03±0.20	7.32±0.66
<b>PLA - CM</b>	56.04±0.57	94.80±1.5	2.71±0.07	3.16±0.07	3.75±0.04	6.28±0.41
<b>PLA/POSS 1 - 3D</b>	64.64±1.64	118.76±6.29	3.36±0.16	4.30±0.12	5.60±0.07	15.85±0.67
<b>PLA/POSS 1 - CM</b>	56.80±0.89	97.43±2.30	2.87±0.01	3.36±0.11	3.92±0.10	8.92±1.17
<b>PLA/POSS 3 - 3D</b>	62.49±0.49	116.51±2.39	3.24±0.09	4.39±0.09	5.38±0.05	15.53±0.67
<b>PLA/POSS 3 - CM</b>	54.24±0.27	91.76±2.90	2.87±0.01	3.19±0.09	4.16±0.06	11.14±0.94

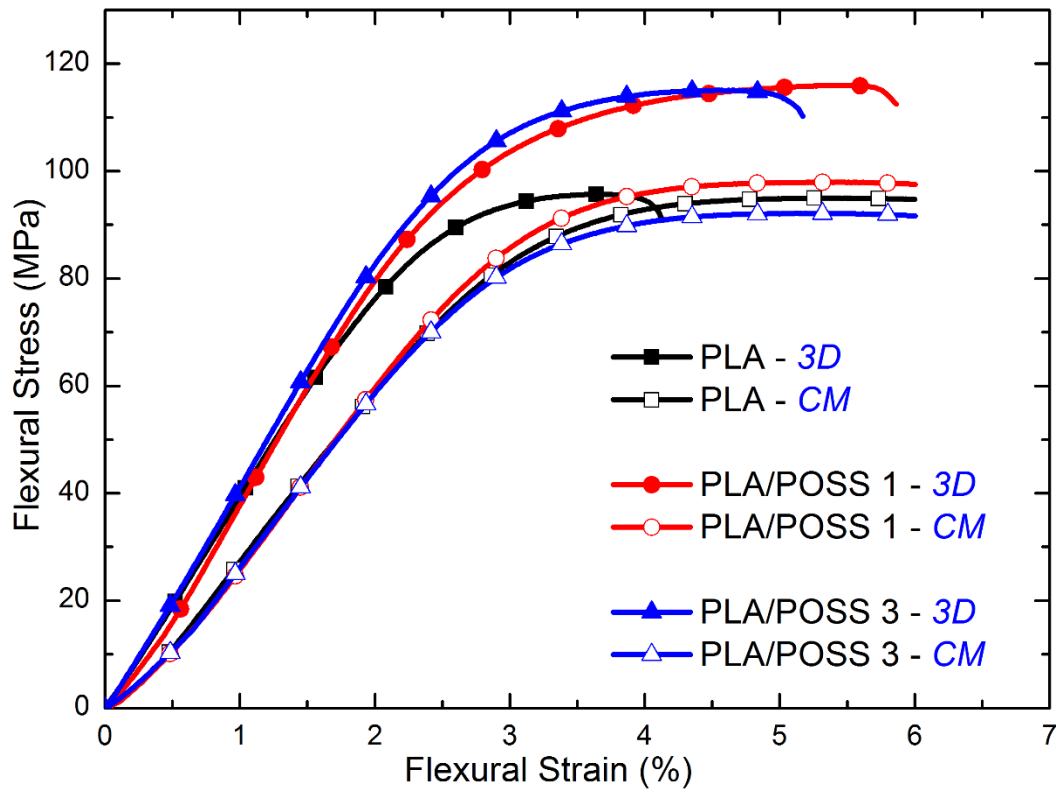


**Figure 4.25** Flexural stress-strain curves of the 3D-printed and compression molded specimens

Moreover, in order to compare strength and stiffness performance of the 3D-printed specimens with respect to compression molded specimens, both tensile and flexural strength data and elastic modulus data were re-evaluated in Figures 4.26 and 4.27, respectively. Note that, %increase values given on top of the columns for PLA/POSS 1 and PLA/POSS 3 nanocomposite specimens were determined as compared to their 3D-printed and compression molded neat PLA specimens.

These figures clearly show that, regardless of the shaping processes of 3D-printing or compression molding, when neat PLA matrix was reinforced with POSS nanoparticles, both strength and elastic modulus values were improved. It is known that two basic “strengthening/stiffening mechanisms”; i.e. “load transfer from the matrix to stronger/stiffer reinforcement” and “the decrease in the macromolecular

chain structure of the matrix by the reinforcements” are also valid in the PLA/POSS composite system.

Nanoparticles having superior Surface Area to Volume (A/V) ratio would be very effective in these strengthening/stiffening mechanisms of composites mentioned above. Of course, uniform distribution of the nanoparticles is a pre-requirement. Since in the second part of this thesis use of 1 wt% POSS particles resulted in more uniform distribution compared to 3 wt% POSS particles, it was generally observed that the improvements in the strength and elastic modulus values of the PLA/POSS 1 specimens were better compared to the PLA/POSS 3 specimens.

Figures 4.26 and 4.27 also revealed that the improvements in the strength and elastic modulus values of the 3D-printed specimens are higher compared to compression molded ones. For example, compared to their neat PLA specimens, the increases in the  $\sigma_{TS}$  and  $\sigma_{Flex}$  values of the 3D-printed PLA/POSS 1 specimen were 11% and 22%, respectively; while these increases in the compression molded specimen were only 0.7% and 3%. Similarly, the increases in the  $E$  and  $E_{Flex}$  values of the PLA/POSS 1 - 3D specimen were 8% and 9%, respectively; while they were only 6% for the PLA/POSS 1 - CM specimen.

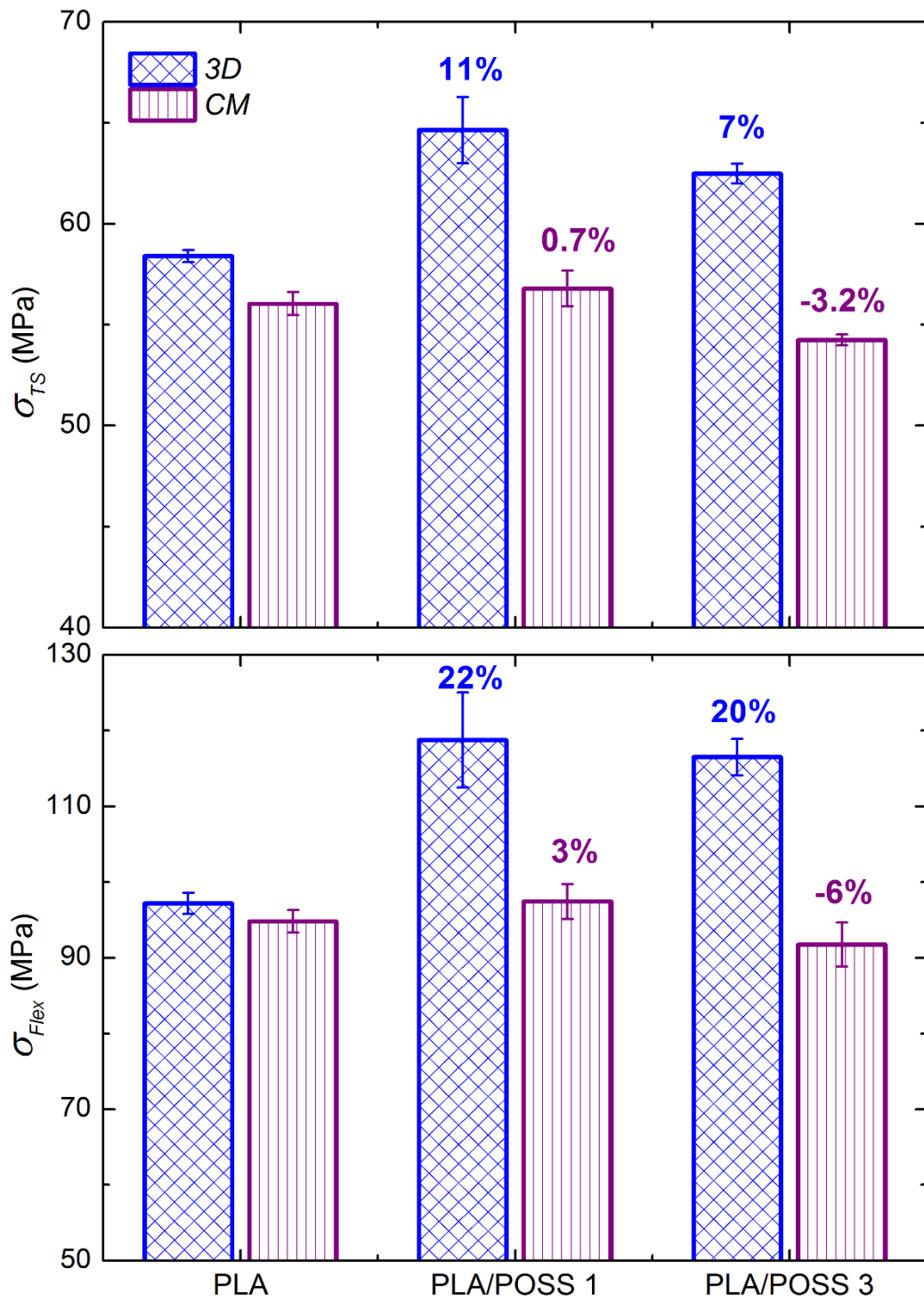
Next, in order to compare “toughness” performance of the 3D-printed specimens with respect to their compression molded counterparts, “Fracture Toughness Tests” were also conducted for all specimen groups. Two values, i.e. “Critical Stress Intensity Factor ( $K_{IC}$ )” and “Critical Strain Energy Release Rate ( $G_{IC}$ )” determined from these tests were also tabulated in Table 4.10, and comparatively evaluated in Figure 4.28. Note that, in this figure %increases compared to their neat PLA specimens were again indicated on top of the columns for the PLA/POSS specimens.

Similar to the Figures 4.26 and 4.27, Figure 4.28 also show that regardless of the 3D-printing and compression molding shaping processes, when POSS nanoparticles

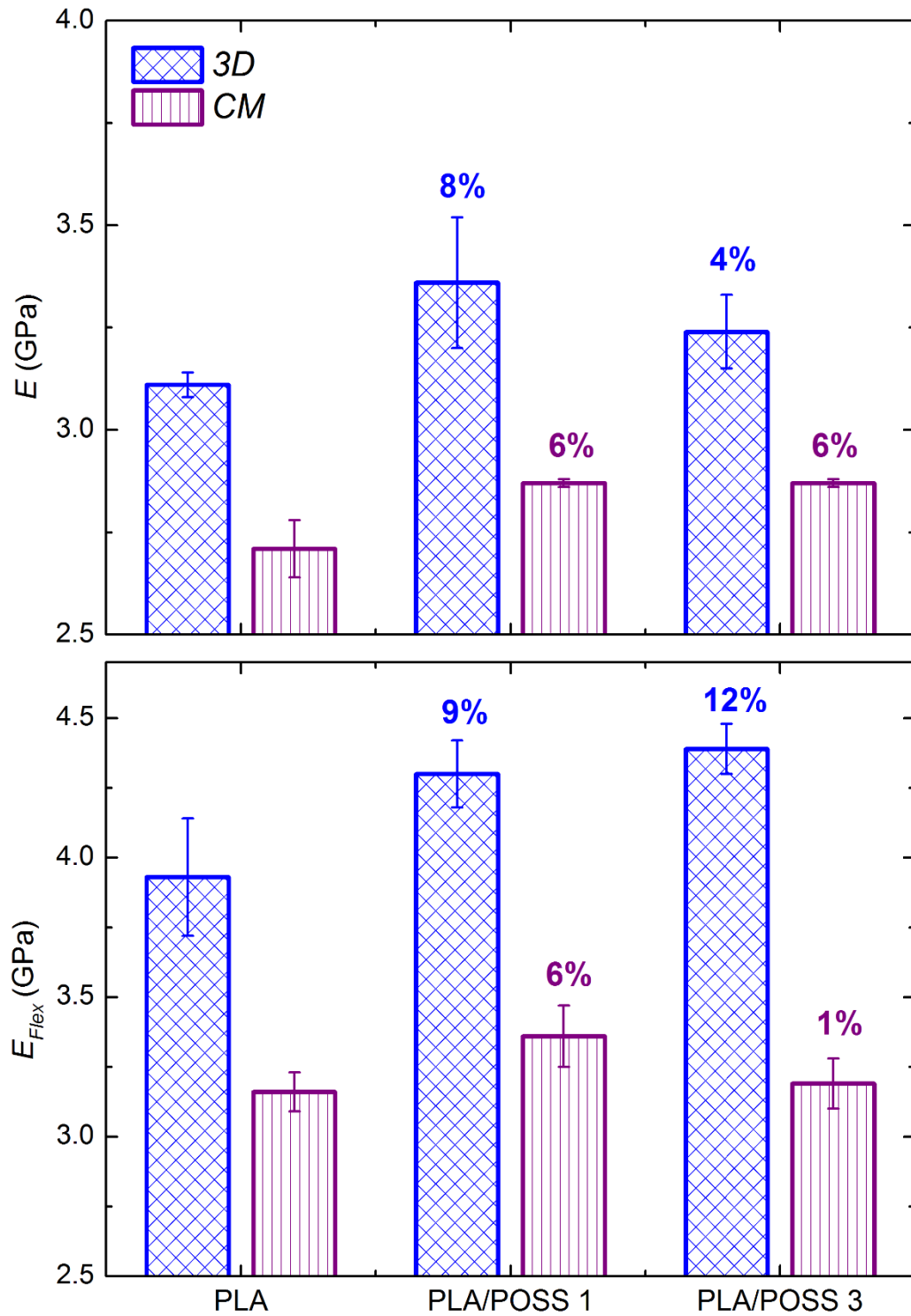
were incorporated into PLA matrix, both  $K_{IC}$  and  $G_{IC}$  fracture toughness values were improved. The main reason would be of course effectiveness of the basic “toughening mechanisms” i.e. “crack pinning, crack deflection, debonding, pull-out” of the POSS nanoparticles leading to decreases in the propagation rate of cracks initiated from the notches.

Figure 4.28 again revealed that the improvements in the  $K_{IC}$  and  $G_{IC}$  fracture toughness values of the 3D-printed specimens were much higher compared to compression molded counterparts. For instance, with respect to their neat PLA specimens, the rises in the  $K_{IC}$  and  $G_{IC}$  values of the 3D-printed PLA/POSS1 specimen were 11% and 117%; while these rises in the compression molded specimen were only 5% and 42%, respectively.

Lastly, in order to determine the degree of “higher mechanical performance” of 3D-printing, all the mechanical properties obtained were re-evaluated in Figure 4.29 in the form of “%Benefits”. The values of the “%Benefits of the 3D-printed Specimens” were calculated with respect to the lower values obtained from their compression molded counterparts. Figure 4.29 simply shows that, in terms of mechanical performance (strength, stiffness, toughness), rather than compression molding, use of 3D-printing is much more beneficial. Benefits in the 3D-printing of PLA/POSS nanocomposites starts from 13% and rises up to 78%. For example, for the PLA/POSS 1 specimen, benefits of using 3D-printing is 22% in  $\sigma_{Flex}$ , 28% in  $E_{Flex}$ , and 43% in  $K_{IC}$ .



**Figure 4.26** Tensile strength and flexural strength of the 3D-printed and compression molded specimens. Note that %increases given on top of the PLA/POSS nanocomposite columns were determined compared to their neat PLA.



**Figure 4.27** Tensile modulus and flexural modulus of the 3D-printed and compression molded specimens. Note that %increases given on top of the PLA/POSS nanocomposite columns were determined compared to their neat PLA.



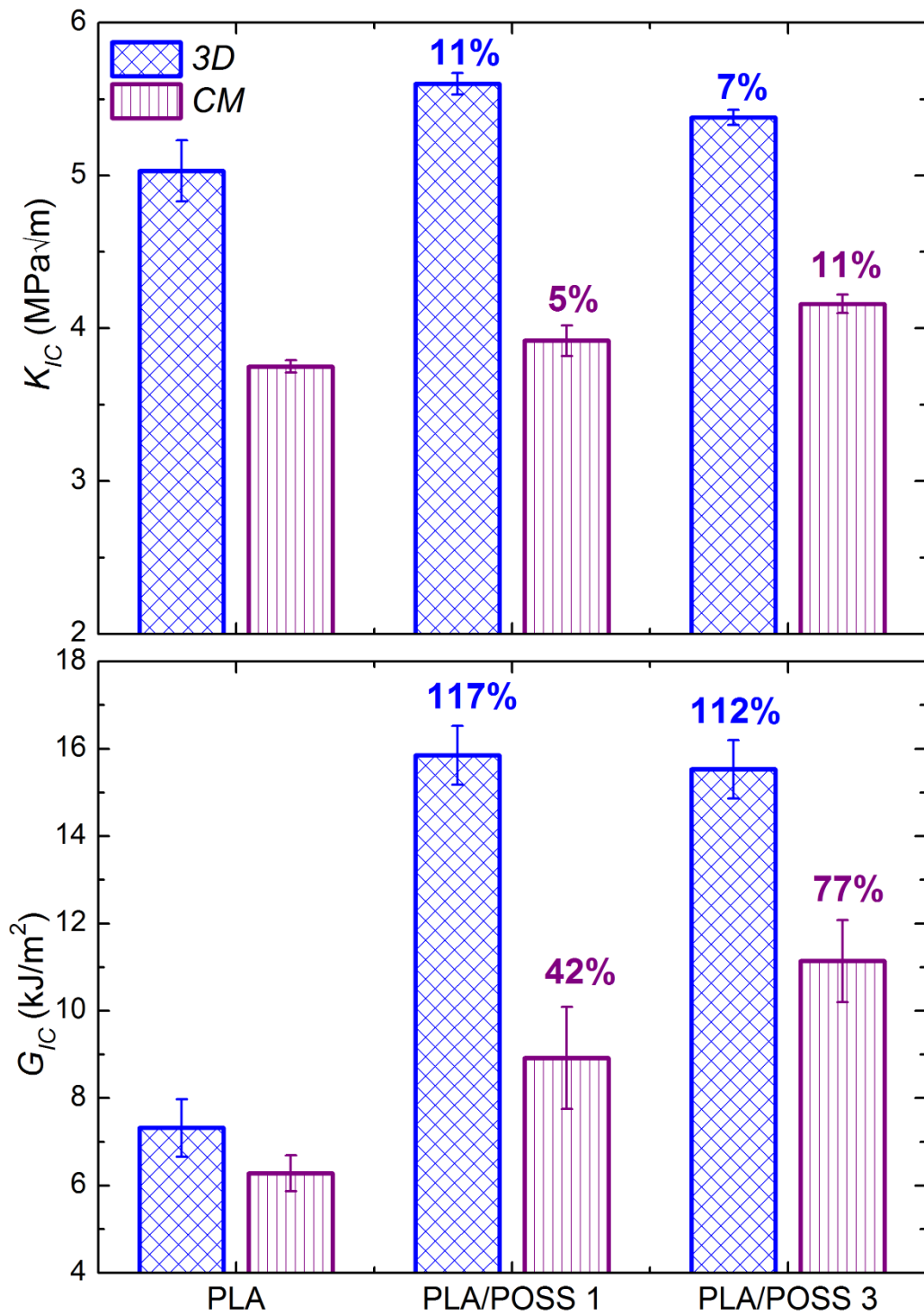


**Figure 4.28** Fracture toughness of the 3D-printed and compression molded specimens. Note that %increases given on top of the PLA/POSS nanocomposite columns were determined compared to their neat PLA.

It could be speculated that the main reason for the very beneficial mechanical performance (i.e. higher strength, elastic modulus and fracture toughness values) of the 3D-printed PLA/POSS specimens would be due to the higher uniformity and higher homogeneity in the distribution of POSS nanoparticles throughout the PLA matrix. Since 3D-printing is an additive manufacturing technique, the structure is formed layer by layer (in the x-y plane) along the thickness (z-direction) of the specimens. Therefore, compared to the compression molding, being a bulk forming technique, the degree of the uniform and homogeneous distribution of POSS nanoparticles in each PLA matrix layer throughout the structure along the thickness of the 3D-printed specimens would be much better. Consequently, the role of these uniformly and homogeneously distributed POSS nanoparticles in the strengthening, stiffening and toughening mechanisms mentioned above would be very effective.

In Figure 4.29, it was seen that, mechanical properties of the 3D-printed neat PLA specimens were also slightly beneficial compared to the compression molded neat PLA specimens. As discussed in a previous study [57], these slightly higher values could be due to the slightly textured structure of the specimens, playing a certain role in the strengthening, stiffening, toughening mechanisms. Formation of the textured structures were normally expected due to the  $\pm 45^\circ$  raster angle orientation used during 3D-printing.

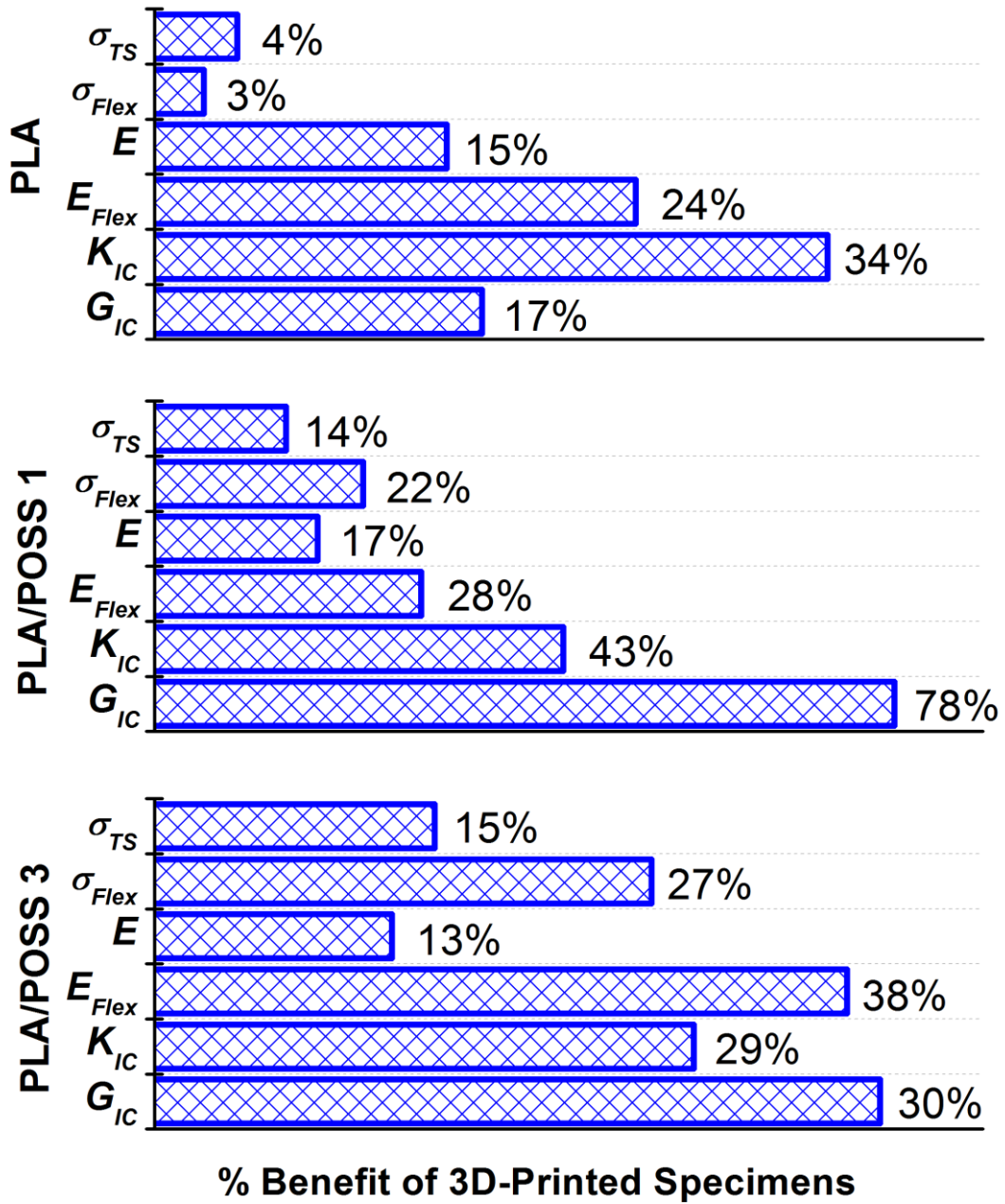


**Figure 4.29** %Benefits in the mechanical properties of the 3D-printed specimens compared to their compression molded counterparts

### 4.2.3 Thermal Behavior of the 3D-Printed and Compression Molded Specimens

For the observation of the differences in the thermal behavior of the 3D-printed PLA/POSS nanocomposites compared to their compression molded counterparts, including their neat PLA specimens, two different thermal analyses; i.e. Differential Scanning Calorimetry and Thermogravimetric Analysis, were conducted. After obtaining first heating DSC thermograms of all specimen groups, as shown in Figure 4.30, the important transition temperatures, i.e. glass transition temperature ( $T_g$ ), cold crystallization temperature ( $T_c$ ), melting temperature ( $T_m$ ); including melting and crystallization enthalpies ( $\Delta H_m$  and  $\Delta H_c$ ), and percent crystallinity amounts ( $X_C$ ) were determined from these curves, and tabulated in Table 4.11. Similarly, after obtaining TGA curves of all specimen groups, as illustrated in Figure 4.31, thermal degradation temperature values ( $T_{5\%}$ ,  $T_{10\%}$ ,  $T_{25\%}$ ,  $T_{max}$ ) determined from these curves were tabulated in Table 4.12.

The most noticeable differences in these figures and tables observed were the values of Crystallinity Amounts ( $\%X_C$ ) in DSC analysis, and the Maximum Thermal Degradation Temperature ( $T_{max}$ ) in TGA. Regardless of the 3D-printing and compression molding processes used,  $\%X_C$  and  $T_{max}$  values of neat PLA specimens increased slightly after incorporation of POSS nanoparticles. It is known that the increase in  $\%X_C$  value was due to the nucleation agent effect of POSS particles, while the increase in  $T_{max}$  value was due to the higher thermal stability of the inorganic cage structure of POSS particles. On the other hand, no significant differences were observed between the thermal properties of the 3D-printed and their compression molded counterparts.

**Table 4.11** Transition temperatures ( $T_g$ ,  $T_c$ ,  $T_m$ ), enthalpies ( $\Delta H_m$ ,  $\Delta H_c$ ) and crystallinity percent ( $X_C$ ) of the 3D-printed and compression molded specimens during DSC first heating

Specimens	$T_g$ (°C)	$T_c$ (°C)	$T_m$ (°C)	$\Delta H_m$ (J/g)	$\Delta H_c$ (J/g)	$X_C$ (%)
PLA - 3D	60.9	120.5	149.7	18.5	13.6	5.27
PLA - CM	60.1	124.6	150.2	17.2	13.7	3.76
PLA/POSS 1 - 3D	60.8	118.4	151.3	22.1	16.5	6.08
PLA/POSS 1 - CM	60.0	121.0	150.0	14.7	6.8	8.56
PLA/POSS 3 - 3D	62.3	118.9	153.2	15.4	10.0	6.03
PLA/POSS 3 - CM	62.2	120.9	150.0	15.3	6.4	9.87

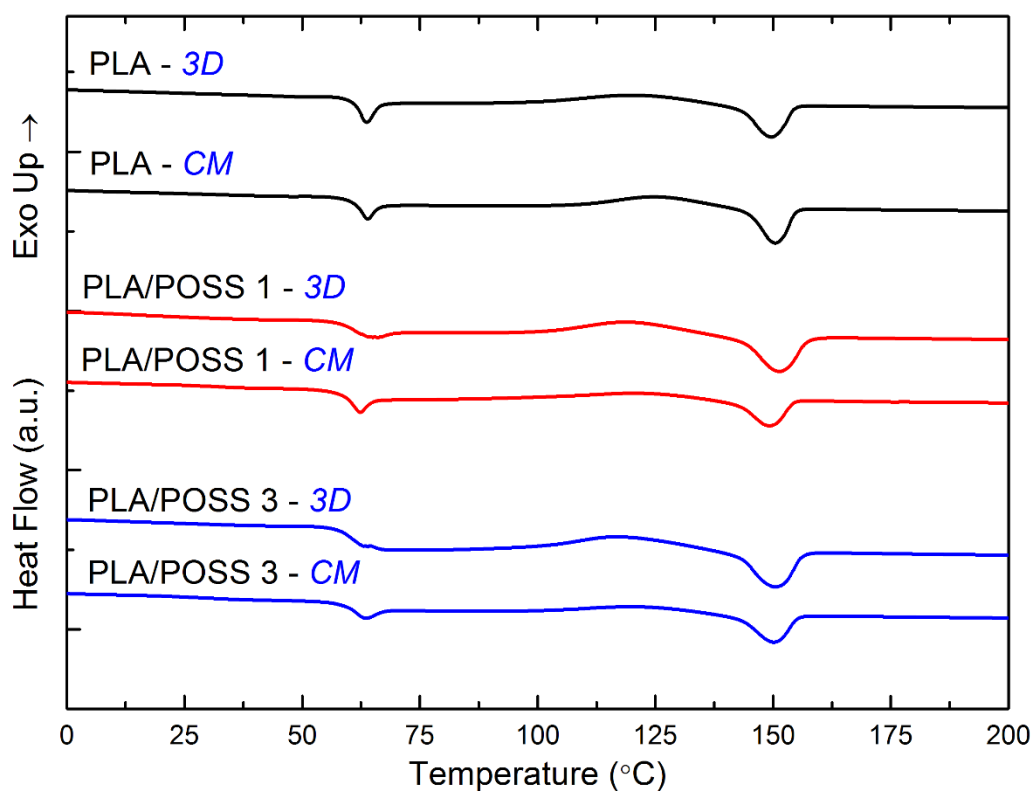


**Figure 4.30** First heating DSC thermograms of the 3D-printed and compression molded specimens

**Table 4.12** Thermal degradation temperatures ( $T_{5\%}$ ,  $T_{10\%}$ ,  $T_{25\%}$ ) of the 3D-printed and compression molded specimens at 5, 10 and 25 wt% mass losses, the maximum mass loss temperature ( $T_{max}$ )

Specimens	$T_{5\%}$ (°C)	$T_{10\%}$ (°C)	$T_{25\%}$ (°C)	$T_{max}$ (°C)
PLA - 3D	328	338	350	366
PLA - CM	332	342	353	362
PLA/POSS 1 - 3D	328	339	352	370
PLA/POSS 1 - CM	327	337	349	365
PLA/POSS 3 - 3D	324	337	351	369
PLA/POSS 3 - CM	321	334	349	368

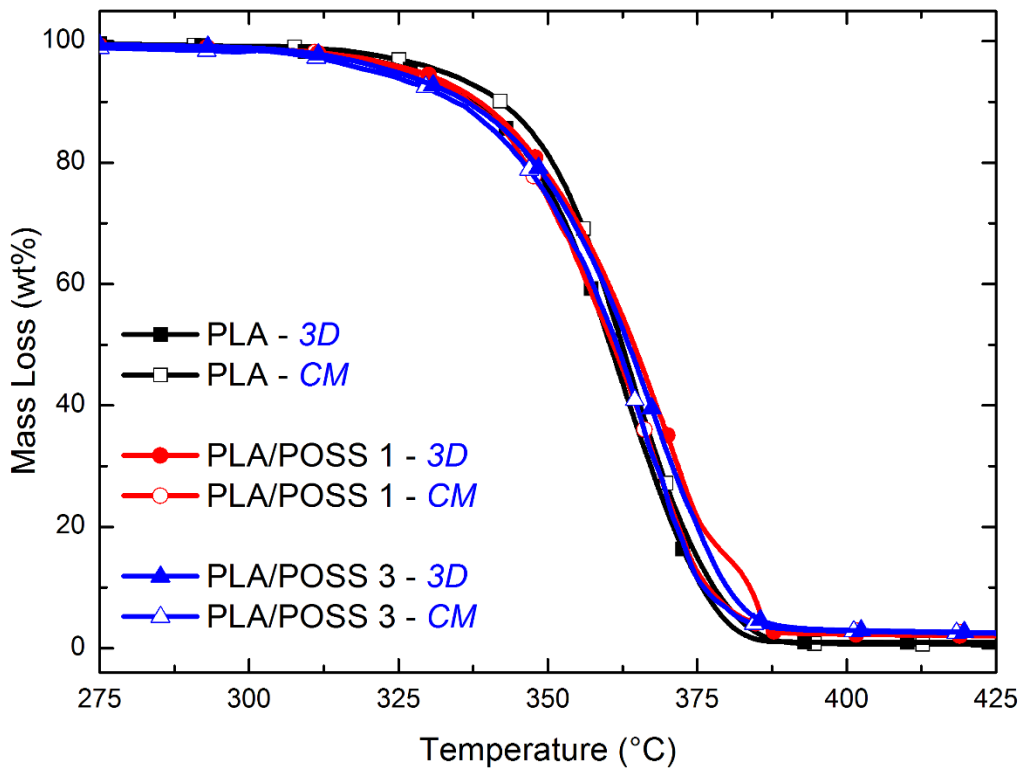


**Figure 4.31** Thermogravimetric curves of the 3D-printed and compression molded specimens

#### **4.2.4 Behavior of the 3D-Printed Specimens in a Physiological Solution**

Since 3D-printing techniques are considered as a significant alternative for shaping biomedical parts, it would be important to investigate behavior of 3D-printed samples in a physiological fluid environment. For this purpose, in order to observe whether there would be any changes in the physical structure and mechanical properties of the only 3D-printed PLA and PLA/POSS specimens, they were followed by soaking them in a physiological saline solution for 120 days at 37°C. For this purpose, the physiological solution was prepared by using the standard PBS (Phosphate Buffered Saline) tablet supplied from Sigma Aldrich. When one tablet was dissolved in 200 mL deionized water, the solution contains 0.01 M phosphate buffer, 0.0027 M potassium chloride (KCl) and 0.137 M sodium chloride (NaCl), having the required pH value of 7.38 at 25°C.

Keeping of the 3D-printed mechanical test specimens in plain PBS solution (i.e. without any other chemical addition) was conducted according to the standard test method “ASTM F1635-11 In Vitro Degradation Testing of Hydrolytically Degradable Polymer Resins and Fabricated Forms for Surgical Implants”. 2 mm thick standard flexural and fracture toughness test specimens immersed in solution bottles were placed in an oven set to 37°C human body temperature for 120 days. Solutions were checked in every 10 days by using a bench type pH meter to provide the pH value at  $7.4 \pm 0.2$ .

At the end of each month, certain number of the specimens were taken out of their solution bottles for three different inspections; (i) visual examination of the specimen surfaces, (ii) weight loss (%) measurements via a precision balance, and (iii) flexural and fracture toughness mechanical tests. It was generally observed that, even at the end of the fourth month, i.e. a total period of 120 days, there was almost no deterioration in the physical structure and mechanical properties of the 3D-printed PLA and PLA/POSS specimens. Thus, it could be interpreted that, 3D-printed

PLA/POSS nanocomposites would be a significant alternative for many biomedical applications.

In the literature, although there is no study investigating the behavior of 3D-printed PLA/POSS structures in PBS solution, there are certain number of works for the conventionally molded PLA-based materials [25, 87, 104-108]. These studies indicated that, there could be certain level of hydrolytic degradation of PLA-based materials in PBS solution, under certain conditions. For instance, if the PBS solution was not at 37°C of human body, but if it was above 50°C, then there might be decreases in the physical mass and mechanical properties [25, 105, 108]. Another important parameter cited was the thickness of the specimens. If PLA-based materials were shaped as films with less than 0.5 mm thickness, then deterioration in the PBS solution could be important [25, 87, 106-108]. Similarly, increasing the porosity in the structure of the specimens might lead to deterioration [87, 104]. Moreover, it was also reported that changing the composition of PBS solution such as with enzymes [117, 118], acid and alkaline media [119, 120] results in various changes in the structure of PLA-based materials.

### **4.3 Use of Taguchi Optimization for the Electrospinning Process Parameters of PLA and PLA/POSS Nanofibers**

#### **4.3.1 Preliminary Studies for the Approximate Process Parameters**

In the third part of this thesis, Taguchi method was applied for the four factors (A, B, C, D), i.e. for the most significant four electron spinning process parameters as:

- (A) PLA Concentration in the Solution, % w/v
- (B) Solution Feeding Rate, mL/h
- (C) Distance between the Collector and the Needle, cm
- (D) Applied Voltage, kV



Before selection of the different levels for each parameter, first an approximate value for these important electrospinning parameters are necessary. For this purpose, certain number of preliminary studies were conducted by using approximate data cited in the literature. First trials were performed to reveal the effects of “solvent type”, by comparing use of only chloroform (CF) versus mixture of CF and dimethylformamide (DMF). It was observed that due to the higher electrical conductivity of DMF, use of the CF/DMF solution mixture (3:1) increased the surface charge of the polymer jet (with high elongation forces) leading to rather more defect-free and uniform electrospun fibers with narrow diameters. Additionally, due to the higher boiling point of DMF, lower volatility i.e. lower evaporation rate of the CF/DMF solvent mixture prevented drying of the polymer jet in the needle tip by decreasing its viscosity.

Second group of preliminary trials revealed that the approximate values for the processing parameter (B) “Solution Feeding Rate” could be around 1.7 mL/h; for (C) “Distance between the Collector and the Needle” could be around 17 cm; and for (D) “Applied Voltage” could be around 12 kV.

The third group of preliminary trials were conducted to determine the most appropriate approximate value for the parameter “(A) PLA Concentration” in the solvent mixture by using the approximate values of the other parameters mentioned above. For this purpose, starting from 1% w/v up to 14% w/v PLA concentrations were tried, by magnetically stirring the PLA powders with the CF/DMF solvent mixture for at least 6 hours at 30°C. In order to observe morphologies of the forms collected during these trials, SEM examinations were performed.

Figure 4.32 shows that when the PLA concentration in the solvent mixture was low (i.e. < 6% w/v), only “droplet” and/or “bead” morphologies could be collected. Because, it is known that [14, 76, 78, 83], in order to obtain “fibrous” morphology, the solution mixture should have sufficient polymer concentration having sufficient

number of entangled macromolecular chains. It is seen in Figure 4.32 that; formation of continuous fibrous morphology starts when the PLA concentration is above 6% w/v. Increasing the PLA concentration decreases the number of “beaded-fibers”. For instance, starting from 8% w/v PLA concentration, electrospun fibers were almost “bead-free” with rather smooth surfaces. It can be detected that two diameter ranges could be obtained; i.e. electrospun fibers having “micron-range” (1-4  $\mu\text{m}$ ) diameter size and “nano-range” (50-200 nm) diameter size. It should be also pointed out that, when the PLA concentration was above 12% w/v, electrospinning was not possible due to the clogging of the needle.

### **4.3.2 Parameter Levels Selected for Taguchi Method**

After determining the approximate values for the four important electrospinning parameters by conducting certain number of preliminary experiments mentioned in the previous section, three different levels for each parameter were selected. Table 4.13 indicates that three levels selected for (A) “PLA solution concentration” are 8, 10, 11% w/v; for (B) “solution feeding rate” are 1, 1.4, 1.8 mL/h; for (C) “the distance between the collector and the needle” are 12, 15, 18 cm; and for (D) “applied voltage” from the high power supply are 15, 18, 22 kV.

Then, in order to determine the number of experiments and the combination of the parameter levels to be used in each experiment, Taguchi Orthogonal Array  $L_9$  ( $3^4$ ) was constructed by using the Minitab 17 software as listed in Table 4.14. It was seen that in order to obtain optimum process parameters only 9 experiments (E1-E9) would be conducted, instead of conducting 81 experiments, i.e. there would be significant reduction in the time, labor, and material consumption.

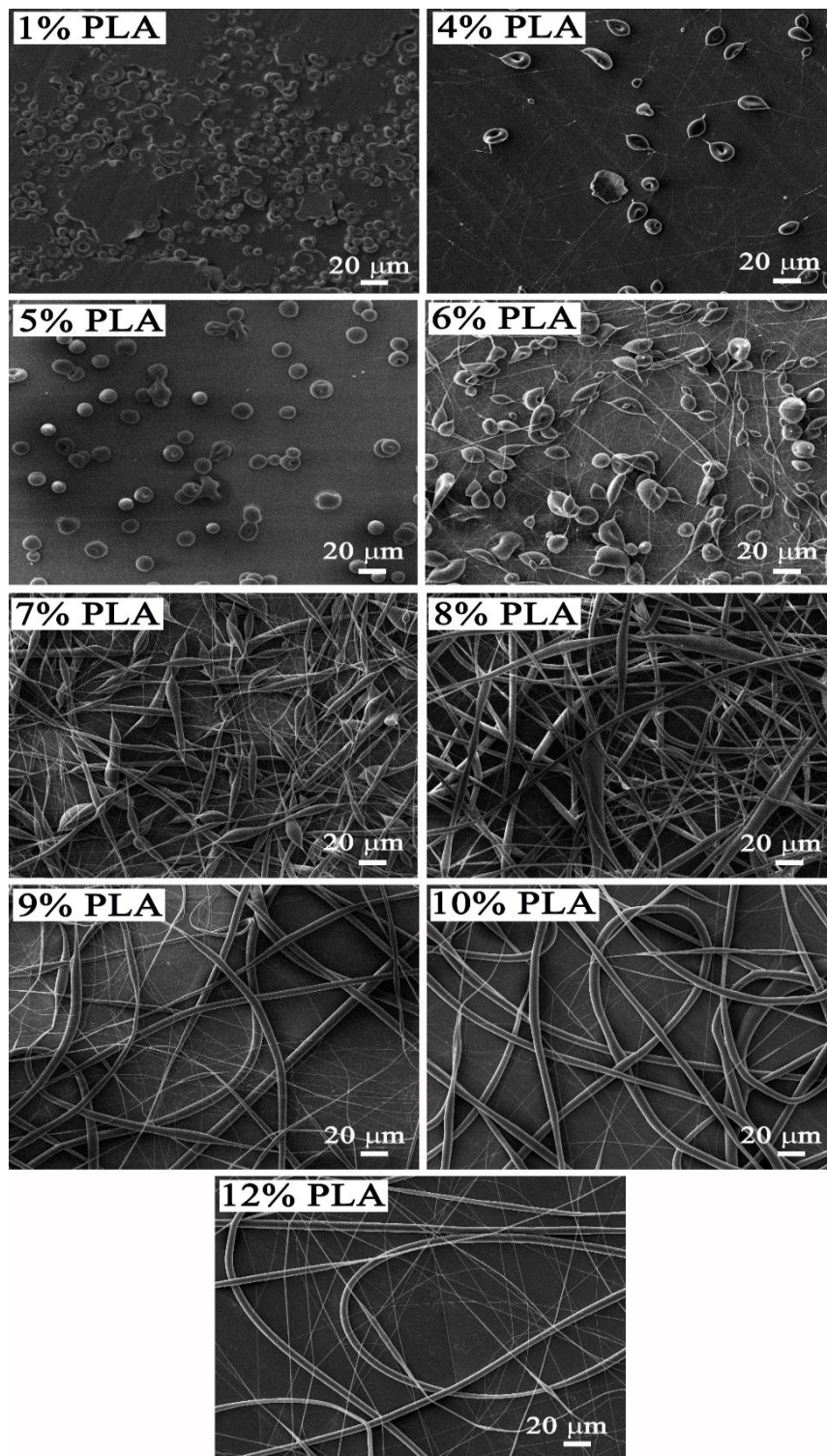


**Figure 4.32** SEM images showing effects of PLA solution concentration on the formation of droplets, beads and fibers determined during preliminary studies

**Table 4.13** Parameters and levels used in the Taguchi method

	(A) Polymer Solution Concentration (% w/v)	(B) Feeding Rate (mL/h)	(C) Needle-to- Collector Distance (cm)	(D) Applied Voltage (kV)
<b>Level 1</b>	8	1	12	15
<b>Level 2</b>	10	1.4	15	18
<b>Level 3</b>	11	1.8	18	22

**Table 4.14** Orthogonal array L<sub>9</sub> (3<sup>4</sup>) used in the Taguchi method

Experiment No	(A) Polymer Solution Concentration (% w/v)	(B) Feeding Rate (mL/h)	(C) Needle-to- Collector Distance (cm)	(D) Applied Voltage (kV)
<b>E1</b>	1	1	1	1
<b>E2</b>	1	2	2	2
<b>E3</b>	1	3	3	3
<b>E4</b>	2	1	2	3
<b>E5</b>	2	2	3	1
<b>E6</b>	2	3	1	2
<b>E7</b>	3	1	3	2
<b>E8</b>	3	2	1	3
<b>E9</b>	3	3	2	1

### 4.3.3 Results of the Nine Taguchi Experiments Applied for the Neat PLA

After determining the Taguchi L<sub>9</sub> orthogonal array experiment matrix, nine different electrospinning experiments (E1-E9) for neat PLA were performed one by one. Then, electrospun fibers collected for each condition were examined under SEM in order to determine their average fiber diameter ranges. SEM images in Figure 4.33 reveal that after each experimental condition rather smooth and almost bead-free electrospun fiber morphology could be obtained. Average fiber diameters measured

from SEM images were tabulated in Table 4.15 together with the process parameters and their levels used in each experiment.

In Table 4.15, values of the S/N (signal-to-noise) ratios were also tabulated. These values were determined by using the “smaller-the-better” approach via the following relation [96]:

$$S/N = -10 \log \left( \frac{1}{n} \sum_{i=1}^n y_i^2 \right) \quad (4.2)$$

where  $n$  is the number of observations in each experiment and  $y_i$  is the measured response data.

Then, Minitab 17 software was used to plot “main effects for S/N ratios” (Figure 4.34) and to tabulate “S/N ratio responses” (Table 4.16) for each nine experiment. In these plots and table, the largest S/N ratio corresponds to the smallest electrospun fiber diameter that could be obtained. Therefore, it can be concluded that the optimum electrospinning parameter combination would be A1B3C3D1; that is “polymer solution concentration” of 8% w/v (A1), “feeding rate” of 1.8 mL/h (B3), “needle-to-collector distance” of 18 cm (C3) and “applied voltage” of 15 kV (D1).

In Table 4.16, “Delta” value is the difference between the maximum and minimum S/N ratios, while the “Rank” data represents the importance of the processing parameters determined by ranking the Delta values from the largest to smallest. Thus, it was seen that for the smallest fiber diameter, the most important processing parameter appears to be “polymer solution concentration”, while the second important was “needle-to collector distance”.

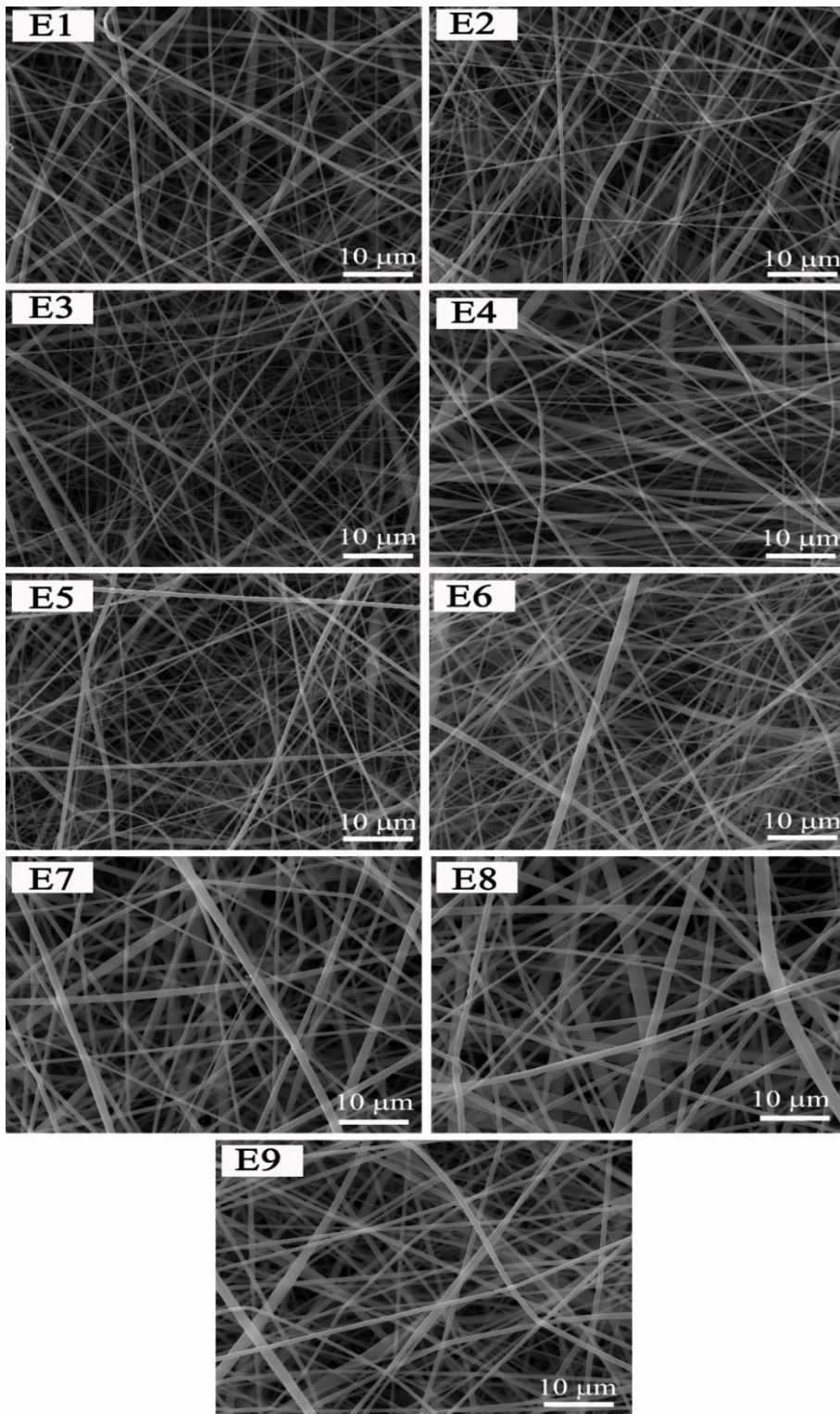


**Figure 4.33** SEM images showing electrospun PLA fibers obtained after nine different Taguchi experiments

**Table 4.15** Results of nine Taguchi experiments in terms of average fiber diameter and S/N Ratios

<b>Experiment No</b>	<b>(A) Polymer Solution Concentration (% w/v)</b>	<b>(B) Feeding Rate (mL/h)</b>	<b>(C) Needle-to-Collector Distance (cm)</b>	<b>(D) Applied Voltage (kV)</b>	<b>Average Fiber Diameter (nm)</b>	<b>S/N Ratio</b>
<b>E1</b>	8	1	12	15	494 ± 250	-53.87
<b>E2</b>	8	1.4	15	18	461 ± 268	-53.27
<b>E3</b>	8	1.8	18	22	385 ± 185	-51.70
<b>E4</b>	10	1	15	22	515 ± 388	-54.44
<b>E5</b>	10	1.4	18	15	415 ± 340	-52.37
<b>E6</b>	10	1.8	12	18	439 ± 235	-52.85
<b>E7</b>	11	1	18	18	669 ± 262	-56.51
<b>E8</b>	11	1.4	12	22	918 ± 491	-59.25
<b>E9</b>	11	1.8	15	15	646 ± 299	-56.21

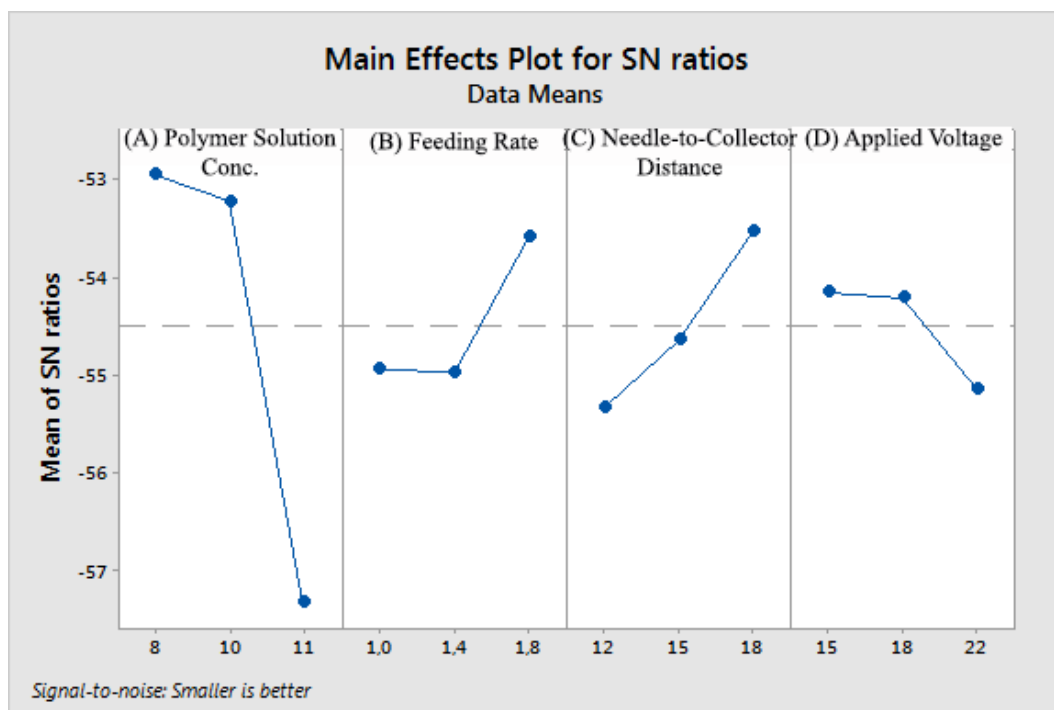


**Figure 4.34** Main effects plot for the S/N ratios

**Table 4.16** S/N ratio response table including delta and rank data

	(A) Polymer Solution Concentration (% w/v)	(B) Feeding Rate (mL/h)	(C) Needle-to- Collector Distance (cm)	(D) Applied Voltage (kV)
<b>Level 1</b>	-52.95	-54.94	-55.32	-54.15
<b>Level 2</b>	-53.22	-54.96	-54.64	-54.21
<b>Level 3</b>	-57.32	-53.58	-53.52	-55.13
<b>Delta</b>	4.38	1.38	1.80	0.98
<b>Rank</b>	1	3	2	4



After the S/N ratio approach of Taguchi method, the same software was used also for the analysis of variation (ANOVA) approach to determine the degree of contribution of each process parameter to the variation in the average diameter of electrospun fibers. So that, it would be possible to compare the “Rank” data determined in S/N response table with the “percent contribution” data determined in ANOVA approach.

Table 4.17 tabulates results of the ANOVA calculations in the form of “degrees of freedom” (DOF), “adjusted sum of squares (Adj SS), “adjusted mean squares” (Adj MS) and “percent contribution” values. In this analysis, DOF for each parameter is the number of levels minus one. Adj SS for each parameter is the square of deviation from the grand mean, while Adj MS is determined by dividing the Adj SS with the respective DOF value [21]. Finally, percent contribution of each parameter can be determined as the ratio of the Adj SS to the total Adj SS, times hundred [21].

Table 4.17 reveals that parameter-A (Polymer Solution Concentration) has the highest contribution (74%) to the variation in the average diameter of electrospun fibers, while parameter-C (Needle-to-Collector Distance) is the second one with 11% contribution. Therefore, it can be concluded that “importance ranking” data of the Taguchi S/N response approach directly coincides with the “percent contribution” data of the ANOVA approach.

**Table 4.17** Results of the analysis of variance (ANOVA) approach used after the Taguchi experiments

	<b>Degrees of Freedom (DOF)</b>	<b>Adjusted Sum of Squares (Adj SS)</b>	<b>Adjusted Mean Square (Adj MS)</b>	<b>Percent Contribution</b>
<b>(A) Polymer Solution Concentration</b>	2	169459	84729	74
<b>(B) Feeding Rate</b>	2	18218	9109	8
<b>(C) Needle-to-Collector Distance</b>	2	24394	12197	11
<b>(D) Applied Voltage</b>	2	15943	7971	7
<b>Total</b>	8	228013		100

#### 4.3.4 Confirmation Experiment for the PLA Nanofibers

As discussed above, after conducting nine Taguchi experiments, S/N ratio approach indicated that the optimum electrospinning parameter combination for PLA would be A1B3C3D1; that is “polymer solution concentration” of 8% w/v (A1), “feeding rate” of 1.8 mL/h (B3), “needle-to-collector distance” of 18 cm (C3) and “applied voltage” of 15 kV (D1). In order to reveal reliability of the Taguchi method, normally “confirmation experiment” should be performed. For this purpose, confirmation experiment for neat PLA by using the optimum A1B3C3D1 parameters were conducted. Figure 4.35 shows SEM images of the electrospun PLA fibers together with the frequency distribution histograms of the fiber diameter. In this confirmation experiment, S/N ratio value and the average diameter electrospun PLA fibers were determined as -51.16 and  $361.4 \pm 196$  nm, respectively.

Furthermore, in order to determine “accuracy”, i.e. confidence level of the Taguchi S/N approach, results of the confirmation experiment could be compared with the

estimated values. For this purpose, the “estimated S/N ratio” and “estimated average diameter” can be calculated by using the following relations [97]:

$$S/N_{estimated} = S/N_M + \sum_{i=1}^n (S/N_i - S/N_M) \quad (4.3)$$

$$S/N_{estimated} = -10 \log(d_{estimated}^2) \quad (4.4)$$

where  $S/N_M$  is the total mean of the S/N ratio while  $S/N_i$  is the mean of the S/N ratios for each parameter level.

After substituting the optimum A1B3C3D1 parameter levels into the above equations, the estimated S/N ratio and the estimated average fiber diameter were determined as -50.72 and 343.5 nm, respectively.

Then, the accuracy (confidence level) of Taguchi method could be quantified by using the following relation:

$$Accuracy = 100 - \frac{Experimental\ Value - Estimated\ Value}{Estimated\ Value} \times 100 \quad (4.5)$$

For instance, when the experimental average fiber diameter (361.4 nm) and the estimated average fiber diameter (343.5 nm) values were substituted in the above relation, it was seen that the accuracy of the Taguchi method used in this thesis was as large as 95%.

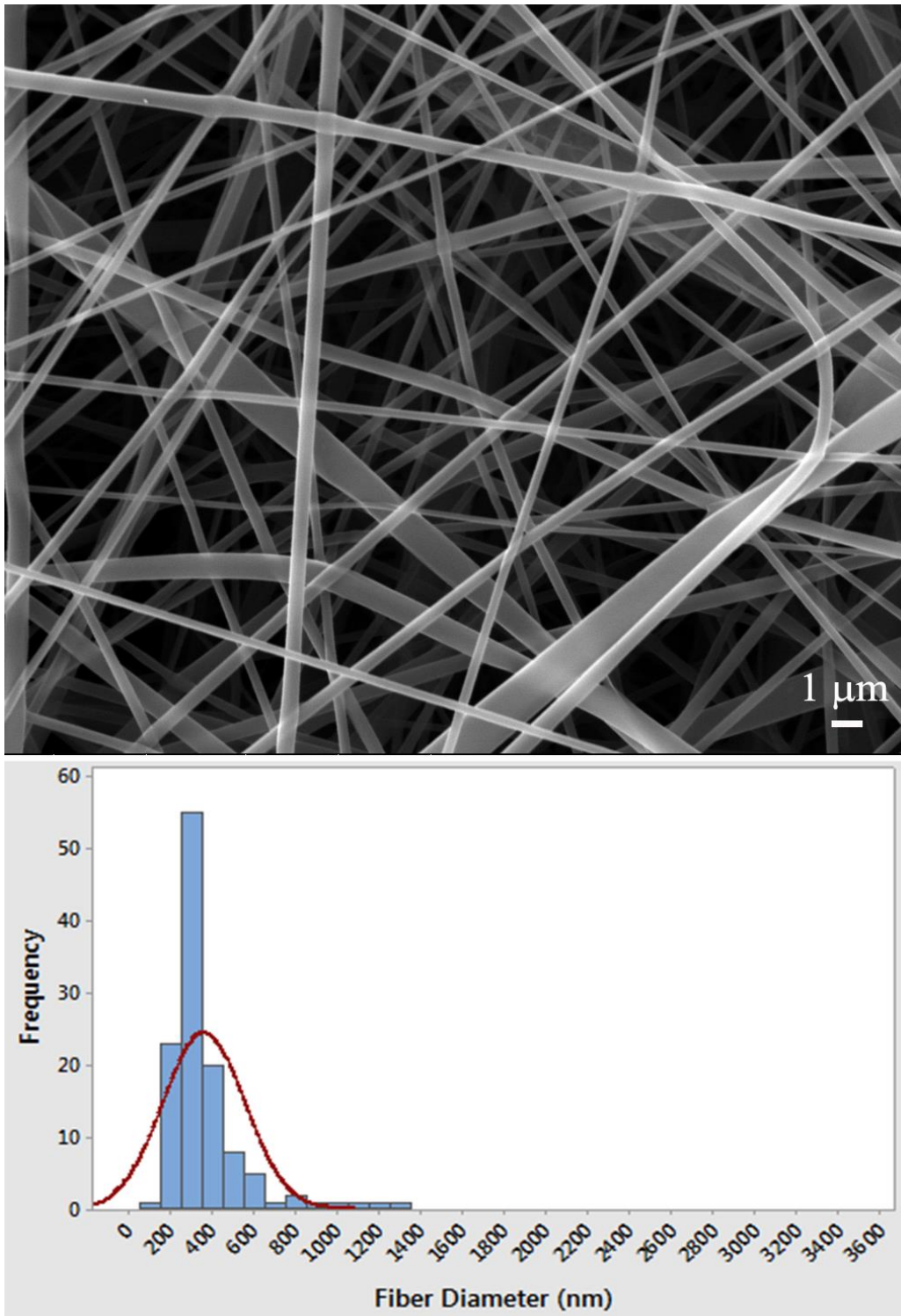


**Figure 4.35** SEM image and the frequency distribution of the electrospun PLA fiber diameters obtained from the confirmation experiment

#### **4.3.5 Applicability of Taguchi Optimum Parameters for the PLA/POSS Nanofibers**

In order to reveal applicability of the Taguchi optimum parameters (A1B3C3D1) determined for neat PLA, electrospinning experiments were also conducted for the PLA/POSS mixtures. For this purpose, again the basic POSS structure explained in Section 3.1 was used. The procedure used for the preparation of the electrospinning solution was the same, as discussed before for the neat PLA. The only difference was the addition of 1, 2, 3, 5 wt% POSS nanoparticles with respect to PLA powders.

After using the same optimum process parameters (A1B3C3D1) determined before, SEM studies were conducted to investigate morphology of the electrospun PLA/POSS nanofibers. Images on the left hand side of Figure 4.36 were taken under low magnification to observe general view of the PLA/POSS electrospun structures, while images on the right hand side were taken under higher magnification for the closer views of the PLA/POSS fibers.

As shown in Figure 4.36 although certain number of bead-free PLA/POSS continuous nanofibers could be obtained; but in general, majority of the PLA/POSS nanofibers have beaded morphology, some of them having spindle-like beads.

Although there are no clear explanations for the reasons of the formation of beaded fiber morphology when the inorganic particles were added to the polymer solution (such as loading POSS particles in this study), it was generally speculated on the increase of viscosity of the polymer solution leading to certain instabilities during electrospinning.

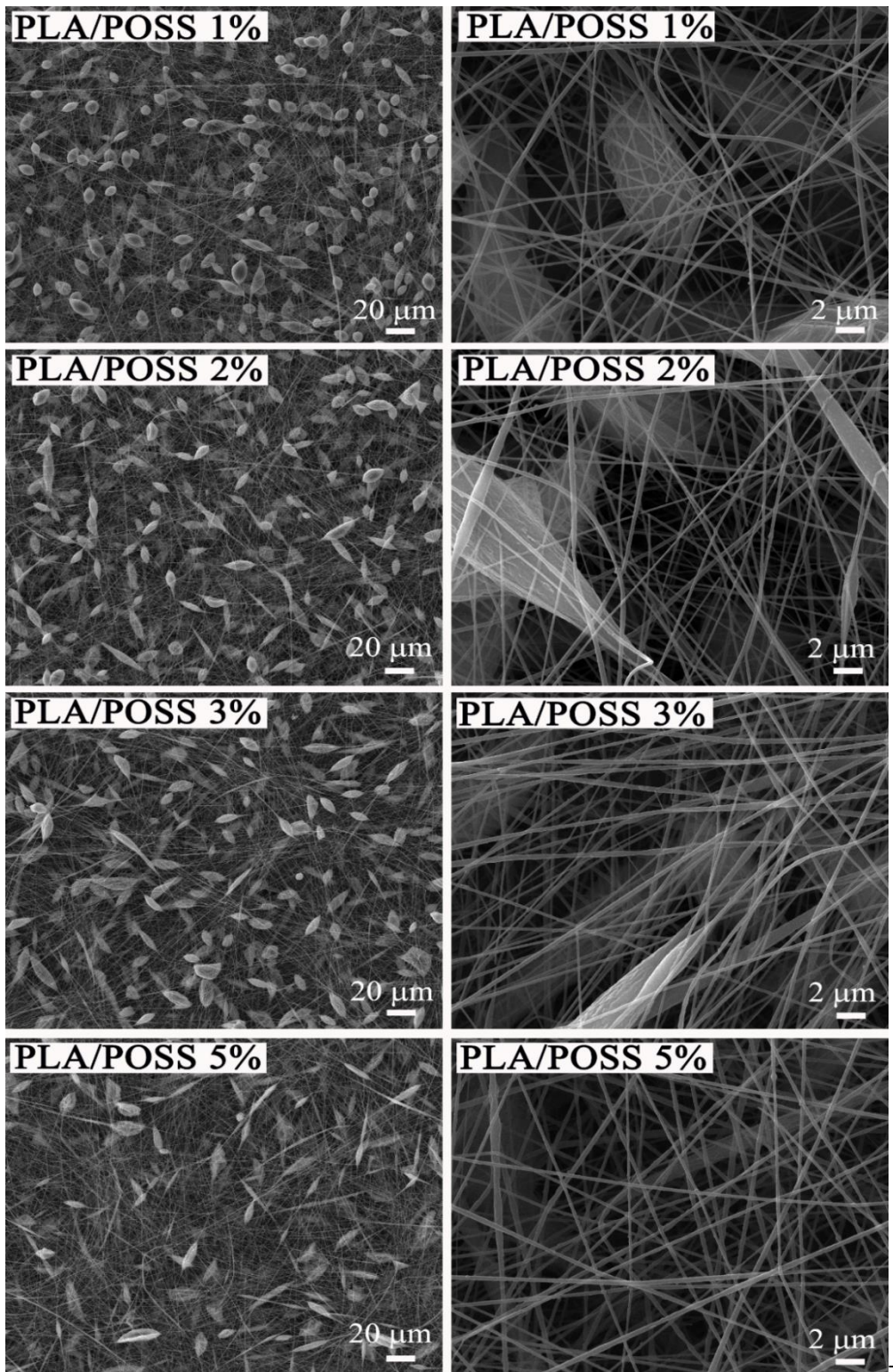


**Figure 4.36** General and closer view SEM images of the PLA/POSS electrospun fibers having generally beaded morphology

It is discussed in the literature [76, 78-80, 83] that increasing the electrical conductivity of the polymer solution might lead to more uniform and lower diameter electrospun fibers. For instance, Zong *et al.* [83] investigated effects of adding 1 wt% three different salts ( $\text{KH}_2\text{PO}_4$ ,  $\text{NaH}_2\text{PO}_4$ ,  $\text{NaCl}$ ) into PLA polymer solution. They indicated that addition of salts resulted in a higher charge density on the surface of ejected polymer jet during electrospinning. Thus, higher elongation forces can be imposed to the jet when the charges carried by the jet increased. It was known that the overall tension in the fibers depends on the self-repulsion of the excess charges on the jet. Hence, increasing the charge density decreases the bead size and fiber diameter.

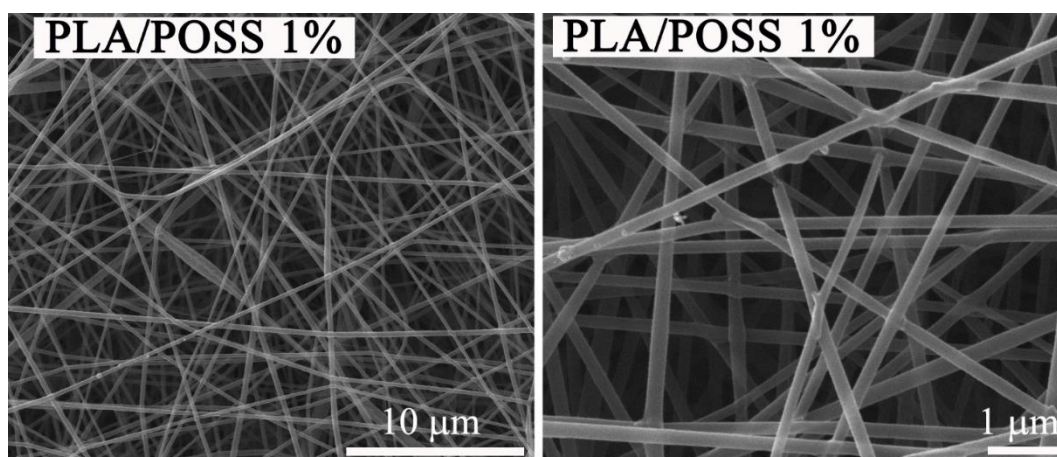


**Figure 4.37** General and closer view SEM images of the PLA/POSS 1% nanofibers with bead-free uniform morphology after the addition of 3 wt% KCl salt into polymer solution

Thus, in this thesis, electrospinning of the PLA/POSS 1% combination was repeated this time also adding 3 wt% KCl salt into the polymer solution. SEM examination (Figure 4.37) conducted for this combination, i.e. PLA/POSS 1% (with 3 wt% KCl salt) revealed that, due to the increased conductivity of the solution, the problem of “bead formation” can be solved. Image analysis for these electrospun PLA/POSS 1% nanofibers revealed that the average fiber diameter was  $207 \pm 71$  nm.

Therefore, it can be generally concluded that optimum process parameters (A1B3C3D1) determined by Taguchi method for the electrospinning of neat PLA nanofibers could be also used for the electrospinning of PLA/POSS nanofibers after addition of only 3 wt% KCl salt into the polymer solution.



## CHAPTER 5

### CONCLUSIONS

The main conclusions drawn from the three different parts of this thesis can be summarized as follows:

#### (i) Effects of POSS Content

- SEM studies revealed that compared to the higher POSS contents of 5 and 7 wt%, lower POSS contents (i.e. 1 and 3 wt%) resulted in rather uniform distribution with lower degree of agglomeration in PLA matrix; the average size range of the agglomerates being less than 100 nm.
- Mechanical tests indicated that due to the higher efficiency of uniformly distributed lower POSS contents in the strengthening, stiffening and toughening mechanisms; use of 1 wt% POSS resulted in highest improvements in strength and modulus, while 3 wt% POSS resulted in highest improvements in fracture toughness values of the PLA matrix.
- DSC analysis showed that due to the nucleation agent effect of the nanoparticles, increasing POSS content increased the crystallinity amount of the PLA matrix; while TGA curves revealed that they have no significant influences on the thermal degradation temperatures.

## **(ii) Effects of POSS Functional Groups**

- Compared to the basic POSS structure having only nonpolar isobutyl groups, SEM images revealed that functionalized POSS structures having aminopropyl groups (ap-POSS), propanediol groups (pd-POSS) and dimethylsilane groups (os-POSS) resulted in more homogeneous distribution with lower degrees of agglomeration in PLA matrix.
- Due to the certain interfacial interactions between the PLA matrix and the organic functional groups of POSS structure, different levels of improvement were observed in the mechanical properties of the nanocomposites. Generally, compared to others, use of pd-POSS structure resulted in slightly higher improvements in strength and modulus values, while use of basic POSS structure was better in terms of fracture toughness values.
- Since efficiency of the nucleation agent action of the more homogeneously distributed POSS particles were higher, use of ap-POSS, pd-POSS and os-POSS led to further increases in the crystallinity amount of PLA matrix, while no significant difference was observed in thermal degradation temperatures.

## **(iii) Effects of MA Compatibilization**

- SEM fractographs revealed that additional use of maleic anhydride (MA) grafted copolymer compatibilization had no detrimental effects on the interfacial morphology between PLA matrix and basic POSS and os-POSS particles; while there were certain levels of debonding with ap-POSS and pd-POSS particles.
- Due to the improved interfacial interactions, all mechanical properties of the nanocomposites with basic POSS and os-POSS particles were increased after their MA compatibilization.

- After MA compatibilization of all nanocomposites, although there were reductions in the crystallinity amounts of their PLA matrices, all thermal degradation temperatures increased substantially.

#### (iv) Effects of 3D-Printing

- Due to the higher effectiveness of the POSS nanoparticles in the well-known composite strengthening/stiffening/toughening mechanisms, mechanical tests (tensile, flexural, toughness) revealed that the improvements in the strength, elastic modulus and fracture toughness values of the 3D-printed specimens were higher compared to compression molded ones. For example, compared to their neat PLA specimens, the increases in the *flexural strength*, *flexural modulus* and *G<sub>IC</sub> fracture toughness* values of the 3D-printed PLA/POSS 1 specimen were 22%, 9% and 117%, respectively; while these increases in the compression molded specimen were only 3%, 6% and 42%, respectively.
- When the mechanical properties of the specimens were compared not according to their neat PLA specimens, but compared with each other; it was again revealed that 3D-printed specimens were much more beneficial compared to their compression molded counterparts. For instance, for the PLA/POSS 1 specimen, benefits of using 3D-printing is 22% in *flexural strength*, 28% in *flexural modulus*, and 78% in *G<sub>IC</sub> fracture toughness* values.
- Since 3D-printed structures are formed layer by layer (in the x-y plane) along the thickness (z-direction) of the specimens, beneficial mechanical performance of the 3D-printed specimens could be due to the higher uniformity and higher homogeneity in the distribution of POSS nanoparticles in each PLA matrix layer.

- Differential Scanning Calorimetry and Thermogravimetric Analysis indicated that there were no significant differences between the thermal properties of the 3D-printed and their compression molded counterparts.
- It was also observed that there was almost no deterioration in the physical structure and mechanical properties of the 3D-printed specimens, even after keeping them 120 days at 37°C in a physiological solution prepared by using the standard PBS (Phosphate Buffered Saline) tablet.

**(v) Use of Taguchi Optimization for Electrospinning Parameters**

- Instead of conducting 81 experiments to determine optimum electrospinning process parameters for PLA, use of Taguchi L<sub>9</sub> orthogonal array experiment matrix, i.e. conducting only 9 experiments, reduced time, labor and material consumption significantly.
- For the smallest electrospun PLA fiber diameter, S/N (signal-to-noise) ratio responses of the Taguchi method indicated that the optimum electrospinning parameter combination would be A1B3C3D1; that is “PLA solution concentration” of 8% w/v (A1), “solution feeding rate” of 1.8 mL/h (B3), “needle-to-collector distance” of 18 cm (C3) and “applied voltage” of 15 kV (D1).
- When compared, “Ranking” data of the Taguchi S/N ratio approach and “Percent Contribution” data of the Analysis of Variation (ANOVA) approach coincided perfectly, both indicating that for the smallest fiber diameter, the most important processing parameter was “PLA solution concentration”, while the second important was “needle-to collector distance”.
- Confirmation experiment conducted for neat PLA (by using the optimum parameter combination A1B3C3D1) resulted in average electrospun fiber

diameter of 361 nm. After comparing this experimental value with the estimated value (344 nm), it was seen that the accuracy of the Taguchi method used in this study was as large as 95%.

- When the same Taguchi optimum parameters (A1B3C3D1) were applied for the electrospinning of PLA solution filled with POSS nanoparticles, SEM images indicated that majority of the PLA/POSS nanofibers have beaded morphology, some of them having spindle-like beads.
- Due to the increase of the electrical conductivity of the polymer solution, it was observed that adding 3 wt% KCl salt into the solution could prevent bead formation and reduce the fiber diameter. For instance, PLA/POSS 1% nanofibers obtained in this way had bead-free morphology with average fiber diameter of 208 nm.
- Therefore, it can be generally concluded that optimum process parameters (A1B3C3D1) determined by Taguchi method for the electrospinning of neat PLA nanofibers could be also used for the electrospinning of PLA/POSS nanofibers after addition of only 3 wt% KCl salt into the polymer solution.



## REFERENCES

- [1] Raquez J-M, Habibi Y, Murariu M, Dubois P. Polylactide (PLA)-based nanocomposites. *Progress in Polymer Science* 2013; 38: 1504-1542. doi: 10.1016/j.progpolymsci.2013.05.014.
- [2] Lim L-T, Auras R, Rubino M. Processing technologies for poly(lactic acid). *Progress in Polymer Science* 2008; 33: 820-852. doi:10.1016/j.progpolymsci.2008.05.004.
- [3] Odent J, Raquez J-M, Dubois P. (2015). Highly Toughened Polylactide-Based Materials through Melt-Blending Techniques. In Fakirov S (Edt), *Biodegradable Polyesters (235-273)*. Weinheim, Germany. Wiley. doi:10.1002/9783527656950.
- [4] Casalini T, Rossi F, Castrovinci A, Perale G. A Perspective on Polylactic Acid-Based Polymers Use for Nanoparticles Synthesis and Applications. *Frontiers in Bioengineering and Biotechnology* 2019; 7. doi: 10.3389/fbioe.2019.00259.
- [5] Sin L T, Rahmat A R, Rahman W A W A (2013). Applications of Poly(lactic Acid). Ebnesajjad S (Edt), *Handbook of Biopolymers and Biodegradable Plastics (55-69)*. Elsevier. doi: 10.1016/C2011-0-07342-8.
- [6] Zuza E, Meaurio E, Sarausa J-R (2016). Biodegradable Polylactide-Based Composites. Poletto M (Edt), *Composites from Renewable and Sustainable Materials (133-150)*. ExLi4EvA. doi: 10.5772/65468.
- [7] Zhou H, Ye Q, Xu J. Polyhedral oligomeric silsesquioxane-based hybrid materials and their applications. *Materials Chemistry Frontiers* 2017; 2. doi: 10.1039/c6qm00062b.

- [8] Ayandele E, Sarkar B, Alexandridis P. Polyhedral Oligomeric Silsesquioxane (POSS)-Containing Polymer Composites. *Nanomaterials* 2012; 2: 445-475. doi:10.3390/nano2040445.
- [9] Hartmann-Thompson C, Matisons J (Edts) (2011) Applications of Polyhedral Oligomeric Silsesquioxanes. Dordrecht Heidelberg London New York. Springer. doi: 10.1007/978-90-481-3787-9.
- [10] Wu J, Mather P T. POSS Polymers: Physical Properties and Biomaterials Applications. *Journal of Macromolecular Science, Part C: Polymer Reviews* 2009; 49: 25-63. doi: 10.1080/15583720802656237.
- [11] Ngo T D, Kashani A, Imbalzano G, Nguyen K T Q, Hui D. Additive Manufacturing (3D printing): A review of materials, methods, applications and challenges. *Composites Part B* 2018;143: 172-196. doi: 10.1016/j.compositesb.2018.02.012.
- [12] Gibson I, Rosen D, Stucker B. (2015). Introduction and Basic Principles. Additive Manufacturing Technologies (1-7). New York Heidelberg Dordrecht London. Springer. doi: 10.1007/978-1-4419-1120-9\_1.
- [13] Alghoraibi I, Alomari S (2019). Different Methods for Nanofiber Design and Fabrication. Barhoum A, Bechelany M, Makhoulouf A S H (Edts), *Handbook of Nanofibers* (81-122). Switzerland. Springer. doi: 10.1007/978-3-319-53655-2\_11.
- [14] Haider A, Haider S, Kang I-K. A comprehensive review summarizing the effect of electrospinning parameters and potential applications of nanofibers in biomedical and biotechnology. *Arabian Journal of Chemistry* (2018); 11: 1165-1188. doi: 10.1016/j.arabjc.2015.11.015.
- [15] Lundstedt T, Seifert E, Abramo L, Thelin B, Nyström A, Pettersen J, Bergman R. Experimental design and optimization. *Chemometrics and Intelligent Laboratory Systems* 1998; 42: 3-40. doi: 10.1016/S0169-7439(98)00065-3.



- [16] Taguchi G (1993). Quality and Productivity. Ragsdell K M (Edt) Taguchi on Robust Technology Development. Newyork. The American Society of Mechanical Engineering. doi: 10.1115/1.800288.
- [17] Taguchi G, Phadke M S. (1984). Quality Engineering Through Design Optimization. IEEE Global Telecommunications Conference, Atlanta: 1106-1113.
- [18] Karanfil G. Importance and applications of DOE/optimization methods in PEM fuel cells: A review. International Journal of Energy Research 2020; 44(1): 1-22. doi: 10.1002/er.4815.
- [19] Wu C-M, Hsu C-H, Su C-I, Liu C-L, Lee J-Y. Optimization parameters for continuous electrospinning of polyacrylonitrile nanofibrous yarn using the Taguchi method. Journal of Industrial Textiles 2018; 48(3): 559-579. doi: 10.1177/1528083717740741.
- [20] Karna S K, Sahai R. An Overview on Taguchi Method. International Journal of Engineering and Mathematical Sciences 2012; 1: 11-18.
- [21] Elkasaby M, Hegab H A, Mohany A, Rizvi G M. Modeling and optimization of electrospinning of polyvinyl alcohol (PVA). Advanced in Polymer Technology 2018; 37: 2114-2122. doi: 10.1002/adv.21869.
- [22] Kontou E, Niaounakis M, Georgiopoulos P. Comparative Study of PLA Nanocomposites Reinforced with Clay and Silica Nanofillers and Their Mixtures. Journal of Applied Polymer Science 2011; 122:1519–29. doi: 10.1002/app.
- [23] Jiang L, Zhang J, Wolcott MP. Comparison of polylactide/nano-sized calcium carbonate and polylactide/montmorillonite composites: Reinforcing effects and toughening mechanisms. Polymer 2007; 48:7632–44. doi: 10.1016/j.polymer.2007.11.001.

- [24] Guo Y, Yang K, Zuo X, Xue Y, Marmorat C, Liu Y, et al. Effects of clay platelets and natural nanotubes on mechanical properties and gas permeability of Poly (lactic acid) nanocomposites. *Polymer* 2016; 83:246–59. doi: 10.1016/j.polymer.2015.12.012.
- [25] Yeniova Erpek CE, Ozkoc G, Yilmazer U. Effects of Halloysite Nanotubes on the Performance of Plasticized Poly(lactic acid)-Based Composites. *Polymer Composites* 2016; 37:3134–48. doi: 10.1002/pc.
- [26] Wu W, Cao X, Zhang Y, He G. Polylactide/halloysite nanotube nanocomposites: Thermal, mechanical properties, and foam processing. *Journal of Applied Polymer Science* 2013; 130:443–52. doi: 10.1002/app.39179.
- [27] Xu W, Luo B, Wen W, Xie W, Wang X, Liu M, et al. Surface modification of halloysite nanotubes with l -lactic acid: An effective route to high-performance poly(l -lactide) composites. *Journal of Applied Polymer Science* 2015; 132:1–9. doi: 10.1002/app.41451.
- [28] Yang C, Chen S, Wang J, Zhu T, Xu G, Chen Z, et al. A facile electrospinning method to fabricate polylactide/graphene/MWCNTs nanofiber membrane for tissues scaffold. *Applied Surface Science* 2016; 362:163–8. doi: 10.1016/j.apsusc.2015.11.142.
- [29] Xin S, Li Y, Zhao H, Bian Y, Li W, Han C, et al. Confinement crystallization of poly(l-lactide) induced by multiwalled carbon nanotubes and graphene nanosheets: A comparative study. *Journal of Thermal Analysis and Calorimetry* 2015; 122:379–91. doi: 10.1007/s10973-015-4695-9.
- [30] Chen H-M, Shao L-N, Shen Y, Yang J-H, Huang T, Zhang N, et al. Largely Improved Crystallization Behavior and Thermal Stability of Poly(L-lactide) via the Synergistic Effects of Graphene Oxide and Carbon Nanotubes. *Journal of Applied Polymer Science* 2014; 131. doi: 10.1002/app.40143.

- [31] Chen H, Du X, Yang A, Yang J, Huang T, Zhang N, et al. Effect of graphene oxides on thermal degradation and crystallization behavior of poly(L-lactide). *RSC Advances* 2014; 4:3443–56. doi: 10.1039/C3RA45480K.
- [32] Girdthep S, Sankong W, Pongmalee A, Saelee T, Punyodom W, Meepowpan P, et al. Enhanced crystallization, thermal properties, and hydrolysis resistance of poly(L-lactic acid) and its stereocomplex by incorporation of graphene nanoplatelets. *Polymer Testing* 2017; 61:229–39. doi: 10.1016/j.polymertesting.2017.05.009.
- [33] Wang Y, Cheng Y, Chen J, Wu D, Qiu Y, Yao X, et al. Percolation networks and transient rheology of polylactide composites containing graphite nanosheets with various thicknesses. *Polymer* 2015; 67:216–26. doi: 10.1016/j.polymer.2015.04.076.
- [34] Xiong Z, Dai X, Na H, Tang Z, Zhang RY, Zhu J. A Toughened PLA/Nanosilica Composite Obtained in the Presence of Epoxidized Soybean Oil. *Journal of Applied Polymer Science* 2014; 132:1–7. doi:10.1002/app.41220.
- [35] Hao X, Kaschta J, Pan Y, Liu X, Schubert DW. Intermolecular cooperativity and entanglement network in a miscible PLA/PMMA blend in the presence of nanosilica. *Polymer* 2016; 82:57–65. doi: 10.1016/j.polymer.2015.11.029.
- [36] Wu JH, Kuo MC, Chen CW. Physical properties and crystallization behavior of poly(lactide)/poly(methyl methacrylate)/silica composites. *Journal of Applied Polymer Science* 2015; 132:2–10. doi: 10.1002/app.42378.
- [37] Li W, Zhang C, Chi H, Li L, Lan T, Han P, et al. Development of Antimicrobial Packaging Film Made from Poly(Lactic Acid) Incorporating Titanium Dioxide and Silver Nanoparticles. *Molecules* 2017; 22. doi: 10.3390/molecules22071170.
- [38] Mofokeng JP, Luyt AS. Morphology and thermal degradation studies of melt-

- mixed poly(lactic acid) (PLA)/poly( $\epsilon$ -caprolactone) (PCL) biodegradable polymer blend nanocomposites with TiO<sub>2</sub> as filler. *Polymer Testing* 2015; 45:93–100. doi: 10.1016/j.polymertesting.2015.05.007.
- [39] Zhang H, Huang J, Yang L, Chen R, Zou W, Lin X, et al. Preparation, characterization and properties of PLA/TiO<sub>2</sub> nanocomposites based on a novel vane extruder. *RSC Advances* 2015; 5:4639–47. doi: 10.1039/C4RA14538K.
- [40] Xiu H, Qi X, Bai H, Zhang Q, Fu Q. Simultaneously improving toughness and UV-resistance of polylactide/titanium dioxide nanocomposites by adding poly(ether)urethane. *Polymer Degradation and Stability* 2017; 143:136–44. doi: 10.1016/j.polymdegradstab.2017.07.002.
- [41] Pan H, Qiu Z. Biodegradable Poly ( L -lactide )/ Polyhedral Oligomeric Silsesquioxanes Nanocomposites : Enhanced Crystallization , Mechanical Properties , and Hydrolytic Degradation. *Macromolecules* 2010; 43:1499–506. doi: 10.1021/ma9023685.
- [42] Turan D, Sirin H, Ozkoc G. Effects of POSS Particles on the Mechanical, Thermal, and Morphological Properties of PLA and Plasticised PLA. *Journal of Applied Polymer Science* 2011; 121:1067–75. doi: 10.1002/app.
- [43] Guo T, Wang B. Isothermal Cold Crystallization and Melting Behaviors of Poly(lactic acid)/Epoxy Vinyl Polyhedral Oligomeric Silsesquioxanes Nanocomposites. *Polymer-Plastics Technology and Engineering* 2014; 53:917–26. doi: 10.1080/03602559.2014.886061.
- [44] Liu Z, Hu D, Huang L, Li W, Tian J, Lu L, et al. Simultaneous improvement in toughness, strength and biocompatibility of poly(lactic acid) with polyhedral oligomeric silsesquioxane. *Chemical Engineering Journal* 2018; 346:649–61. doi: 10.1016/j.cej.2018.03.077.
- [45] Fernández MD, Fernández MJ, Cobos M. Effect of polyhedral oligomeric silsesquioxane (POSS) derivative on the morphology, thermal, mechanical and

- surface properties of poly(lactic acid)-based nanocomposites. *Journal of Materials Science* 2016; 51:3628–42. doi: 10.1007/s10853-015-9686-5.
- [46] Kodal M, Sirin H, Ozkoc G. Effects of Reactive and Nonreactive POSS Types on the Mechanical, Thermal, and Morphological Properties of Plasticized Poly(lactic acid). *Polymer Engineering and Science* 2014; 54:264–75. doi: 10.1002/pen.
- [47] Kodal M, Sirin H, Ozkoc G. Investigation of Relationship Between Crystallization Kinetics and Interfacial Interactions in Plasticized Poly(lactic acid)/POSS Nanocomposites: “Effects of Different POSS Types.” *Polymer Composites* 2018; 39. doi: 10.1002/pc.
- [48] Wang R, Wang S, Zhang Y. Morphology, Rheological Behavior, and Thermal Stability of PLA/PBSA/POSS Composites. *Journal of Applied Polymer Science* 2009; 113:3095–102. doi: 10.1002/app.
- [49] Wang BT, Zhang P, Gao D. PLA-Based Biodegradable Copolyester Nanocomposites: Preparation, Characterization and Mechanical Properties. *Advanced Materials Research* 2011; 380:290–3. doi: 10.4028/www.scientific.net/AMR.380.290.
- [50] Gardella L, Colonna S, Fina A, Monticelli O. On novel bio-hybrid system based on PLA and POSS. *Colloid and Polymer Science* 2014; 292:3271–8. doi: 10.1007/s00396-014-3369-7.
- [51] Jia H, Gu S-Y, Chang K. 3D printed self-expandable vascular stents from biodegradable shape memory polymer. *Advance in Polymer Technology* 2018; 37(8): 3222-3228. doi: 10.1002/adv.22091
- [52] Li N, Li Y, Liu S. Rapid prototyping of continuous carbon fiber reinforced polylactic acid composites by 3D printing. *Journal of Materials Processing Technology* 2016; 238: 218-225. doi: 10.1016/j.jmatprotec.2016.07.025

- [53] Tian X, Liu T, Wang Q, Dilmurat A, Li D, Ziegmann G. Recycling and remanufacturing of 3D printed continuous carbon fiber reinforced PLA composites. *Journal of Cleaner Production* 2017; 142: 1609-1618. doi: 10.1016/j.jclepro.2016.11.139
- [54] Luo H, Tan Y, Zhang F, Zhang J, Tu Y, Cui K. Selectively Enhanced 3D Printing Process and Performance Analysis of Continuous Carbon Fiber Composite Material. *Materials* 2019; 12: 3529-3542. doi: 10.3390/ma12213529
- [55] Butt J, Hewavidana Y, Mohaghegh V, Sadeghi-Esfahlani S, Shirvani H. Hybrid Manufacturing and Experimental Testing of Glass Fiber Enhanced Thermoplastic Composites. *Journal of Manufacturing and Materials Processing* 2019; 3: 96-111. doi: 10.3390/jmmp3040096
- [56] He L, Zhong J, Zhu C, Liu X. Mechanical properties and in vitro degradation behavior of additively manufactured phosphate glass particles/fibers reinforced Polylactide. *Journal of Applied Polymer Science* 2019; 136(44): 48171. doi: 10.1002/APP.48171
- [57] Kaynak C, Varsavas S D, Performance comparison of the 3D-printed and injection-molded PLA and its elastomer blend and fiber composites. *Journal of Thermoplastic Composite Materials* 2019; 32(4): 501-520. doi: 10.1177/0892705718772867.
- [58] Najera S, Michel M, Kyung-Hwan J, Nam-Soo K. Characterization of 3D Printed PLA/PCL/TiO<sub>2</sub> Composites for Cancellous Bone. *Journal of Material Sciences and Engineering* 2018; 7(1). DOI: 10.4172/2169-0022.1000417.
- [59] Nadernezhad A, Unal S, Khani N, Koc B. Material extrusion-based additive manufacturing of structurally controlled poly(lactic acid)/carbon nanotube nanocomposites. *The International Journal of Advanced Manufacturing Technology* 2019; 102: 2119-2132. doi: 10.1007/s00170-018-03283-9.

- [60] Shi S, Chen Y, Jing J, Yang L. Preparation and 3D-printing of highly conductive polylactic acid/carbon nanotube nanocomposites via local enrichment strategy. *RSC Advances* 2019; 9(51): 29980-29986. doi: 10.1039/c9ra05684j.
- [61] Luo J, Wang H, Zuo D, Ji A, Liu Y. Research on the Applications of MWCNTs/PLA Composite Material in the Manufacturing of Conductive Composite Products in 3D Printing. *Micromachines* 2018; 9: 635-647. doi: 10.3390/mi9120635.
- [62] Caminero M A, Chacon J M, Garcia-Plaza E, Nunez P J, Reverte J M, Bear J P. Additive Manufacturing of PLA-Based Composites Using Fused Filament Fabrication: Effect of Graphene Nanoplatelet Reinforcement on Mechanical Properties, Dimensional Accuracy and Texture. *Polymer* 2019; 11: 799-820. doi: 10.3390/polym11050799.
- [63] Bustillos J, Montero D, Nautiyal P, Loganathan A, Boesl B, Agarwal A. Integration of Graphene in Poly(Lactic) Acid by 3D Printing to Develop Creep and Wear-Resistant Hierarchical Nanocomposites. *Polymer Composites* 2018; 39(11): 3877-3888. doi: 10.1002/pc.24422.
- [64] Camargo J C, Machado A R, Almeida E C, Sousa Silva E F M. Mechanical properties of PLA-graphene filament for FDM 3D printing. *The International Journal of Advanced Manufacturing Technology* 2019; 103: 2423-2443. doi: 10.1007/s00170-019-03532-5.
- [65] Prashantha K, Roger F. Multifunctional properties of 3D printed poly(lactic acid)/graphene nanocomposites by fused deposition modelling. *Journal of Macromolecular Science, Part A* 2017; 54(1): 24-29. doi: 10.1080/10601325.2017.1250311.
- [66] Chen X, Gao C, Jiang J, Wu Y, Zhu P, Chen G. 3D printed porous PLA/nHA composites scaffolds with enhanced osteogenesis and osteoconductivity in

- vivo for bone regeneration. *Biomedical Materials* 2019; 14(6). doi: 10.1088/1748-605X/ab388d.
- [67] Song Y, Li Y, Song W, Yee K, Lee K Y, Tagarielli V L. Measurements of the mechanical response of unidirectional 3D-printed PLA. *Materials and Design* 2017; 123: 154-164. doi: 10.1016/j.matdes.2017.03.051.
- [68] Lay M, Thajudin N L N, Abdul Hamid Z A, Rusli A, Abdullah M K, Shuib R K. Comparison of physical and mechanical properties of PLA, ABS and nylon 6 fabricated using fused deposition modeling and injection molding. *Composites Part B* 2019; 176: 107341. doi: 10.1016/j.compositesb.2019.107341.
- [69] Priya M S, Naresh K, Jayaganthan R, Velmurugan R. A comparative study between in-house 3D printed and injection molded ABS and PLA polymers for low-frequency applications. *Materials Research Express* 2019; 6. doi: 10.1088/2053-1591/ab2776.
- [70] Benwood C, Anstey A, Andrzejewski J, Misra M, Mohanty A K. Improving the Impact Strength and Heat Resistance of 3D Printed Models: Structure, Property, and Processing Correlations during Fused Deposition Modeling (FDM) of Poly(Lactic Acid). *ACS Omega* 2018; 3: 4400-4411. doi: 10.1021/acsomega.8b00129.
- [71] Andrzejewski J, Pejkowski L, Topolinski T. Tensile and Fatigue Behavior of Additive Manufactured Polylactide. *3D Printing and Additive Manufacturing* 2019; 6(5): 272-280. doi: 10.1089/3dp.2017.0154.
- [72] Askanian H, de Lima D M, Commereuc S, Verney V. Toward a Better Understanding of the Fused Deposition Modeling Process: Comparison with Injection Molding. *3D Printing and Additive Manufacturing* 2018; 5(4): 319-327. doi: 10.1089/3dp.2017.0060.



- [73] Daver F, Lee K P M, Brandt M, Shanks R. Cork-PLA composite filaments for fused deposition modelling. *Composites Science and Technology* 2018; 168: 230-237. doi: 10.1016/j.compscitech.2018.10.008.
- [74] Rasselet D, Caro-Bretelle A-S, Taguet A, Lopez-Cuesta J-M. Reactive Compatibilization of PLA/PA11 Blends and Their Application in Additive Manufacturing. *Materials* 2019; 12: 485-502. doi: 10.3390/ma12030485.
- [75] Alghoraibi I, Alomari S. Different Methods for Nanofiber Design and Fabrication. *Handbook of Nanofibers*, Springer; 2019, 79–124. doi: 10.1007/978-3-319-53655-2\_11.
- [76] Touny AH, Lawrence JG, Jones AD, Bhaduri SB. Effect of electrospinning parameters on the characterization of PLA/HNT nanocomposite fibers. *Journal of Materials Research* 2010; 25:857–65. doi: 10.1557/jmr.2010.0122.
- [77] Sonseca A, Peponi L, Sahuquillo O, Kenny JM, Giménez E. Electrospinning of biodegradable polylactide/hydroxyapatite nanofibers: Study on the morphology, crystallinity structure and thermal stability. *Polymer Degradation and Stability* 2012; 97:2052–9. doi: 10.1016/j.polymdegradstab.2012.05.009.
- [78] Yang T, Wu D, Lu L, Zhou W, Zhang M. Electrospinning of Polylactide and Its Composites With Carbon Nanotubes. *Polymer Composites* 2011; 32:1280–8. doi: 10.1002/pc.
- [79] Kim ES, Kim SH, Lee CH. Electrospinning of polylactide fibers containing silver nanoparticles. *Macromolecular Research* 2010; 18:215–21. doi: 10.1007/s13233-010-0316-4.
- [80] Casasola R, Thomas NL, Trybala A, Georgiadou S. Electrospun poly lactic acid (PLA) fibres: Effect of different solvent systems on fibre morphology and diameter. *Polymer* 2014; 55:4728–37. doi: 10.1016/j.polymer.2014.06.032.
- [81] Tian R, Zhang P, Lv R, Na B, Liu Q, Ju Y. Formation of highly porous

- structure in the electrospun polylactide fibers by swelling-crystallization in poor solvents. *RSC Advances* 2015; 5:37539–44. doi: 10.1039/c5ra05738h.
- [82] Zhang X, Nakagawa R, Chan KHK, Kotaki M. Mechanical property enhancement of polylactide nanofibers through optimization of molecular weight, electrospinning conditions, and stereocomplexation. *Macromolecules* 2012; 45:5494–500. doi: 10.1021/ma300289z.
- [83] Zong X, Kim K, Fang D, Ran S, Hsiao BS, Chu B. Structure and process relationship of electrospun bioabsorbable nanofiber membranes. *Polymer* 2002; 43:4403–12. doi: 10.1016/S0032-3861(02)00275-6.
- [84] Lu Y, Chen YC, Zhang PH. Preparation and characterisation of polylactic acid (PLA)/polycaprolactone (PCL) composite microfibre membranes. *Fibres and Textiles in Eastern Europe* 2016; 24:17–25. doi: 10.5604/12303666.1196607.
- [85] Gómez-Pachón EY, Vera-Graziano R, Campos RM. Structure of poly(lactic-acid) PLA nanofibers scaffolds prepared by electrospinning. *IOP Conference Series: Materials Science and Engineering* 2014; 59. doi: 10.1088/1757-899X/59/1/012003.
- [86] Forouharshad M, Putti M, Basso A, Prato M, Monticelli O. Biobased System Composed of Electrospun sc-PLA/POSS/Cyclodextrin Fibers To Remove Water Pollutants. *ACS Sustainable Chemistry and Engineering* 2015; 3:2917–24. doi: 10.1021/acssuschemeng.5b00892.
- [87] Gomez-Sanchez C, Kowalczyk T, Ruiz De Eguino G, Lopez-Arraiza A, Infante A, Rodriguez CI, et al. Electrospinning of poly(lactic acid)/polyhedral oligomeric silsesquioxane nanocomposites and their potential in chondrogenic tissue regeneration. *Journal of Biomaterial Science, Polymer Edition* 2014; 25:802–25. doi: 10.1080/09205063.2014.910151.
- [88] Monticelli O, Putti M, Gardella L, Cavallo D, Basso A, Prato M, et al. New Stereocomplex PLA-Based Fibers: Effect of POSS on Polymer

- Functionalization and Properties. *Macromolecules* 2014;47:4718–27. doi: 10.1021/ma500528a.
- [89] Gardella L, Basso A, Prato M, Monticelli O. PLA/POSS nanofibers: A novel system for the immobilization of metal nanoparticles. *ACS Applied Materials and Interfaces* 2013;5:7688–92. doi: 10.1021/am402280j.
- [90] Kim B, Kim K, Kim I. Poly ( L-Lactide ) Composite Nanofibers Incorporating POSS-MWNTs. *Advanced Materials Research* 2011; 175–176:341–4. doi: 10.4028/www.scientific.net/AMR.175-176.341.
- [91] Albetran H, Dong Y, Low IM. Characterization and optimization of electrospun TiO<sub>2</sub>/PVP nanofibers using Taguchi design of experiment method. *Journal of Asian Ceramic Societies* 2015; 3:292–300. doi: 10.1016/j.jascer.2015.05.001.
- [92] Khanlou HM, Ang BC, Talebian S, Afifi AM, Andriyana A. Electrospinning of polymethyl methacrylate nanofibers : optimization of processing parameters using the Taguchi design of experiments. *Textile Research Journal* 2015;85:356–68. doi: 10.1177/0040517514547208.
- [93] Veerabhadraiah A, Ramakrishna S, Angadi G, Venkatram M, Ananthapadmanabha VK, Narasimha MHN, et al. Development of polyvinyl acetate thin films by electrospinning for sensor applications. *Applied Nanoscience* 2017; 7:355–63. doi: 10.1007/s13204-017-0576-9.
- [94] Pirsalami S, Zebarjad SM, Daneshmanesh H. Evaluation and Optimization of Electrospun Polyvinyl Alcohol Fibers via Taguchi Methodology. *International Polymer Processing* 2016; 31:503–7. doi: 10.3139/217.3278.
- [95] Celep GK, Dincer K. Optimization of Parameters for Electrospinning of Polyacrylonitrile Nanofibers by the Taguchi Method. *International Polymer Processing* 2017; 32:508–14. doi: 10.3139/217.3411.

- [96] Senthil T, Anandhan S. Electrospinning of non-woven poly(styrene-co-acrylonitrile) nanofibrous webs for corrosive chemical filtration: Process evaluation and optimization by Taguchi and multiple regression analyses. *Journal of Electrostatics* 2015;73:43–55. doi:10.1016/j.elstat.2014.10.002.
- [97] Amini N, Kalaei M, Mazinani S, Pilevar S, Ranaei-Siadat SO. Morphological optimization of electrospun polyacrylamide/MWCNTs nanocomposite nanofibers using Taguchi's experimental design. *The International Journal of Advanced Manufacturing Technology* 2013;69:139–46. doi:10.1007/s00170-013-5006-x.
- [98] Zhao P, Cao M, Gu H, Gao Q, Xia N, He Y, et al. Research on the electrospun foaming process to fabricate three-dimensional tissue engineering scaffolds. *Journal of Applied Polymer Science* 2018;135:46898. doi: 10.1002/app.46898.
- [99] Nazir A, Khenoussi N, Schacher L, Hussain T, Adolphe D, Hekmati AH. Using the Taguchi method to investigate the effect of different parameters on mean diameter and variation in PA-6 nanofibres produced by needleless electrospinning. *RSC Advances* 2015;5:76892–7. doi: 10.1039/c5ra13649k.
- [100] Sadeghi D, Karbasi S, Razavi S, Mohammadi S, Shokrgozar MA, Bonakdar S. Electrospun poly(hydroxybutyrate)/chitosan blend fibrous scaffolds for cartilage tissue engineering. *Journal of Applied Polymer Science* 2016; 133:1–9. doi: 10.1002/app.44171.
- [101] Patra SN, Easteal AJ, Bhattacharyya D. Parametric study of manufacturing poly(lactic) acid nanofibrous mat by electrospinning. *Journal of Materials Science* 2009;44:647–54. doi: 10.1007/s10853-008-3050-y.
- [102] Su C, Liu Y, Hsu C, Lee J, Lu C. Optimum Parameters of the Continuous Process of Electrospun Nanofibrous Yarn. *Fibers and Polymers* 2015;16:826–33. doi: 10.1007/s12221-015-0826-y.
- [103] Dong Y, Bickford T, Haroosh HJ, Lau K, Takagi H. Multi-response analysis

in the material characterisation of electrospun poly (lactic acid)/halloysite nanotube composite fibres based on Taguchi design of experiments : fibre diameter , non-intercalation and nucleation effects. *Applied Physics A Materials Science and Processing* 2013;112:747–57. doi: 10.1007/s00339-013-7789-x.

- [104] Diaz E, Molpeceres A L, Sandonis I, Puerto I. PLLA/nHA Composite Films and Scaffolds for Medical Implants: In Vitro Degradation, Thermal and Mechanical Properties. *Journal of Inorganic and Organometallic Polymers and Materials* 2019; 29: 121-131. doi: 10.1007/s10904-018-0972-y
- [105] Felfel R M, Hossain K M Z, Parsons A J, Rudd C D, Ahmed I. Accelerated in vitro degradation properties of polylactic acid/phosphate glass fibre composites. *Journal of Materials Science* 2015; 50: 3942-3955. doi: 10.1007/s10853-015-8946-8.
- [106] Tsuji H, Ikada Y. Properties and morphology of poly(L-lactide) 4. Effects of structural parameters on long-term hydrolysis of poly(L-lactide) in phosphate-buffered solution. *Polymer Degradation and Stability* 2000; 67: 179-189. doi: 10.1016/S0141-3910(99)00111-1.
- [107] Tsuji H, Mizuno A, Ikada Y. Properties and Morphology of Poly(L-lactide). III. Effects of Initial Crystallinity on Long-Term In Vitro Hydrolysis of High Molecular Weight Poly(L-lactide) Film in Phosphate-Buffered Solution. *Journal of Applied Polymer Science* 2000; 77 (7): 1452-1464. doi: 10.1002/1097-4628.
- [108] Li K, Colonna S, Fina A, Monticelli O. Polyhedral Oligomeric Silsesquioxane (POSS) Surface Grafting: A Novel Method to Enhance Polylactide Hydrolysis Resistance. *Nanomaterials* 2019; 9: 1144. doi: 10.3390/nano9081144.
- [109] Kaynak C, Meyva Y. Use of maleic anhydride compatibilization to improve toughness and other properties of polylactide blended with thermoplastic

- elastomers. *Polymers for Advanced Technologies* 2014; 25:1622–32. doi: 10.1002/pat.3415.
- [110] Fischer EW, Sterzel HJ, Wegner G. Investigation of Structure of Solution Grown Crystals of Lactide Copolymers by Means of Chemical Reactions. *Colloid and Polymer Science* 1973; 251:980–90. doi: 10.1007/bf01498927.
- [111] Chen C, Huang S, Chen M, Lu Q. Synthesis and characterization of three kinds of bifunctionalized polyhedral oligomeric silsesquioxanes with the same cage structure. *High Performers Polymers* 2012; 24:119–24. doi: 10.1177/0954008311434560.
- [112] Lin-Vien D, Colthup NB, FateleyWG GJ. (1991) *The Handbook of Infrared and Raman Characteristic Frequencies of Organic Molecules*. San Diego: CA: Academic Press.
- [113] Kolel-Veetil MK, Dominguez DD, Keller TM. Dendritic Networks Containing Polyhedral Oligomeric Silsesquioxane (POSS) and Carborane Clusters. *Journal of Polymer Science Part A: Polymer Chemistry* 2008; 46:2581–7. doi: 10.1002/pola.
- [114] Kastner J, Lorret O, Rank A, Schwarzinger C, Dittert B, Mühlberger M. Nanocontact printing stamp material via bi-functionalization of polyhedral oligomeric silsesquioxanes. *European Polymer Journal* 2015; 65:221–31. doi: 10.1016/j.eurpolymj.2014.11.015.
- [115] Domenek S, Ducruet V. (2016) *Characteristics and Applications of PLA. Biodegradable and Biobased Polymers for Environmental and Biomedical Applications*, Wiley. doi: 10.1002/9781119117360.
- [116] Hwang SW, Lee SB, Lee CK, Lee JY, Shim JK, Selke SEM, et al. Grafting of maleic anhydride on poly(L-lactic acid). Effects on physical and mechanical properties. *Polymer Testing* 2012; 31:333–44. doi:

10.1016/j.polymertesting.2011.12.005.

- [117] Jung C-H, Hwang I-T, Jung C-H, Choi J-H. Preparation of flexible PLA/PEG-POSS nanocomposites by melt blending and radiation crosslinking. *Radiation Physics and Chemistry* 2014; 102: 23-28. doi: 10.1016/j.radphyschem.2014.04.020.
- [118] Yuan X, Mak A F T, Yao K. Comparative Observation of accelerated degradation of (L-lactic acid) fibres in phosphate buffered saline and a dilute alkaline solution. *Polymer Degradation and Stability* 2002; 75: 45-53. doi: 10.1016/S0141-3910(01)00203-8.
- [119] Araque-Monros M C, Vidaurre A, Gil-Santos L, Bernabe S G, Monleon-Pradas M, Mas-Estelles J. Study of the degradation of a new PLA braided biomaterial in buffer phosphate saline, basic and acid media, intended for the regeneration of tendons and ligaments. *Polymer Degradation and Stability* 2013; 98: 1563-1570. doi: 10.1016/j.polymdegradstab.2013.06.031.
- [120] Tsuji H, Nakahara K. Poly(L-lactide). IX. Hydrolysis in Acid Media. *Journal of Applied Polymer Science* 2002; 86: 186-194. doi: 10.1002/app.10813.





## CURRICULUM VITAE

**Yelda MEYVA ZEYBEK**

**Date of Birth** : March 8, 1987

**Address** : Middle East Technical University  
Faculty of Engineering  
Department of Metallurgy and Materials Engineering  
D-307 Çankaya/ANKARA

**E-mail** : yeldameyva@gmail.com; yeldameyva@kmu.edu.tr

**Phone Number** : 0507 605 0816

### EDUCATION

***Doctor of Philosophy*** **2014-2020**  
Department of Polymer and Science Technology **CPA: 3.93/4**  
Middle East Technical University (METU), Ankara, Turkey  
Thesis Subject: Studies on Polylactide Nanocomposites with Polyhedral Oligomeric  
Silsesquioxane  
Advisor: Prof. Dr. Cevdet KAYNAK

***Master of Science*** **2011-2014**  
Department of Polymer and Science Technology **CPA: 3.50/4**  
Middle East Technical University (METU), Ankara, Turkey  
Thesis Subject: Toughening of Polylactide by Blending with Various Elastomeric  
Materials  
Advisor: Prof. Dr. Cevdet KAYNAK

***Bachelor of Science***

**2005- 2010**

Department of Chemical Engineering

**CPA: 3.04/4**

Ege University, Izmir, Turkey

Thesis Subject: Removal of Arsenic by Oxides of Titanium, Iron and Manganase

Advisor: Prof. Dr. Mustafa DEMİRCİOĞLU

## **PROFESSIONAL EXPERIENCE**

<i>02/2018 - Present</i>	Res Assist/Metallurgical and Materials Eng/KMU
<i>01/2012 - 02/2018</i>	Res Assist/Polymer Science and Technology Dept/METU
<i>08/2011 - 01/2012</i>	Res Assist/Materials Science and Eng/KMU
<i>09/2010 - 08/2011</i>	TÜBİTAK Project Asist/Chem Eng Dept/IZTECH
<i>07/2009 - 08/2009</i>	Summer Internship/Abalıoğlu Inc./Production
<i>06/2008 - 07/2008</i>	Summer Internship/Sanovel Drug Inc./Quality Control

## **INTERNATIONAL PUBLICATIONS (SCI)**

1. C. Kaynak and **Y. Meyva** “*Use of Maleic Anhydride Compatibilization to Improve Toughness and Other Properties of Polylactide Blended with Thermoplastic Elastomers*”, *Polymers for Advanced Technologies*, 25 (12) , 1622-1632 (December 2014)
2. **Y. Meyva** and C. Kaynak, “*Toughening of Polylactide by Bio-based and Petroleum-based Thermoplastic Elastomers*”, *International Polymer Processing*, 30 (5) , 593-602 (November 2015).
3. **Y. Meyva** and C. Kaynak, “*Influences of Three Different Ethylene Copolymers on the Toughness and other Properties of Polylactide*”, *Plastics, Rubber and*

Composites: Macromolecular Engineering, 45 (5) , 189-198 (July 2016), (DOI: 10.1080/14658011.2016.1153821)

4. **Y. Meyva-Zeybek** and C. Kaynak, “*Loss of Thermoplastic Elastomer Toughening in Polylactide After Weathering*”, Journal of Applied Polymer Science, (March 2019), (DOI: 10.1002/app.47177)
5. **Y. Meyva-Zeybek** and C. Kaynak, “*Behaviour of PLA/POSS Nanocomposites: Effects of Filler Content, Functional Group, Copolymer Compatibilization*”, Journal of Thermoplastic Composite Materials, (Submitted)
6. **Y. Meyva-Zeybek** and C. Kaynak, “*Electrospinning of PLA and PLA/POSS Nanofibers: Use of Taguchi Optimization for Process Parameters*”, Journal of Applied Polymer Science, (Under Review)
7. **Y. Meyva-Zeybek** and C. Kaynak, “*A Comparative Study for the Behavior of 3D-Printed and Compression Molded PLA/POSS Nanocomposites*”, Composites Communications, (Submitted)

#### **INTERNATIONAL CONFERENCE PROCEEDINGS**

1. **Y. Meyva**, S. Kurklu, N. Gizli, M. Demircioglu, “*Arsenic Removal by Nanoparticle Media*”, Abstract Book of the **6<sup>th</sup> Nanoscience and Nanotechnology Conference**, İzmir Yüksek Teknoloji Enstitüsü, İzmir, Turkey, (15-18 June 2010)
2. E. Ozdemir, M. Molva, **Y. Meyva**, Ö. Fidan, S. K. Ozdemir, “*Production of Calcite from Aggregated Nano Clusters*”, Abstract Book of the **7<sup>th</sup> Nanoscience and Nanotechnology Conference**, Sabancı University, Istanbul, (June 27, 2011)

3. C. Kaynak, Y. Meyva, A.R. Erdogan, I. Kaygusuz, “*Morphological Studies of Polylactide Blends and Composites by Scanning Electron Microscopy*”, Abstract Book of the **17th International Conference of Focus on Microscopy – FOM 2014**, University of Sydney, Australia, page 69 , (13-16 April 2014)
4. Y. Meyva and C. Kaynak, “*Changes in the Thermal and Other Properties of Polylactide by Blending with Thermoplastic Polyurethane*”, Book of Abstracts of the **International Conference on Thermophysical and Mechanical Properties of Advanced Materials – THERMAM 2014**, University of Rostock & Dokuz Eylul University, Izmir, Turkey, page 55 , (12-15 June 2014)
5. Y. Meyva and C. Kaynak, “*Effects of Maleic Anhydride Compatibilization on the Toughness and Other Properties of Polylactide Blended with Thermoplastic Elastomers*”, Abstract Book of the **8th European Symposium on Biopolymers – ESBP 2015**, Sapienza University, Rome, Italy, page 107, (16-18 September 2015)
6. C. Kaynak and Y. Meyva, “*Toughening of Polylactide (PLA) by Blending with Elastomeric Materials*” (**invited talk**), Abstract Book of the **Energy Materials Nanotechnology – EMN Meeting on Polymer 2016**, The Hong Kong Polytechnic University, Hong Kong, China, page 69-70, (12-15 January 2016)
7. Y. Meyva and C. Kaynak, “*Blending of Polylactide with Different Elastomeric Materials for Toughening*”, Book of Abstract of the **46th IUPAC World Polymer Congress – MACRO 2016**, International Union of Pure and Applied Chemistry, Istanbul, Turkey, page 178, (17-21 July 2016)
8. Y. Meyva-Zeybek and C. Kaynak, “*Mechanical Properties of PLA Nanocomposites Filled with Various Polyhedral Oligomeric Silsesquioxane Structures*”, Abstract of the **17. E-MRS (European Materials Research**

Society) 2018 Fall Meeting, Warsaw, Poland, 1 page on USB (17-20 September 2018)

## NATIONAL CONFERENCE PROCEEDINGS

1. Y. Meyva and C. Kaynak, “*Polilaktitin Farklı Elastomerik Malzemelerle Toklaştırma Amaçlı Harmanlanması*”, **6. Ulusal Polimer Bilim ve Teknoloji Kongresi**, Hacettepe Üniversitesi, Ankara, Bildiri Özetleri, sayfa:88, (4-7 Eylül 2016)

## PROJECTS

PROJECT NAME	PROJECT TYPE	BUDGET	DATE	PROJECT NUMBER
Design of Plant for Methanol Production	Ege University	--	2009-2010	--
Removal of <i>Arsenic</i> by Oxides of Titanium, Iron and Manganase	Ege University	--	2009-2010	--
Synthesis of Nanocalcite (CaCO <sub>3</sub> )	TUBITAK1001	300000 TL	2010-2011	110M104
Investigation of Rubber Toughening Mechanisms in the Brittle Polylactide Biopolymer	TUBITAK1002	30000 TL	2013-2014	113M586
Preparation and Characterization of Polylactide (PLA)/Elastomer Blends	OYP-YOK Project	10000 TL	2012-2013	--
Production of PLA/POSS Composite Nanofiber Structure with Electrospinning Method	OYP-YOK Project	10000 TL	2015-2016	--

## **AWARDS**

- Publication incentive award from the METU Development Foundation (December, 2014)
- Publication incentive award from the METU Development Foundation (November, 2015)
- Publication incentive award from the METU Development Foundation (December, 2018)

## **ASSISTED COURSES**

- PST 502 Polymer Science and Technology (Coordinator)
- PST 508 Characterization Techniques for Polymeric Materials
- CENG 107 General Chemistry Laboratory
- IE 107 General Chemistry Laboratory
- METE 215 Materials Processing Laboratory
- METE 470 Composite Materials
- METE 560 Polymer Nanocomposites

## **LANGUAGE**

English : Fluent (Yökdil: 85)

## **CITATIONS**

Sum of times cited (ISI Web of Science):	48
H-index (ISI Web of Science)	2